



Discovery of novel *N*-benzylbenzamide derivatives as tubulin polymerization inhibitors with potent antitumor activities

Huajian Zhu^a, Wenlong Li^a, Wen Shuai^a, Yang Liu^a, Limei Yang^a, Yuchen Tan^a, Tiandong Zheng^a, Hong Yao^a, Jinyi Xu^{a,*}, Zheyang Zhu^b, Dong-Hua Yang^c, Zhe-Sheng Chen^c, Shengtao Xu^{a,*}

^a State Key Laboratory of Natural Medicines and Department of Medicinal Chemistry, China Pharmaceutical University, 24 Tong Jia Xiang, Nanjing, 210009, PR China

^b Division of Molecular Therapeutics & Formulation, School of Pharmacy, The University of Nottingham, University Park Campus, Nottingham NG7 2RD, UK

^c College of Pharmacy and Health Sciences, St. John's University, 8000 Utopia Parkway, Queens, New York, 11439, United States

ARTICLE INFO

Article history:

Received 18 November 2020

Received in revised form

16 February 2021

Accepted 17 February 2021

Available online 24 February 2021

Keywords:

N-benzylbenzamide

Anti-vascular

Druggability

Tubulin inhibitors

Antitumor

ABSTRACT

A series of novel *N*-benzylbenzamide derivatives were designed and synthesized as tubulin polymerization inhibitors. Among fifty-one target compounds, compound **20b** exhibited significant anti-proliferative activities with IC₅₀ values ranging from 12 to 27 nM against several cancer cell lines, and possessed good plasma stability and satisfactory physicochemical properties. Mechanism studies demonstrated that **20b** bound to the colchicine binding site and displayed potent anti-vascular activity. Notably, the corresponding disodium phosphate **20b-P** exhibited an excellent safety profile with the LD₅₀ value of 599.7 mg/kg (i.v. injection), meanwhile, it significantly inhibited tumor growth and decreased microvessel density in liver cancer cell H22 allograft mouse model without obvious toxicity. Collectively, **20b** and **20b-P** are novel promising anti-tubulin agents with more druggable properties and deserve to be further investigated for cancer therapy.

© 2021 Elsevier Masson SAS. All rights reserved.

1. Introduction

Microtubules are stiff, cylindrical polymers of α , β -tubulins, and the head-to-tail association of α - β heterodimers forms linear protofilaments [1,2]. They play diverse roles in cells, such as protein transport, maintaining cell structure, chromosome segregation and mitosis [3–5]. Microtubule targeting agents (MTAs) such as paclitaxel or vincristine, have been widely used in clinics for the treatment of various cancers [6,7].

Six binding sites for taxane, laulimalide, vinca alkaloid, pironetin, maytansine and colchicine have been identified in microtubules. Inhibitors targeting taxane and laulimalide binding sites can stabilize microtubules while those targeting other four binding sites can destabilize microtubules [6,8]. Currently, all FDA approved drugs that disrupt microtubule polymerization for cancer treatment bind to either the taxane binding site or the vinca alkaloids

binding site. In recent decades, colchicine binding site inhibitors (CBSIs) have held great potential as a new generation of tubulin inhibitors, which can overcome the limitations of existing tubulin inhibitors such as structure complexity, poor aqueous solubility, narrow therapeutic index, wide inter-patient variability and high toxicity [9–18]. Notably, CBSIs exhibit promising ability to rapidly disrupt existing tumor blood vessels, leading to the collapse of blood vessels and tumor cell death [19,20].

Several typical small-molecular inhibitors of tubulin targeting the colchicine binding site were evaluated in clinical trials as vascular disrupting agents (VDAs) (Fig. 1A). Combretastatin A-4 (**1**, CA-4) is a natural *cis*-stilbene derivative isolated from the bark of the African willow tree *Combretum caffrum* [9], which was identified as a typical CBSI [21]. CA-4 displayed both potent anti-proliferative activity against multiple human cancer cell lines [22] and anti-vascular activity [23]. The phosphate CA-4 (CA-4P) had been evaluated in clinical trials, however, it was discontinued due to the lack of a meaningful improvement in progression-free survival (PFS) and unfavorable partial response data [24]. Verubulin (**3**), also known as MPC-6827, was a very potent tubulin polymerization inhibitor and demonstrated low nanomolar (nM) potency

* Corresponding author.

** Corresponding author.

E-mail address: cpuxst@cpu.edu.cn (S. Xu).

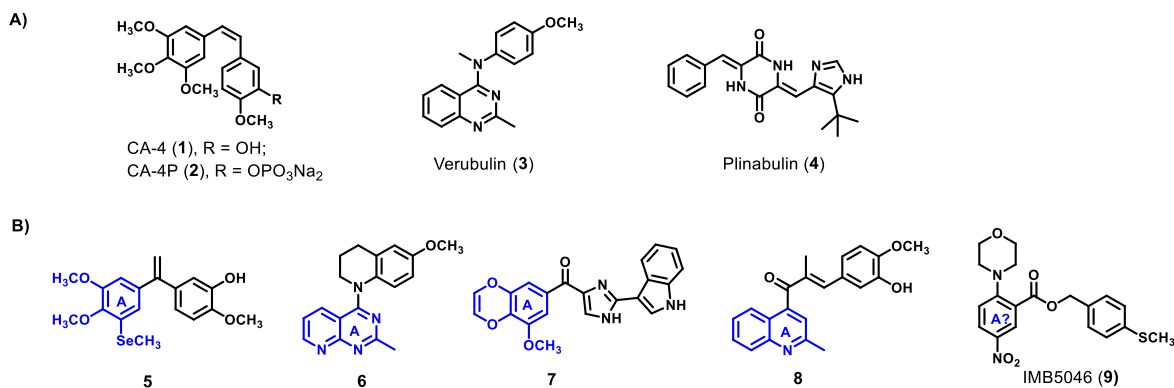


Fig. 1. A) Typical CBSIs under clinical trials; B) Reported CBSIs by modifying TMP or replacing TMP moiety. The 4-methylthiophenyl moiety of IMB5046 was predicted to act as ring A in Zheng's work, however, in this study, we speculated that 2-morpholine-5-nitrophenyl moiety located in the position of TMP acting as ring A of known CBSIs according to our SARs and docking study below.

against diverse cancer cell lines [25], and it was found to act as a VDA by inducing rapid shutdown of tumor blood flow [26]. Some verubulin derivatives have been reported to exhibit potent anti-tumor efficacy and improved therapeutic index [27–29]. Verubulin was also evaluated in clinical trials; however, it was discontinued due to cardiovascular toxicity revealed in phase I and phase II studies [30]. Plinabulin (4), developed from phenylahistin as a metabolite isolated from *Aspergillus ustus* [31], was another typical CBSI which attracted much attention [32]. Currently, a combination of plinabulin and docetaxel is being evaluated in clinical phase III trials for the treatment of non-small cell lung cancer [33].

3,4,5-Trimethoxyphenyl (TMP) is a common moiety which serves as ring A of classical CBSIs, such as colchicine, combretastatin A-4, podophyllotoxin. TMP is crucial for interacting with tubulin and producing the maximum antiproliferative activities [34]. Though modifications on the TMP moiety of CBSIs are usually reported to significantly reduced anticancer potency [35,36], there are still many reports in which modifying TMP or replacing TMP with other moieties led to the improvement of activity. In 2017, Pang et al. introduced a selenium atom to the TMP moiety of iso-combretastatin A-4 (isoCA-4), the 3-methylseleno derivative (structure 5 in Fig. 1B) displayed comparable *in vitro* anti-proliferative activity to isoCA-4 while the *in vivo* antitumor activity was significantly improved [37]. The quinazoline of compound 6 was thought to be a surrogate of TMP moiety when binding to the colchicine site, and this was supported by its crystal structure complexed with tubulin [29]. In 2018, Wang et al. reported a modification on the TMP moiety of lead VERU-111, and compound 7 with a unique 3-methoxybenzo [4,5]-dioxene ring was found to be 2–8 times more potent than VERU-111 against three cancer cell lines [38]. Our group also discovered a quinoline-chalcone compound 8, and its antiproliferative activity was improved by 8–10 fold when compared to its parent compound bearing a TMP moiety [39].

A novel nitrobenzoate IMB5046 (9, 2-morpholin-4-yl-5-nitrobenzoic acid 4-methylsulfanylbenzyl ester), which was reported by Zheng et al. in 2016, was found to display both potent *in vitro* and *in vivo* antitumor activities, and mechanism studies indicated that it bound to the colchicine binding site [40]. IMB5046 is distinct from any other known CBSIs; however, its structure-activity relationships (SARs) have not been investigated. Though IMB5046 had a remarkable antitumor activity in several mouse xenograft models, the ester bond, which may be unstable *in vivo*, and the nitro group, which is often associated with mutagenicity and genotoxicity [41], might complicate the further development of IMB5046. In addition, its docking study showed that the 4-

methylthiophenyl moiety occupied the position where TMP of colchicine was located [40], which structurally differs from the SARs of classical CBSIs [14]. Thus, the binding mode of IMB5046 with tubulin should be further investigated.

Based on our previous works on discovering and developing novel anticancer agents targeting the tubulin-microtubule system [39,42–48], we further considered to design and synthesize novel *N*-benzylbenzamide derivatives based on IMB5046 with the wish to obtain promising anti-tubulin agents with more druggable properties (Fig. 2). We set for ourselves the goal of designing new analogs with (a) equal or higher potency compared to IMB5046, (b) substantially low toxicity as tested in mouse models, and (c) improved plasma stability.

Herein, we would like to report the synthesis of these *N*-benzylbenzamide derivatives, their SARs and mechanism studies, evaluation of preliminary druggability, *in vitro* and *in vivo* anti-tumor and anti-vascular activities as well as the illustration of the 2-morpholinophenyl moiety as a structurally novel ring A of CBSIs.

2. Results and discussion

2.1. Synthesis of target *N*-benzylbenzamide derivatives

In our first-round modification, we investigated the SARs of ring B. Seventeen compounds **13a–q** including two indolyl benzoates **13a** and **13b** and fifteen *N*-benzylbenzamides **13c–q** were synthesized. As shown in Scheme 1, 2-fluoro-5-nitrobenzoic acid **11** was prepared by the nitration of the starting material 2-fluorobenzoic acid **10**, which underwent a nucleophilic attack by morpholine to give 2-morpholino-5-nitrobenzoic acid **12**. The esterification or amidation of intermediate **12** with different indolylcarbinols or benzylamines yielded target compounds **13a–q**.

In the second-round modification, the SARs of C-2 position on ring A were investigated. Eight compounds **16a–h**, of which different amino groups were substituted at the C-2 position while ring B was maintained as an isovanillic ring, were synthesized as shown in Scheme 2. Intermediate **11** underwent nucleophilic substitutions by different amines to give **14a–h**, which were reacted with TBS-protected benzylamine **15** followed by deprotection of TBS to yield target compounds **16a–h**.

In the third-round modification, the effects of C-4 and C-5 positions on activity was further examined, thus, twenty-six compounds **20a–p** and **34a–j** were synthesized, of which ring B was an isovanillic ring and C-2 was substituted with morpholine or piperidine. As illustrated in Scheme 3, benzoic acids **19a–d** in which R were hydrogen or fluorine were prepared by the reactions of their

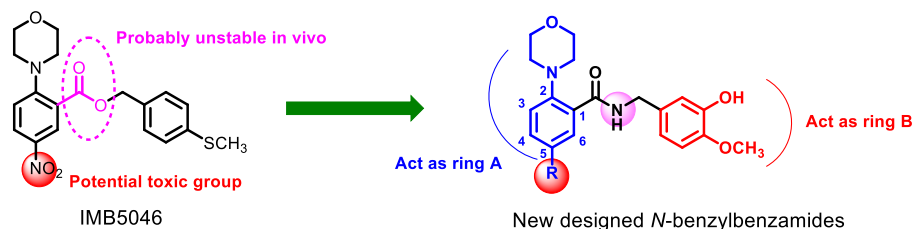
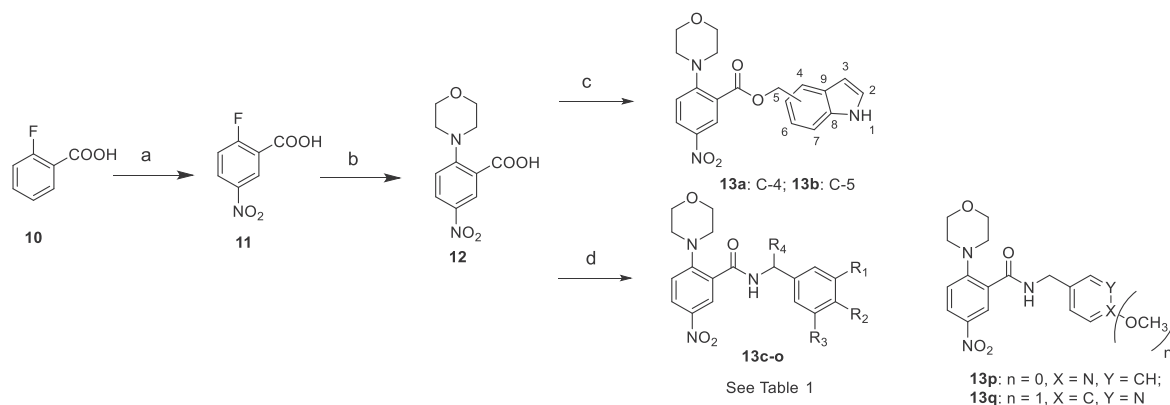
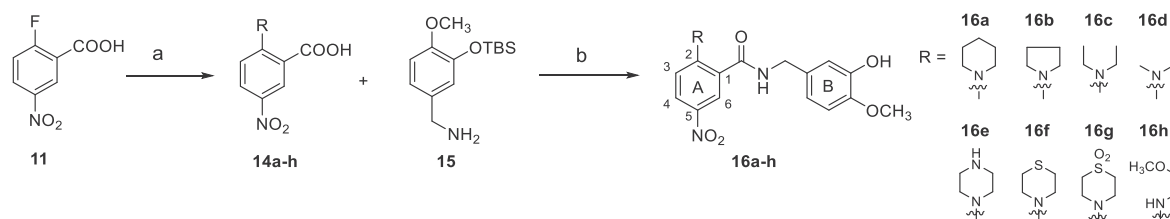


Fig. 2. The designing concept for *N*-benzylbenzamide derivatives.



Scheme 1. Reagents and conditions: (a) con. HNO_3 , con. H_2SO_4 , 0 °C to rt, 2 h, 71.2%; (b) morpholine, dioxane, rt, 2 h, yield 76.4%; (c) 4-indolylcarbinol or 5-indolylcarbinol, EDCI, DMAP (cat.), DCM, rt, 2 h, 60.3–67.8%; (d) i) various benzylamines, EDCI, HOBT, DMAP (cat.), DCM, rt, 2 h, 42.0–88.0%; ii) when R_1 or $R_2 = OTBS$, TBAF, THF, rt, 15 min, 61.5–81.1%.



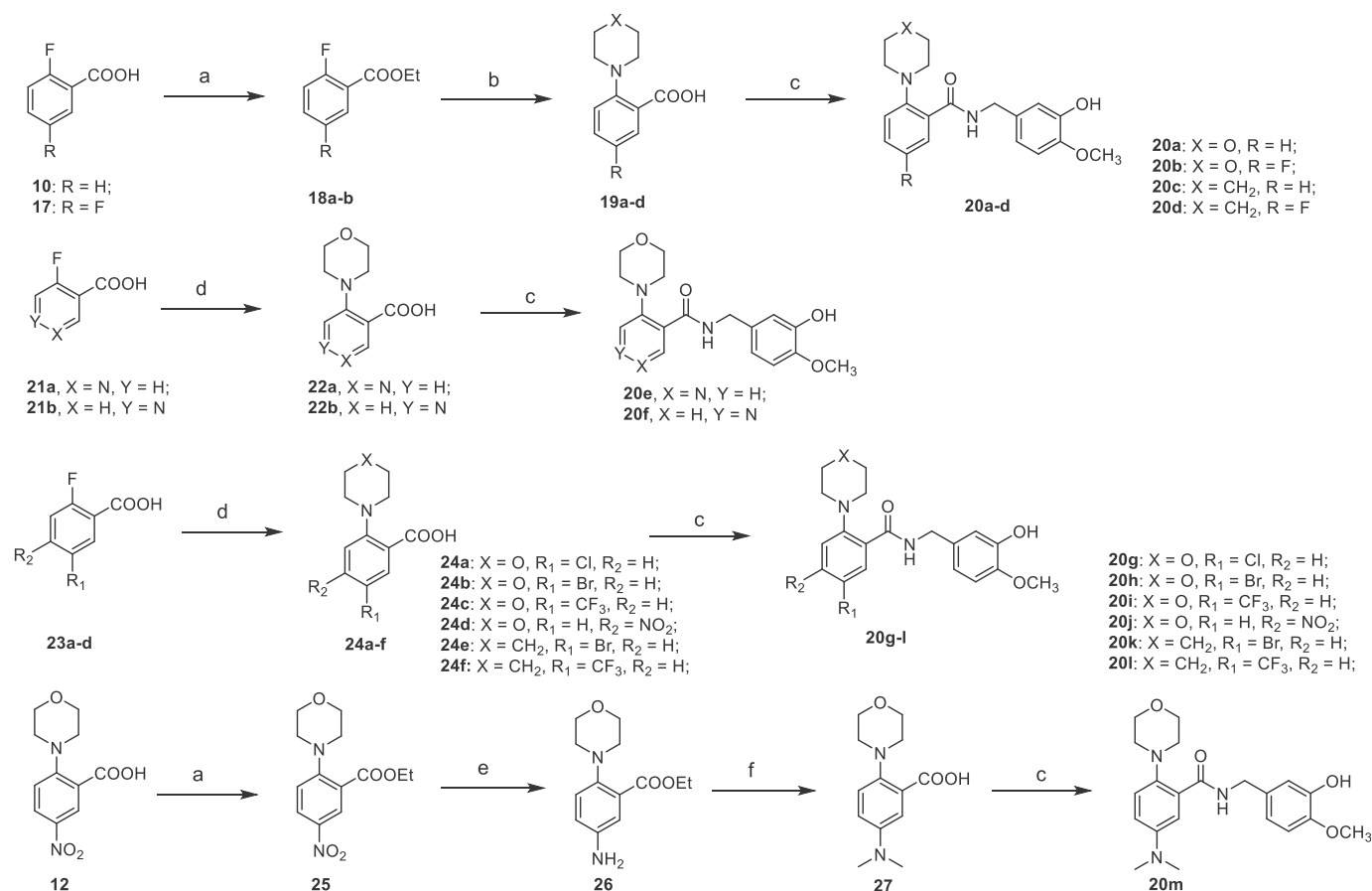
Scheme 2. Reagents and conditions: (a) various amines, dioxane, rt, 2 h, 70.3–90.3%; (b) i) EDCI, HOBT, DMAP (cat.), DCM, rt, 2 h; ii) TBAF, THF, rt, 15 min, 44.4–62.9% over 2 steps; when R was *N*-Boc piperazine, Boc was removed under condition: CF_3COOH , DCM, rt, 2 h, 43.9% over 2 steps.

corresponding ethyl 2-fluorobenzoates **18a–b** with morpholine or piperidine and following hydrolysis of the ethyl ester. Benzoic acids **22a–b** and **24a–f** were prepared by refluxing their corresponding 2-fluorobenzoic acids with morpholine or piperidine in dioxane (Scheme 3). 5-(Dimethylamino)-2-morpholinobenzoic acid **27** was prepared by reductive amination of 5-amino-2-morpholinobenzoic acid **26** with paraformaldehyde followed by the hydrolysis of ethyl ester (Scheme 3). Benzoic acids **32a–c** in which R were methoxy or benzyloxy groups were prepared by a different method as shown in Scheme 4. Benzoic acid pinacol esters **30a–b** were prepared by Miyaura borylations of their corresponding bromobenzenes **29a–b**, followed by oxidation using hydrogen peroxide gave **31a–b**, and the intermediates **31a–b** underwent etherification and saponification to produce benzoic acids **32a–c**. Larger R groups were also introduced to the C-5 position of ring A. As shown in Scheme 5, benzoic acids **33a–c** and **33d–g** were prepared by reductive aminations and amidations of intermediate **26**, respectively, and **33h–j** were prepared by Suzuki coupling reactions of intermediate **30a**. All prepared benzoic acids reacted with TBS-protected benzylamine **15** followed by deprotection of TBS to afford their corresponding target compounds **20a–p** and **34a–j**.

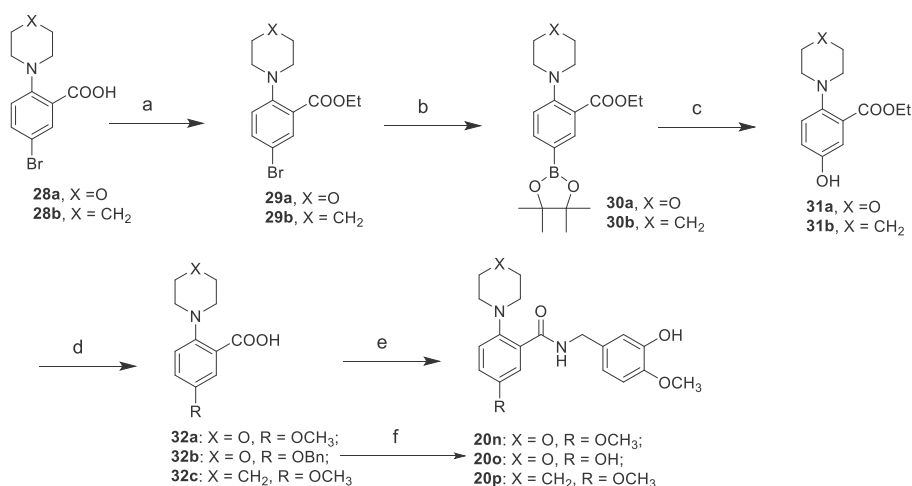
Finally, considering the excellent antiproliferative activity and satisfactory druggability of compound **20b**, its disodium phosphate **20b-P** was prepared as shown in Scheme 6. Dibenzyl phosphoryl chloride was prepared according to the literature method [49]. **20b-PBn** was prepared by the reaction of **20b** with newly prepared dibenzylphosphoryl chloride, which was then debenzylated and neutralized with NaOH to afford the target disodium phosphate **20b-P**.

2.2. Antiproliferative activities and SARs

We first investigated the SARs of ring B. A431 epidermoid cancer cell line was chosen to test the antiproliferative activities since it was the most sensitive cell line in Zheng's work [40]. As the indole moiety has long been considered to be a privileged structure in ring B of CBSIs [50,51], we first evaluated the activities of **13a** and **13b**, of which the indole moiety took the place of 4-methylthiophenyl moiety in IMB5046. However, they all displayed a significant decrease of activity ($IC_{50} > 1 \mu M$) (Table 1). The following modifications led to fifteen *N*-benzylbenzamide derivatives **13c–q** by replacing the ester bond of IMB5046 with amide linkage.



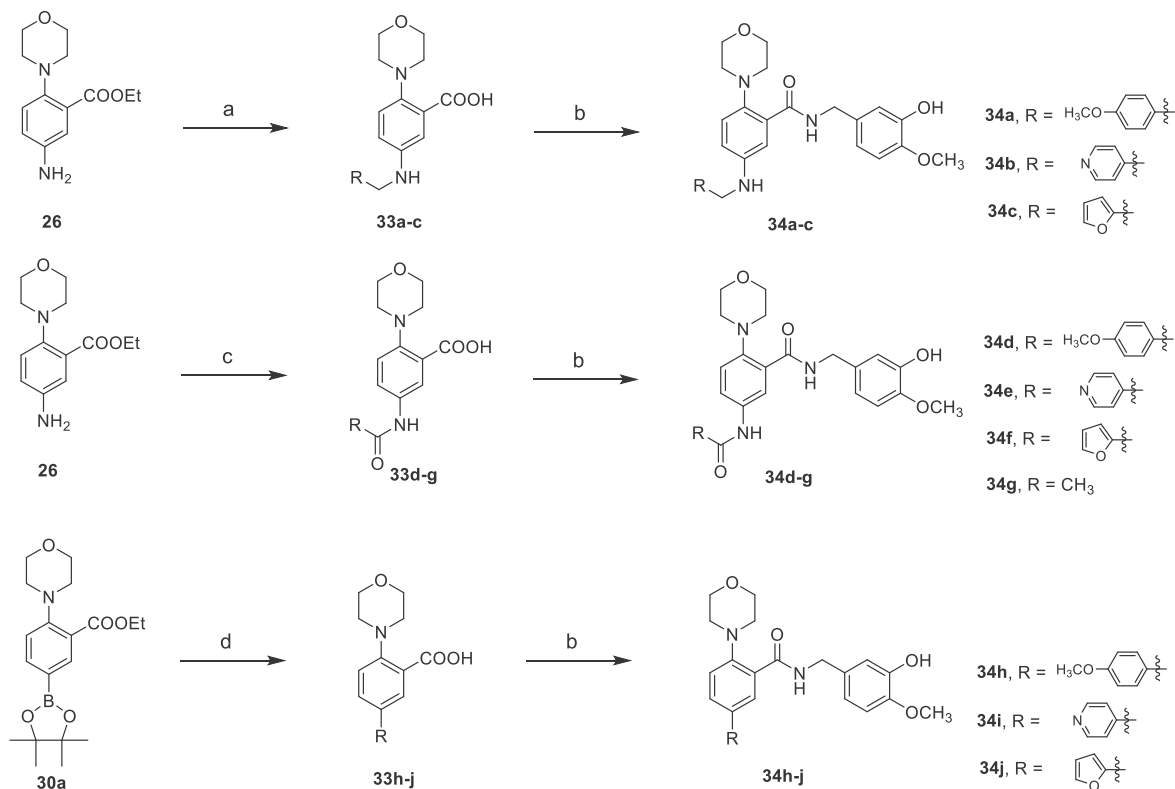
Scheme 3. Reagents and conditions: (a) Con. H₂SO₄ (Cat.), EtOH, overnight, reflux; (b) i) morpholine or piperidine, DMSO, 120 °C, 6 h; ii) 10% NaOH aqueous, CH₃OH, 80 °C, 30 min; 44.9–55.4% over 2 steps; (c) method A: i) EDCI, HOBT, DMAP (cat.), DCM, rt, 2 h; ii) TBAF, THF, rt, 15 min, 40.7–59.0% over 2 steps; method B: i) HATU, Et₃N, CH₃CN, rt, 2 h; ii) TBAF, THF, rt, 15 min, 39.5–55.7% over 2 steps; (d) i) morpholine or piperidine, dioxane, reflux, 2 h-overnight, ii) neutralized by 10% HCl aqueous, 73.8–93.6% over 2 steps; (e) Fe, EtOH, AcOH, reflux, 30 min, 76.1%; (f) i) paraformaldehyde, NaBH(CN)₃, AcOH, 30 min, rt; ii) 10% NaOH aqueous, CH₃OH, 80 °C, 30 min; 65.4% over 2 steps.



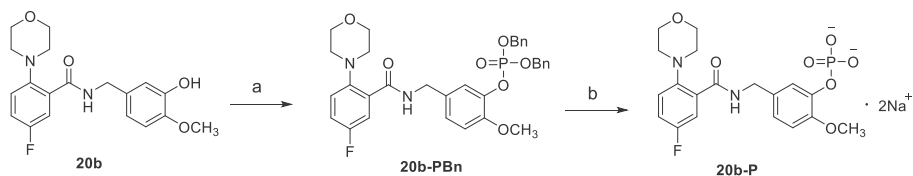
Scheme 4. Reagents and conditions: (a) Con. H₂SO₄ (Cat.), EtOH, overnight, reflux; (b) Bis(pinacolato)diboron, KOAc, PdCl₂(CH₃CN)₂, dioxane, 80 °C, 3 h, 78.5–86.1%; (c) H₂O₂, CH₃OH, rt, 30 min, 89.7–93.4%; (d) i) NaH, (CH₃)₂SO₄, 0 °C to rt, 30 min; ii) 10% NaOH aqueous, CH₃OH, 80 °C, 30 min; 54.6–63.3% over 2 steps; (e) i) HATU, Et₃N, CH₃CN, rt, 2 h; ii) TBAF, THF, rt, 15 min; 39.5–54.5% over 2 steps; (f) i) HATU, Et₃N, CH₃CN, rt, 2 h; ii) TBAF, THF, rt, 15 min; iii) Pd–C, H₂, CH₃OH, rt, 2 h, 16.8% over 3 steps.

Unfortunately, the amide linkage replacement of ester bond led to about a 22-fold decrease in activity (**13c** vs. IMB5046). Compound **13d** in which R₂ was substituted with methoxy, was more potent than compounds in which R₂ was substituted with other groups

such as ethoxy (**13e**), trifluoromethyl (**13f**), trifluoromethoxy (**13g**), dimethylamino (**13h**), chlorine (**13i**) and hydroxy (**13j**). The introduction of methyl into the linkage (**13k**) led to a roughly 2-fold drop of potency when compared with **13d**. Encouragingly, the

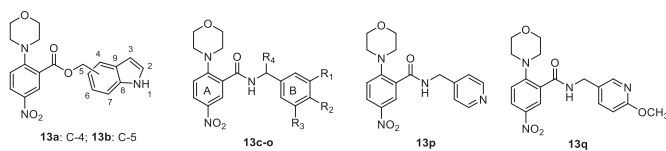


Scheme 5. Reagents and conditions: (a) i) Various benzaldehydes, CH_3OH , rt, 30 min; ii) NaBH_4 , CH_3OH , rt, 15 min; iii) 10% NaOH aqueous, CH_3OH , 80°C , 30 min; 49.8–66.9% over 3 steps; (b) i) HATU, Et_3N , CH_3CN , rt, 2 h; ii) TBAF, THF, rt, 15 min, 42.9–57.9% over 2 steps; (c) HATU, Et_3N , CH_3CN , rt, 2 h; ii) 10% NaOH aqueous, CH_3OH , 80°C , 30 min; 42.5–64.5% over 2 steps; (d) i) Various bromobenzenes, K_2CO_3 , $\text{Pd}(\text{PPh}_3)_4$, DMF, 90°C , 2 h, ii) 10% NaOH aqueous, CH_3OH , 80°C , 30 min, 44.3–57.9% over 2 steps.



Scheme 6. Reagents and conditions: (a) NaH , dibenzylphosphoryl chloride, 0°C to rt, 2 h, 63.8%; (b) i) $\text{Pd}-\text{C}$, H_2 , CH_3OH , rt, 30 min; ii) NaOH , CH_3OH , rt, 30 min, 89.6% over 2 steps.

Table 1
SARs of ring B.



Compd.	R ₁	R ₂	R ₃	R ₄	A431 IC ₅₀ values (μM) ^a	Compd.	R ₁	R ₂	R ₃	R ₄	A431 IC ₅₀ values (μM) ^a
13a	—	—	—	—	>1	13j	H	OH	H	H	>1
13b	—	—	—	—	>1	13k	H	OCH ₃	H	CH ₃	0.241 ± 0.015
13c	H	SCH ₃	H	H	0.221 ± 0.015	13l	F	OCH ₃	H	H	0.093 ± 0.007
13d	H	OCH ₃	H	H	0.127 ± 0.010	13m	OCH ₃	OCH ₃	H	H	>1
13e	H	OC ₂ H ₅	H	H	0.143 ± 0.012	13n	OH	OCH ₃	H	H	0.045 ± 0.005
13f	H	CF ₃	H	H	>1	13o	OCH ₃	OCH ₃	OCH ₃	H	>1
13g	H	OCF ₃	H	H	>1	13p	—	—	—	—	>1
13h	H	N(CH ₃) ₂	H	H	0.145 ± 0.015	13q	—	—	—	—	>1
13i	H	Cl	H	H	>1	IMB5046	—	—	—	—	0.010 ± 0.005

^a IC₅₀ values are indicated as the mean ± SD of three independent experiments.

introduction of fluorine (**13l**) and hydroxy (**13n**) increased the potency and **13n** was the most potent compound with an IC_{50} of 45 nM though it was 4.5-fold less potent than IMB5046 (IC_{50} = 10 nM). Interestingly, the isovanillic ring, which can be found in numerous known CBSIs, was the most beneficial moiety as ring B of the *N*-benzylbenzamides, indicating that the 4-methylthiophenyl moiety of IMB5046 might act as ring B of CBSIs, which is contrary to its predicted binding mode [40]. Consequently, the decision was made to maintain the isovanillic ring as ring B and focus on efforts to improve potency on other areas of *N*-benzylbenzamide derivatives.

We further made our efforts to optimize C-2 position of ring A, which indicated that substitutions at this position exert great influences on antiproliferative activity (Table 2). When a piperidine moiety was introduced (**16a**), the activity was improved by about 4-fold when compared to the morpholine counterpart **13n**. The IC_{50} of **16a** was 12 nM in A431 cells, which was comparable to that of IMB5046. However, the activity significantly decreased when the piperidine was changed to pyrrole (**16b**) or dimethylamine (**16d**), while the diethylamine compound **16c** still retained potency (IC_{50} = 51 nM). The replacement of oxygen in morpholine by nitrogen (**16e**) and sulfone (**16g**) led to loss of activity while **16f** bearing a thiomorpholine exhibited a slightly decreased activity (IC_{50} = 60 nM). Furthermore, compound **16h** bearing a secondary amino group mimicking the structure of morpholine also displayed loss of activity.

With the above SARs information in hand, we further investigated SARs of the C-4 and C-5 positions of ring A, and found that substituents at the C-5 position were well-tolerated while those at the C-4 position were not (Table 3). Unexpectedly, when R_1 was hydrogen, fluorine, bromine, trifluoromethyl and methoxy groups, the morpholine derivatives were slightly more potent than the piperidine counterparts (**20a** vs **20c**, **20b** vs **20d**, **20h** vs **20j**, **20i** vs **20l** and **20n** vs **20p**). Moreover, in the case of morpholine derivatives, halogens (**20b**, **20g** and **20h**) substituted at the C-5 position was favorable for activity, while trifluoromethyl (**20i**), dimethylamino (**20m**) and hydroxy (**20o**) containing compounds was slightly less potent. Compound **20n** bearing a methoxy group also exhibited potent activity with an IC_{50} value of 28 nM. Incorporation of nitrogen heterocycles as ring A (**20e** and **20f**) also led to a significant drop of potency. The C-4 position did not tolerate modifications as compound **20j** bearing a nitro group at C-4 position displayed much less potent activity compared to compound

13n. We further introduced moieties with more steric hindrance to the C-5 position of ring B. As shown in Table 4, compounds **34a-j** all displayed decreased activity while **34h** with a biphenyl skeleton had moderate activity with an IC_{50} value of 154 nM, indicating that there might exist an ample space where the C-5 position is located in the colchicine binding pocket.

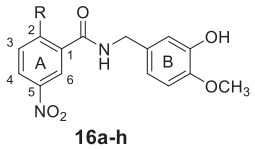
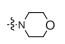
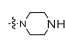
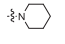
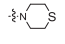
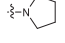
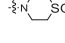
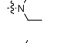
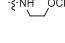
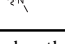
Five additional cancer cell lines and one human normal hepatocytes L-O2 cell line were chosen for further evaluation of representative compounds. As shown in Table 5, all these selected compounds displayed potent activities against these five cancer cell lines in nanomolar ranges, and the SARs were generally consistent with their performances in A431 cells. All these compounds also had less potent cytotoxicity against L-O2 cells, which indicated that these *N*-benzylbenzamide derivatives might have low toxicity. Even though **16a** was the most active compound with IC_{50} values ranging from 11 to 29 nM, the existence of an undesired nitro group in the structure of **16a** prompted us to choose another compound **20b**, which had comparable IC_{50} values (19–27 nM) to those of **16a**, for further biological evaluation. The comprehensive SARs of the newly designed *N*-benzylbenzamide derivatives were summarized as shown in Fig. 3.

Multidrug resistance (MDR) is one of the main reasons for tumor chemotherapy failure [52]. As IMB5046 was reported to overcome multidrug resistance [40], we investigated the antiproliferative efficacy of compound **20b** in the drug-resistant and parental sensitive cells by MTT assays, and the results were shown in Table 6. The drug-resistant indexes (DRIs) of **20b** were comparable to those of CA-4 and were slightly better than those of IMB5046. Except for the Adriamycin-resistant cell line Bel-7402/ADR, **20b** had DRIs of 5.3–10.8 while positive drugs paclitaxel and vincristine showed 92.5–241.0-fold resistances to the drug-resistant cells, indicating that **20b** had a moderate antiproliferative effect on drug resistant cancer cells.

2.3. Physicochemical and drug-like properties of **20b** and **20d**

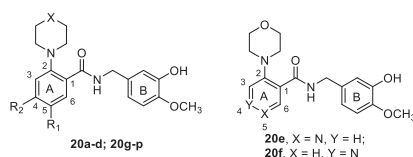
Morpholine was a ubiquitous unit in drug discovery, such as Gefitinib and Linezolid. Aqueous solubility of lipophilic scaffolds is often improved by the attachment of a morpholine unit, and morpholine was reported to have improved solubility and reduced logP when compared to piperidine [53]. Since compound **20b** with a morpholine unit and **20d** with a piperidine unit exhibited similar antiproliferative activities, their physicochemical and drug-like

Table 2
SARs of C-2 position of ring A.

 16a-h					
Compd.	R	A431 IC_{50} values (μ M) ^a	Compd.	R	A431 IC_{50} values (μ M) ^a
13n		0.045 ± 0.005	16e		>1
16a		0.012 ± 0.002	16f		0.060 ± 0.005
16b		0.372 ± 0.025	16g		>1
16c		0.051 ± 0.025	16h		>1
16d		>1	IMB5046		0.010 ± 0.005

^a IC_{50} values are indicated as the mean ± SD of three independent experiments.

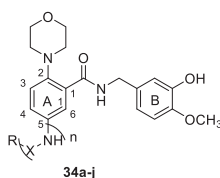
Table 3
SARs of C-4 and C-5 position of ring A.



Compd.	R ₁	R ₂	X	A431 IC ₅₀ values (μM) ^a	Compd.	R ₁	R ₂	X	A431 IC ₅₀ values (μM) ^a
13n	NO ₂	H	O	0.045 ± 0.005	20h	Br	H	O	0.030 ± 0.003
16a	NO ₂	H	CH ₂	0.012 ± 0.002	20i	CF ₃	H	O	0.037 ± 0.005
16f	NO ₂	H	S	0.060 ± 0.005	20j	H	NO ₂	O	0.224 ± 0.018
20a	H	H	O	0.020 ± 0.002	20k	Br	H	CH ₂	0.092 ± 0.010
20b	F	H	O	0.014 ± 0.003	20l	CF ₃	H	CH ₂	0.097 ± 0.010
20c	H	H	CH ₂	0.030 ± 0.004	20m	N(CH ₃) ₂	H	O	0.105 ± 0.009
20d	F	H	CH ₂	0.025 ± 0.004	20n	OCH ₃	H	O	0.028 ± 0.004
20e	—	—	—	0.977 ± 0.085	20o	OH	H	O	0.121 ± 0.008
20f	—	—	—	0.118 ± 0.020	20p	OCH ₃	H	CH ₂	0.057 ± 0.005
20g	Cl	H	O	0.025 ± 0.003	IMB5046	—	—	—	0.010 ± 0.005

^a IC₅₀ values are indicated as the mean ± SD of three independent experiments.

Table 4
Further SARs of C-5 position of ring A.



Compd.	R	X	n	A431 IC ₅₀ values (μM) ^a	Compd.	R	X	n	A431 IC ₅₀ values (μM) ^a
34a		CH ₂	1	0.306 ± 0.023	34f		C=O	1	0.478 ± 0.035
34b		CH ₂	1	1.080 ± 0.102	34g	CH ₃	C=O	1	0.220 ± 0.016
34c		CH ₂	1	0.315 ± 0.024	34h		—	0	0.154 ± 0.013
34d		C=O	1	>1	34i		—	0	0.388 ± 0.022
34e		C=O	1	0.962 ± 0.085	34j		—	0	0.215 ± 0.015

^a IC₅₀ values are indicated as the mean ± SD of three independent experiments.

Table 5
Antiproliferative activities of selected compounds against five cancer cell lines and normal human liver cells.

Compd.	IC ₅₀ values (μM) ^a					
	HepG2	K562	HCT-8	MDA-MB-231	H22	L-O2
13n	0.061 ± 0.008	0.059 ± 0.005	0.060 ± 0.008	0.057 ± 0.003	0.050 ± 0.008	0.116 ± 0.015
16a	0.012 ± 0.002	0.019 ± 0.003	0.011 ± 0.002	0.029 ± 0.004	0.025 ± 0.003	0.120 ± 0.010
16f	0.058 ± 0.004	0.049 ± 0.003	0.060 ± 0.004	0.062 ± 0.005	0.055 ± 0.004	0.113 ± 0.011
20a	0.048 ± 0.003	0.030 ± 0.005	0.062 ± 0.008	0.055 ± 0.006	0.049 ± 0.007	0.105 ± 0.012
20b	0.025 ± 0.003	0.019 ± 0.004	0.020 ± 0.005	0.027 ± 0.004	0.024 ± 0.005	0.112 ± 0.012
20c	0.031 ± 0.004	0.030 ± 0.005	0.029 ± 0.003	0.029 ± 0.003	0.029 ± 0.005	0.097 ± 0.009
20d	0.026 ± 0.002	0.011 ± 0.001	0.029 ± 0.006	0.086 ± 0.009	0.032 ± 0.006	0.088 ± 0.012
20g	0.029 ± 0.004	0.032 ± 0.003	0.025 ± 0.002	0.030 ± 0.004	0.031 ± 0.005	0.095 ± 0.010
20h	0.031 ± 0.003	0.024 ± 0.002	0.030 ± 0.003	0.029 ± 0.005	0.024 ± 0.004	0.108 ± 0.012
20i	0.062 ± 0.007	0.040 ± 0.005	0.056 ± 0.006	0.057 ± 0.006	0.055 ± 0.007	0.103 ± 0.013
20n	0.029 ± 0.004	0.061 ± 0.005	0.027 ± 0.003	0.029 ± 0.003	0.032 ± 0.004	0.052 ± 0.005
IMB5046	0.033 ± 0.004	0.010 ± 0.001	0.027 ± 0.003	0.031 ± 0.006	0.025 ± 0.005	0.044 ± 0.008
CA-4	0.010 ± 0.001	0.007 ± 0.002	0.012 ± 0.004	0.015 ± 0.003	0.015 ± 0.003	0.046 ± 0.009

^a IC₅₀ values are indicated as the mean ± SD of three independent experiments.

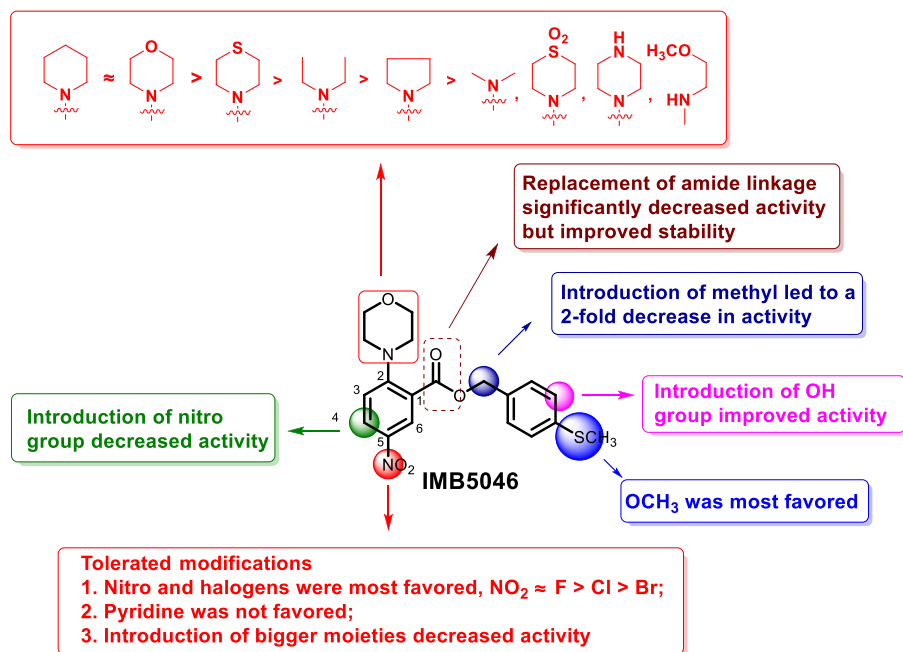


Fig. 3. The comprehensive SARs of newly designed *N*-benzylbenzamide derivatives.

Table 6

The IC₅₀ values of compound 20b in different drug-resistant cancer cells.

Compd.	IC ₅₀ values (μM) ^a								
	Bel-7402	Bel-7402/ADR	DRI	HCT-8	HCT-8/Taxol	DRI	K562	K562/VCR	DRI
20b	0.027 ± 0.003	0.104 ± 0.012	3.9	0.020 ± 0.002	0.106 ± 0.009	5.3	0.019 ± 0.003	0.205 ± 0.015	10.8
IMB-5046	0.056 ± 0.004	0.268 ± 0.022	4.8	0.027 ± 0.002	0.221 ± 0.023	8.2	0.010 ± 0.001	0.297 ± 0.031	29.7
CA-4	0.011 ± 0.002	0.058 ± 0.004	5.3	0.011 ± 0.002	0.087 ± 0.005	7.9	0.007 ± 0.001	0.057 ± 0.005	8.1
ADR	0.274 ± 0.086	1.732 ± 0.202	6.3	ND	ND	—	ND	ND	—
Taxol	ND	ND	—	0.028 ± 0.004	2.590 ± 0.122	92.5	ND	ND	—
VCR	ND	ND	—	ND	ND	—	0.021 ± 0.004	5.060 ± 0.562	241.0

^bDRI: drug-resistant index = (IC₅₀ of drug resistant cancer cell)/(IC₅₀ of parental cancer cell).

^cND: not detected.

^a IC₅₀ values are indicated as the mean ± SD of three independent experiments.

properties were further assessed with CA-4 as the reference. As shown in Table 7, the reference CA-4 showed low solubility (<1 μg/

Table 7

Physicochemical and drug-like properties of compounds 20b and 20d.

Compd.	MW ^a	clogP ^b	TPSA ^c	Drug-Score	Aqueous Solubility ^e (μg/mL)		logD _{7.4} ^f
					pH 2.0	pH 7.4	
20b	360.0	1.87	71.03	0.82	323.2	76.6	1.61
20d	358.0	3.03	61.80	0.71	1108.2	<1	2.97
CA-4	316.0	3.24	57.15	0.48	<1	1 [55]	2.68
20b-P	—	—	—	—	>1000	>1000	—

^a MW: molecular weight.

^b clogP: calculated logarithm of the octanol-water partition coefficient.

^c tPSA: topological polar surface area, predicted by Osiris calculations in <https://www.organic-chemistry.org/prog/peo/>.

^e A general solubility guideline for human oral absorption is < 10 μg/mL, low; 10–60 μg/mL, moderate; > 60 μg/mL, high.

^f Experimental logarithm of the n-octanol/water distribution coefficient at pH 7.4.

mL) both at pH 2.0 and pH 7.4. Notably, the morpholine derivative **20b** had aqueous solubility of 323.2 μg/mL at pH 2.0 and 76.6 μg/mL at pH 7.4, while the piperidine derivative **20d** showed low solubility (<1 μg/mL) at pH 7.4. Interestingly, the aqueous solubility of **20d** (1108.2 μg/mL) under acidic conditions was much greater than **20b** in the same assay, which may be due to its more basic nature and ability to form a salt at pH 2.0. Compound **20b-P**, the disodium phosphate of **20b**, was soluble in water (>1000 μg/mL at pH 2.0 and 7.4). Additionally, the lipophilicity of **20b** and **20d** were also assessed by measuring their octanol/water (aqueous buffer pH 7.4) partition coefficients through the HPLC/UV method [54]. The logD_{7.4} value of **20b** was lower than that of **20d**, which was consistent with its aqueous solubility (pH 7.4) and predicted clogP. Moreover, the predicted topological polar surface area (TPSA) values for **20b** and **20d** were in a desirable range (a criterion of <140 Å²). Their drug-score values, which is a value used to judge a compound's overall potential to qualify for a drug, were also predicted by Osiris calculations. The results showed that **20b** had a higher drug-score value than that of **20d** and CA-4, indicating that **20b** might be more druggable than **20d** and CA-4.

2.4. Tubulin polymerization by binding to the colchicine binding site

To investigate whether these *N*-benzylbenzamide derivatives are tubulin targeting agents, a representative compound **20b** was selected to undergo tubulin polymerization assay *in vitro*. In this assay, tubulin monomer was self-polymerized to microtubules, increasing light scattering at 340 nm. Microtubule-destabilizing agent (MDA) colchicine is known to inhibit self-polymerization of tubulin. On the contrary, microtubule-stabilizing agent (MSA) paclitaxel promotes self-polymerization of tubulin. As shown in Fig. 4, **20b** produced a significant inhibition of tubulin polymerization with a similar action to that of colchicine, indicating that **20b** acted as an MDA. The IC_{50} values of **20b** in inhibiting tubulin polymerization were further determined as shown in Table 8. The results showed that **20b** exhibited a comparable activity to IMB5046 with an IC_{50} value of 3.03 μ M, which was slightly less potent than that of CA-4 (IC_{50} = 2.64 μ M). In addition, **20b** was examined for its potential inhibition of the binding of [3H]-colchicine to tubulin. The binding potency of **20b** to the colchicine binding site was 82.9% at 5 μ M while those of IMB5046 and CA-4 were 85.7% and 90.3%, respectively, at the same concentration (Table 8), suggesting that **20b** bound to the colchicine binding site almost as well as IMB5046 and CA-4. Besides, the IC_{50} value of **20b**-phosphate in inhibiting tubulin polymerization was 6.18 ± 0.50 μ M.

2.5. Docking profiles of compound **20b** with tubulin

In Zheng's work, the 4-methylthiophenyl moiety of IMB5046 was predicted to act as ring A resembling the TMP of colchicine [40]. However, our SARs have showed that the isovanillic ring was the most beneficial moiety when replacing the 4-methylthiophenyl of IMB5046, indicating that the 4-methylthiophenyl moiety might act as ring B of CBSIs. In addition, C-5 position on ring A of *N*-benzylbenzamide tolerated modifications with even more sterically demanding moieties introduced, indicating that there might exist an ample space where the C-5 position fits in the colchicine binding pocket. As reported before [56], a hydrophobic pocket, named as zone 3, was buried deeper in the β -subunit of tubulin, which could be occupied by some CBSIs [44,57,58]. Thus, we speculated that 4-methylthiophenyl of IMB5046 resembles the binding mode of isovanillic ring of ring B while the 2-morpholine-5-nitrophenyl moiety located in the position of TMP acting as ring A of known CBSIs. To further support this hypothesis, docking studies of compound **20b** and IMB5046 with tubulin were performed using the Glide module in the Schrodinger software. The original ligand CA-4 in the crystal structure (PDB:5lyj) [59] was first redocked into

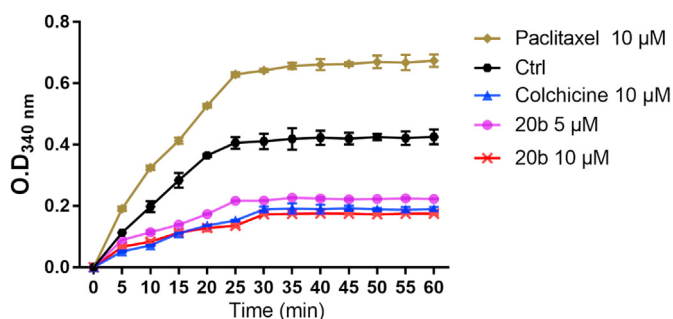


Fig. 4. Effects of **20b** on tubulin polymerization *in vitro*. After incubation of purified tubulin protein with tested compounds, polymerizations were followed by an increase in absorbance at 340 nm over a 60 min period at 37 °C. The experiments were performed three times.

Table 8

Inhibition of tubulin polymerization^a and colchicine binding to tubulin^b.

Compd.	Inhibition of tubulin polymerizaion IC_{50} (μ M)	Inhibition of colchicine binding (%) inhibition \pm SD	
		1 μ M	5 μ M
20b	3.03 ± 0.31	56.9 ± 4.4	82.9 ± 4.7
IMB5046	2.99 ± 0.23	58.0 ± 0.6	85.7 ± 2.2
CA-4	2.64 ± 0.22	80.2 ± 1.5	90.3 ± 3.4
20b-P	6.18 ± 0.50	ND ^c	ND ^c

^a All Data are presented as the mean \pm SD from three independent experiments.

^b Tubulin, 1 μ M; [3H]-colchicine, 5 μ M; and inhibitors, 1 or 5 μ M.

^c ND = not determined.

the colchicine site, which was quite close to that in the crystal structure (RMSD value = 0.72 Å), indicating the feasibility of our docking method. As shown in Fig. 5A and C, the phenolic hydroxyl of **20b** and CA-4 formed hydrogen bonds with the residue Thr179. The binding mode of 5-fluorine-2-morpholine phenyl moiety was slightly different from that of TMP. Morpholine located at the position of a methoxy group of TMP interacted with residues Ala 316, Ala 317 and Ala 354, and the fluorine pointed towards the deeper pocket which was surrounded by residues Tyr 202, Leu 242, Ala 250, and Leu 255. The binding mode of IMB5046 with tubulin was similar to that of **20b** (Fig. 5B and D), which was in accordance with their SARs.

2.6. Anti-microtubule effects in A431 cancer cells

Immunofluorescent staining assay was further performed in A431 cells to evaluate the inhibitory effects of **20b** on microtubule organization at the cytological level. As shown in Fig. 6, the microtubule in vehicle-treated A431 cells formed an intact network with fine filaments. However, cells treated with **20b** at various concentrations (7.5 nM, 15 nM, and 30 nM) for 24 h resulted in significant disruption of microtubule networks, loss of cellular structure, and formation of cell membrane rounding. These results indicated that **20b** significantly caused microtubule network disruption at the cytological level.

2.7. Cell cycle analysis

Most microtubule polymerization inhibitors interrupt the tubulin-microtubule balance thus causing mitotic arrest at the G2/M phase, and ultimately leading to apoptosis [60]. Therefore, the effects of **20b** on cell cycle progression of A431 cells were evaluated by flow cytometry. As illustrated in Fig. 7A and C, treatment of **20b** at concentrations of 7.5, 15, and 30 nM caused a rise of cells in G2/M population from 7.27% (control) to 13.84%, 16.25%, and 24.95%, respectively, indicating that **20b** arrested A431 cell cycle at the G2/M phase. Effects of **20b** on the expression of cell cycle regulatory proteins were further tested and the results were shown in Fig. 7B and D. It was found that **20b** decreased cdc2, cyclin B1 and p-histone H3 protein levels in a concentration-dependent manner, suggesting that the **20b**-induced G2/M arrest may be correlated with the regulation of cdc2, cyclin B1 and p-Histone H3 protein.

2.8. Cell apoptosis assay

Mitotic arrest of tumor cells by tubulin-targeted agents is generally associated with cellular apoptosis. Thus, the effects of **20b** on A431 cell apoptosis were examined by fluorescent microscopy in Hoechst 33342 assays. As shown in Fig. 8A and C, A431 cells treated with **20b** (7.5 nM, 15 nM, and 30 nM) for 48 h displayed significant

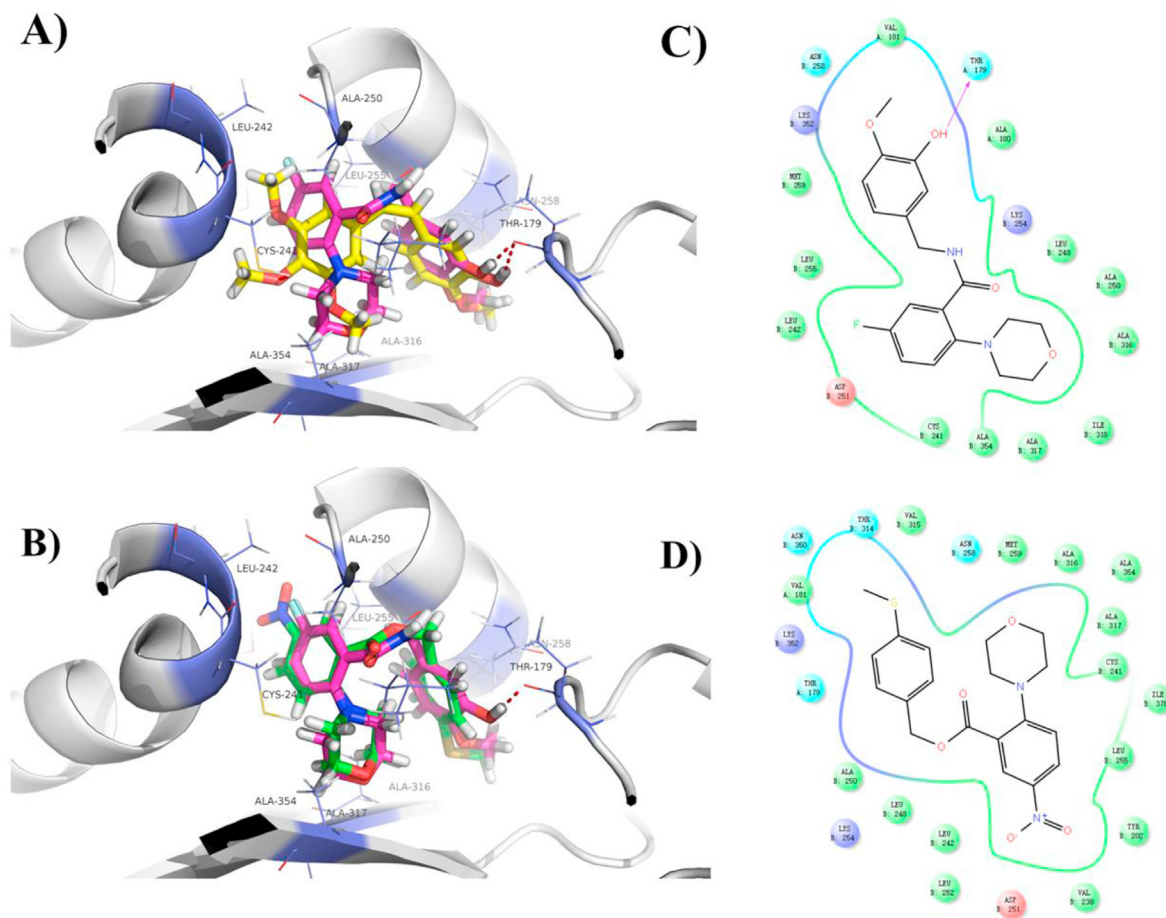


Fig. 5. Proposed binding models for **20b** and IMB5046 with tubulin (PDB code: 5lyj). (A) CA-4 (shown in yellow) and **20b** (magenta); (B) **20b** (shown in magenta) and IMB5046 (green); (C) The 2D interactions between **20b** and tubulin; (D) The 2D interactions between IMB5046 and tubulin.

changes in cell morphology, such as nucleus fragmentation and chromatin condensation. The results of flow cytometry analysis in Annexin-V/PI assays also indicated that **20b** induced A431 cell apoptosis in a dose-dependent manner (Fig. 8B and D). A431 cells treated with **20b** at concentrations of 7.5, 15, and 30 nM showed an accumulation of apoptotic cells (Annexin-V+/PI− and Annexin-V+/PI+) from 2.84% (control) to 20.73%, 44.78%, and 66.14%, respectively.

As compound **20b** could effectively induced A431 cell apoptosis, we further evaluated its effects on the expression of apoptosis-related proteins by Western blot analysis. The Bcl-2 family has been considered as important proteins that control the mitochondrial pathway of apoptosis [61]. As shown in Fig. 9A and B, **20b** upregulated the expression of the pro-apoptotic protein Bax and downregulated the expression of the anti-apoptotic protein Bcl-2 in a dose-dependent manner. The caspase families are considered to be markers for cells undergoing apoptosis and can facilitate cellular disassembly. Caspase-3 is one of the most important “executioner” caspases, which cleaves many important cellular substrates [62]. As shown in Fig. 9A and C, **20b** produced a concentration-dependent activation of caspase-3. Furthermore, a significant increase of caspase-9 was also observed, which interacted with caspase-3 and activated apoptosis. The downstream substrate poly (ADP-ribose) polymerase (PARP) of caspase-3 was also observed to be cleaved after incubations with **20b**. Moreover, p53, which can act in the cytosol and mitochondria to promote apoptosis through transcription-independent mechanisms [63], was activated after

treatments of **20b**. Taken together, **20b**-induced cell apoptosis may be correlated with upregulation of pro-apoptotic proteins, down-regulation of anti-apoptotic proteins, caspase activation, cleaved PARP and p53 activation.

2.9. In vitro evaluation of mitochondrial membrane potential and reactive oxygen species (ROS) generation

Mitochondrial membrane potential (MMP) reduction is considered an early event of apoptosis. The lipophilic cationic JC-1 staining method was used to determine the effect of compound **20b** on MMP of A431 cells. As presented in Fig. 10A and C, with the concentration of **20b** increasing from 0 to 30 nM, the red fluorescence intensity decreased from 93.83% to 33.88%, and the green fluorescence intensity increased from 5.98% to 65.96%, indicating that **20b** decreased the MMP of A431 cells during the apoptosis process.

Mitochondria is an important source of ROS in cells [64]. To further explore the mechanism of **20b** for inhibiting tumor cells, the fluorescent probe 2',7'-dichlorofluorescein diacetate (DCF-DA) was used to evaluate the intracellular ROS levels after incubation with **20b**. As shown in Fig. 10B and D, **20b** induced intracellular ROS generation in a dose-dependent manner. The ratio of DCF positive cells was increased from 6.17% in cells incubated with DMSO to 21.99% in cells incubated with 30 nM of **20b**. Collectively, **20b** was able to increase ROS levels of A431 cells and eventually triggered apoptotic cell death.

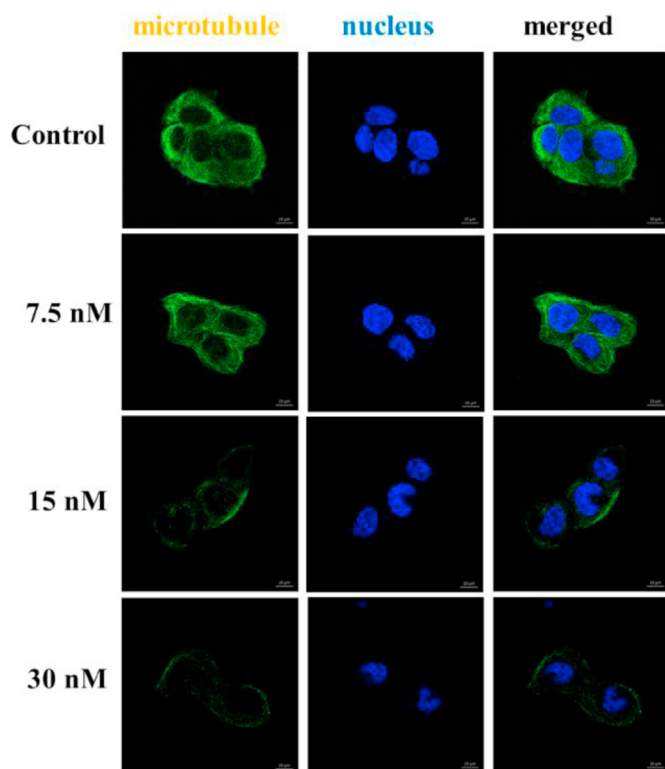


Fig. 6. Effects of **20b** on the cellular microtubule network visualized by immunofluorescence.

2.10. Plasma stability of compound **20b**

To assess whether compound **20b**, of which amide linkage was introduced, had improved stability, the *in vitro* assay using rat plasma was performed. As shown in Fig. 11, the positive control Enalapril quickly degraded within 1 h after incubation with rat plasma at 37 °C, while **20b** and IMB5046 were relatively stable in the same assay. Consistently, **20b** had an improved plasma stability profile compared to IMB5046. After a 3-h incubation, there remained 91.5% of **20b** and only 72.6% of IMB5046. The unexpected stability of IMB5046, which bears an ester bond, is most likely attributable to the steric hindrance adjacent to the ester bond, which might hinder the esterase-catalyzed hydrolysis reaction. Nevertheless, the remarkable plasma stability of **20b** prompted us to further investigate its safety profile and *in vivo* antitumor efficacy.

2.11. The safety profile of **20b** in mice

To understand the safety of **20b**, the acute toxicity of its disodium phosphate prodrug **20b-P** was assessed in ICR mice. **20b-P** dissolved into saline was intravenously injected at doses of 327.7, 409.6, 512.0, 640, and 800 mg/kg ($n = 10$ per group) and mice were observed during two weeks. As shown in Table 10, treatment with **20b-P** at a dose of 327.7 mg/kg only caused one death in ten mice, while treatment with **20b-P** at 800 mg/kg killed eight mice. Finally, the median lethal dose (LD_{50}) value of **20b-P** was calculated to be 599.7 mg/kg, implying the low toxicity of **20b-P**.

2.12. *In vivo* anti-tumor activity of compound **20b** and **20b-P**

In order to verify the potential antitumor effect of **20b** and **20b-P** *in vivo*, a liver cancer allograft mouse model was established by

subcutaneous injection of H22 cells into the right flank of mice. Paclitaxel (PTX), IMB5046, CA-4 and its disodium phosphate prodrug CA-4P were used as the positive controls. As shown in Fig. 12A and B, **20b** and **20b-P** had a significant inhibitory effect on tumor growth. PTX caused a reduction of tumor weight by 72.7% at a dose of 6 mg/kg every other day (*i.v.*) after three weeks as compared to vehicle, while **20b** and **20b-P** reduced tumor weights by 66.0% and 71.4% at a dose of 20 mg/kg per day (*i.v.*), respectively (Fig. 12D). Particularly, **20b-P** (20 mg/kg) displayed more potent antitumor activity than CA-4P (62.7%) at the same dose. **20b** exhibited a comparable inhibitory rate to IMB5046 at the dose of 20 mg/kg while that of the disodium phosphate prodrug **20b-P** was much higher. Additionally, PTX caused a significant loss of body weight (Fig. 12C) while **20b** and **20b-P** did not obviously affect body weight even at doses up to 20 mg/kg, indicating the low toxicities of **20b** and **20b-P** toward mice. Further H&E staining of some important organs including heart, liver, spleen, lung and kidney collected from the **20b-P**-treated group (20 mg/kg) also implied low toxicity of **20b-P** (Fig. 13). Taking these results together, **20b** and **20b-P** were efficacious and safe in inhibiting the growth of cancer *in vivo*, and should be further investigated as potential anticancer agents.

2.13. *In vitro* and *in vivo* evaluation of anti-vascular activity

Some microtubule binding drugs possess vascular disrupting activity due to their disruption ability to microtubule dynamics of endothelial cells [65]. Thus, wound healing assays was performed to evaluate the anti-vascular activity of **20b** by using human umbilical vein endothelial cells (HUVECs). Standardized scratches (wounds) were made in confluent monolayers of HUVECs and then incubated with increasing concentrations (7.5, 15 and 30 nM) of **20b**. As shown in Fig. 14A, **20b**-treatment resulted in significant inhibition of migration capacity of HUVECs especially at the dose of 30 nM, which indicated that **20b** had significant anti-vascular activity.

The formation of HUVEC tube is the key step in angiogenesis. Thus, we further evaluated the anti-vascular activity of **20b** by performing a tube formation assay. As shown in Fig. 14B, HUVECs in the control group form capillary-like tubules with multicentric junctions, while treatment with **20b** at the concentration of 30 nM completely inhibited HUVEC cord formation. The IC_{50} value of **20b** against HUVECs after 6-h treatment was $0.12 \pm 0.03 \mu M$, indicating that the *in vitro* potent anti-vascular activity of **20b** was not caused by its cytotoxicity.

CD31 is commonly used as an endothelial cell marker to high-light tumor blood vessels reflecting the degree of angiogenesis [66]. To assess whether **20b** could exert anti-vascular effects *in vivo*, immunohistochemical staining against CD31 was performed to quantify the microvessel density (MVD) of tumors treated with vehicle and **20b** (20 mg/kg). The **20b**-treated group exhibited significantly lower tumor microvessel density (MVD) as compared with the control group (Fig. 14C), suggesting that **20b** exhibited potent anti-vascular activity *in vivo*.

3. Conclusions

With the aim of discovering novel drug candidate with better druggable profiles as well as illustrating their binding modes with tubulin, we have performed a comprehensive SARs study of *N*-benzylbenzamide derivatives based on the structure of the lead compound IMB5046. These compounds have a new type of A ring segment with better drug-like properties, replacing the traditional 3,4,5-trimethoxyphenyl group. Due to the simplicity in the structure, the target compounds can be obtained through a convenient and efficient synthetic route from cheap and easily available

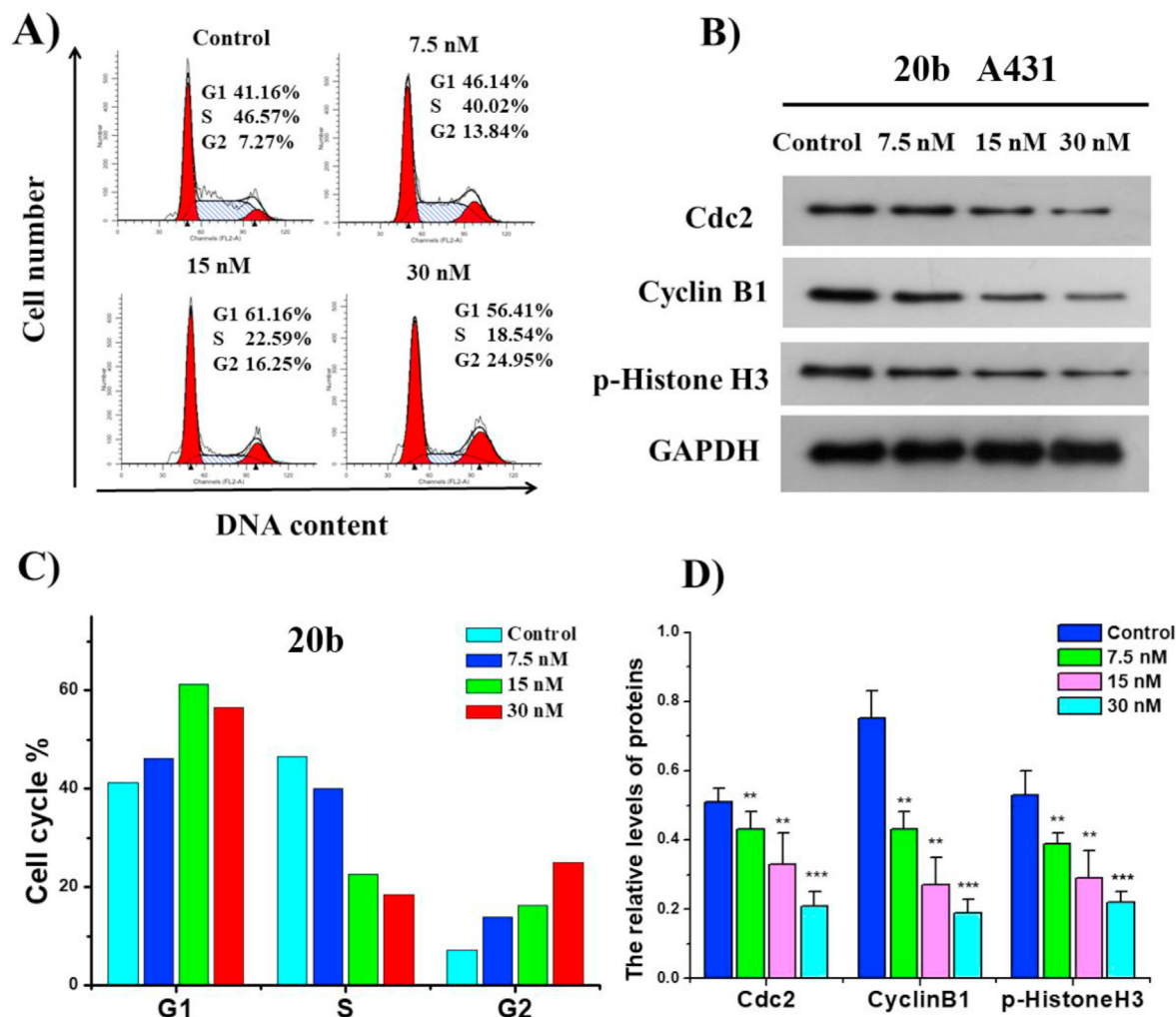


Fig. 7. Compound **20b** induced G2/M arrest in A431 cancer cells. (A) The percentages of cells at different phases of the cell cycle after treatment with various concentrations of **20b**. (B) Western blotting analysis on the effect of **20b** on the G2/M regulatory proteins. (C) Histograms display the percentage of cell cycle distribution. (D) Histograms display the density ratios of cdc2, cdc25c and p-histone-H3 to GAPDH. ** $p < 0.01$, *** $p < 0.001$ vs. control group.

starting materials. As a result, the representative compound **20b** was eventually found to exhibit potent antiproliferative activity comparable to IMB5046 with the IC_{50} values ranging from 12 to 27 nM against six cancer cell lines. Compound **20b** displayed a moderate selectivity for human normal hepatocytes LO2 cells, and its antiproliferative efficacies against three drug-resistant cancer cells were also evaluated with the DRIs comparable to those of CA-4 and slightly better than those of IMB5046. Compound **20b**, which has a morpholine unit, and compound **20d**, which has a piperidine unit, were further assessed for their physicochemical and drug-like properties. Our experiments showed that **20b** had satisfactory physicochemical parameters and its drug-score value was predicted to be higher than that of **20d** or CA-4.

In addition, compound **20b** significantly inhibited tubulin polymerization and disrupted microtubule networks of A431 cells, and it was further confirmed that **20b** binds to the colchicine binding pocket by colchicine competition inhibition assay and molecular docking studies through colchicine competition inhibition assay and molecular docking studies. Notably, our SARs and docking studies suggested that the binding mode of **20b** resembles that of classical CBSI CA-4 with the 5-fluorine-2-morpholinephenyl moiety proposed to be a novel ring A of CBSIs. Moreover, **20b**

induced A431 cell cycle arrest at the G2/M phase by regulation of G2/M-related protein expression of cdc2, cyclin B1 and p-Histone H3 protein. **20b** also induced A431 cell apoptosis, which might be the resulting effects of upregulation of pro-apoptotic protein, downregulation of anti-apoptotic protein, caspase activation, cleaved PARP and p53 activation. Additionally, **20b** depolarized the mitochondria membrane potentials and induced ROS generation in A431 cells.

Furthermore, **20b** possessed good plasma stability (remaining = 91.5% after 3-h incubation) and safety profiles (LD_{50} value of acute toxicity = 599.7 mg/kg). The antitumor effects of **20b** and its disodium phosphate **20b-P** were validated in liver cancer xenograft mouse model without obvious toxicity. Compounds **20b** and **20b-P** reduced tumor weights by 66.0% and 71.4% at a dose of 20 mg/kg per day (i.v.), respectively, which were more potent than the reference CA-4. Finally, the anti-vascular activity of **20b** was confirmed in *in vitro* HUVEC wound healing and tube formation assays as well as *in vivo* microvessel formation in xenograft tumor tissues. Therefore, **20b** and **20b-P** deserved further investigations as novel, safe and efficacious anti-tubulin drug candidates for the treatment of cancers.

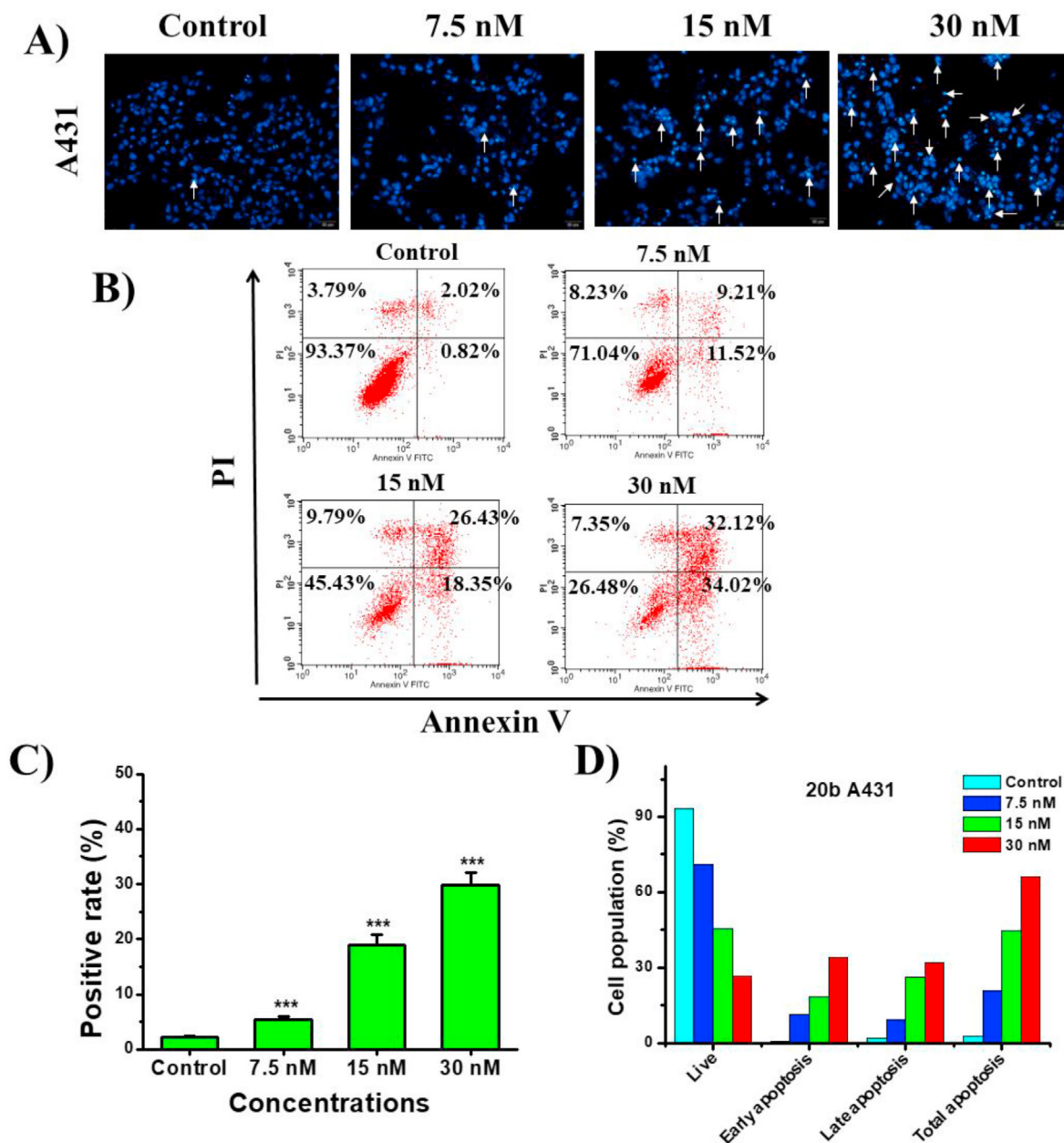


Fig. 8. Compound **20b** induced apoptosis in A431 cancer cells. (A) Cell morphological alterations and nuclear changes (white arrows) associated with A431 cells after incubation with **20b**; (B) A431 cells stained with Annexin V/PI, followed by flow cytometric analysis; (C) Histograms display the percentage of positive cells; (D) Histograms display the percentage of cell distribution. *** $p < 0.001$ vs. control group.

4. Experimental

4.1. Chemistry

4.1.1. General

All commercially available reagents were used without further purification. Solvents were dried through routine protocols. Flash column chromatography was carried out on 200–300 mesh silica gel (Qingdao Haiyang Chemical, China). Reactions were monitored by thin-layer chromatography (TLC) on 0.25 mm silicagel plates (GF254) and visualized under UV light. ^1H NMR and ^{13}C NMR spectra were recorded with a Bruker AV-300 spectrometer (Bruker Company, Germany) in the indicated solvents (CDCl_3 or $\text{DMSO}-d_6$, TMS as internal standard); the values of the chemical shifts are expressed in δ values (ppm) and the coupling constants (J) in Hz.

Low- and high-resolution mass spectra (LRMS and HRMS) were measured on Finnigan MAT 95 spectrometer (Finnigan, Germany). Purity of all tested compounds was $\geq 95\%$, as estimated by HPLC (SHIMADZU Labsolutions, UV detection at $\lambda = 254$ nm) analysis on the Agilent C18 column (4.6×150 mm, $5 \mu\text{m}$) eluting at 1 mL/min of methanol and water (80:20), representative HPLC trace see [Supporting Information](#).

4.1.2. 2-Morpholino-5-nitrobenzoic acid (**12**)

To a solution of 2-fluorobenzoic acid (**10**) (5.0 g, 35.7 mmol) in 10 mL concentrated H_2SO_4 , 10 mL concentrated HNO_3 was added dropwise at 0°C . After stirring for 2 h at room temperature, the mixture was slowly poured into ice water. The resulting precipitate were collected by filtration, which were washed by water, and dried to give 4.7 g 2-fluoro-5-nitrobenzoic acid (**11**) as yellow solid, yield

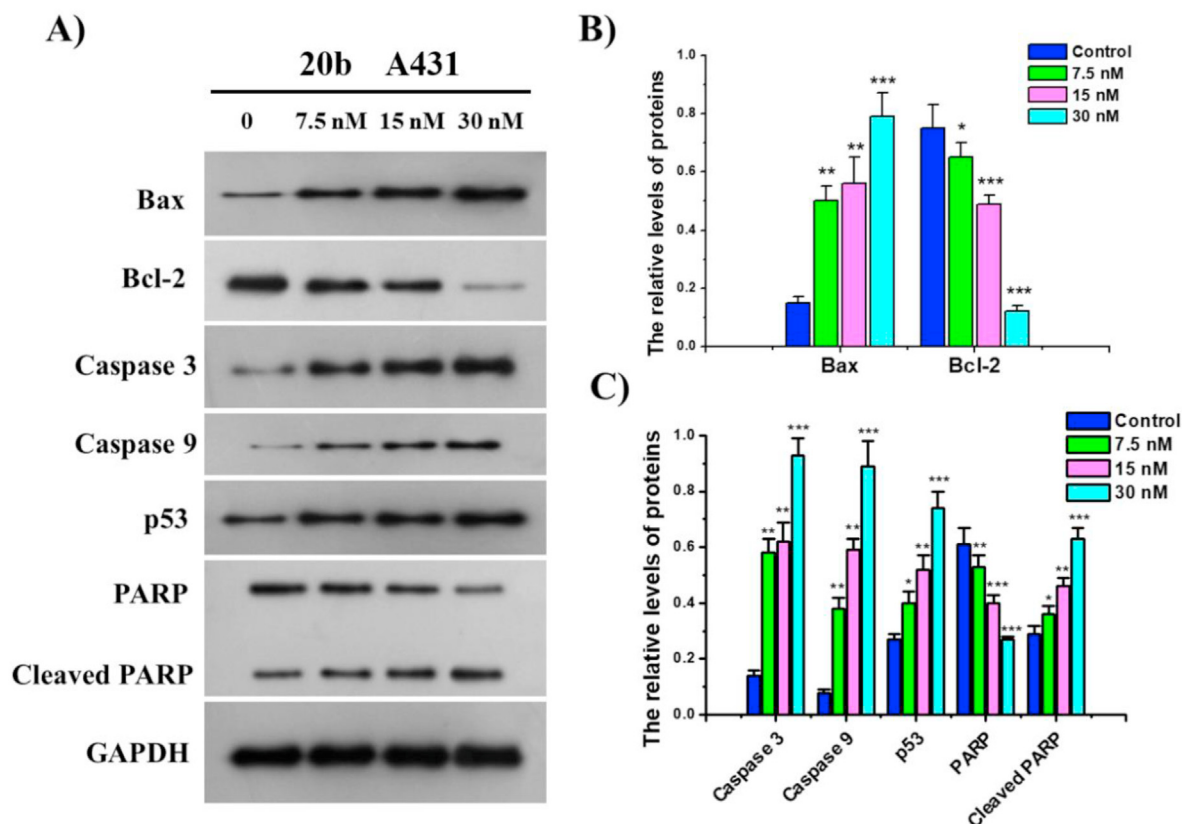


Fig. 9. (A) Western blot analysis of apoptosis-related proteins. (B) Histograms display the density ratios of Bax and Bcl-2 to GAPDH. (C) Histograms display the density ratios of caspase 3, caspase 9, p53 and PARP to GAPDH. * $p < 0.05$, ** $p < 0.01$, *** $p < 0.001$ vs. control group.

71.2%; To the solution of **11** (500 mg, 2.7 mmol) in 10 mL dioxane, morpholine (1.2 mL, 13.5 mmol) was added in one portion. After stirring for 2 h at room temperature, the solvent and remaining morpholine were removed in vacuo. Then, the residues were dissolved into water and neutralized by 10% HCl aqueous. The resulting precipitate were collected, washed by water, and dried to give 520 mg 2-morpholino-5-nitrobenzoic acid (**12**) as yellow solid, yield 76.4%. ^1H NMR (300 MHz, DMSO- d_6) δ 8.40 (d, $J = 2.9$ Hz, 1H), 8.20 (dd, $J = 9.2, 2.9$ Hz, 1H), 7.19 (d, $J = 9.2$ Hz, 1H), 3.72 (d, $J = 4.8$ Hz, 4H), 3.28 (d, $J = 4.7$ Hz, 4H); ^{13}C NMR (75 MHz, DMSO- d_6) δ 167.39, 155.09, 138.17, 127.42, 127.28, 120.86, 117.75, 65.70, 50.95; ESI-MS m/z 252.1 [M - H] $^-$ 251.1.

4.1.3. General procedures for the preparation of **13a** and **13b**

To a solution of **12** (80 mg, 0.32 mmol) in 10 mL anhydrous DCM, indolylcarbinol (56 mg, 0.38 mmol), EDCI (296 mg, 1.6 mmol) and catalytic amount of DMAP were added. The mixtures were stirred for 2 h, and extracted with DCM (3 \times 25 mL). The combined organic layers were then washed with brine, dried over anhydrous Na_2SO_4 , and concentrated in vacuo to provide the crude products, which were purified by column chromatography with petroleum/ethyl acetate (4:1) to give target compounds **13a** and **13b**.

(1H-indol-4-yl)methyl 2-morpholino-5-nitrobenzoate (13a). Yellow solid, 60.3%. ^1H NMR (300 MHz, CDCl_3) δ 8.62 (d, $J = 2.8$ Hz, 1H), 8.36 (s, 1H), 8.20 (dd, $J = 9.1, 2.8$ Hz, 1H), 7.43 (d, $J = 7.6$ Hz, 1H), 7.30–7.18 (m, 3H), 6.92 (d, $J = 9.2$ Hz, 1H), 6.73 (d, $J = 2.9$ Hz, 1H), 5.70 (s, 2H), 3.61 (t, $J = 4.6$ Hz, 4H), 3.09 (t, $J = 4.7$ Hz, 4H); ^{13}C NMR (75 MHz, CDCl_3) δ 166.32, 155.94, 139.75, 136.06, 128.47, 127.88, 127.12, 126.89, 124.94, 121.96, 121.33, 120.97, 117.23, 112.02, 100.92, 72.80, 66.28, 51.66; HR-MS (ESI) m/z : calcd for $\text{C}_{20}\text{H}_{20}\text{N}_3\text{O}_5$ [M+Na] $^+$ 404.1217 found 404.1211.

(1H-indol-5-yl)methyl 2-morpholino-5-nitrobenzoate (13b). Yellow solid, 67.8%. ^1H NMR (300 MHz, CDCl_3) δ 8.59 (d, $J = 2.8$ Hz, 1H), 8.40–8.28 (m, 1H), 8.19 (dd, $J = 9.2, 2.8$ Hz, 1H), 7.77 (d, $J = 1.5$ Hz, 1H), 7.41 (d, $J = 8.3$ Hz, 1H), 7.30 (dd, $J = 8.4, 1.6$ Hz, 1H), 7.24 (t, $J = 2.8$ Hz, 1H), 6.91 (d, $J = 9.2$ Hz, 1H), 6.57 (ddd, $J = 3.1, 2.1, 1.0$ Hz, 1H), 5.47 (s, 2H), 3.69–3.63 (m, 4H), 3.13–3.07 (m, 4H); ^{13}C NMR (75 MHz, CDCl_3) δ 166.28, 155.78, 139.64, 135.79, 128.22, 127.89, 127.74, 126.59, 125.13, 123.38, 122.10, 121.41, 117.10, 111.28, 102.85, 68.60, 66.26, 51.57. HR-MS (ESI) m/z : calcd for $\text{C}_{20}\text{H}_{20}\text{N}_3\text{O}_5$ [M+H] $^+$ 404.1217 found 404.1212.

4.1.4. General procedures for the preparation of **13c-q**

To a solution of **12** (80 mg, 0.32 mmol) in 10 mL anhydrous DCM, various benzylamines (0.38 mmol), EDCI (296 mg, 1.6 mmol), HOBT (52 mg, 0.38 mmol) and catalytic amount of DMAP were added. The mixtures were stirred for 2 h, and extracted with DCM (3 \times 25 mL). The combined organic layers were then washed with brine, dried over anhydrous Na_2SO_4 , and concentrated in vacuo to provide the crude products, which were purified by column chromatography with petroleum/ethyl acetate (4:1) to give target compounds. For benzylamines that containing TBS-protected phenolic hydroxyl, the products obtained in above procedure were dissolved into 10 mL THF, and TBAF (1.2 e.q) was added. The mixtures were stirred for 15 min, and extracted with DCM (3 \times 25 mL). The combined organic layers were then washed with brine, dried over anhydrous Na_2SO_4 , and concentrated in vacuo to provide the crude products, which were purified by column chromatography with petroleum/ethyl acetate (2:1) to give target compounds **13j** and **13n**.

N-(4-methylthiobenzyl)-2-morpholino-5-nitrobenzamide (13c). Yellow solid (78 mg, yield 63.5%). ^1H NMR (300 MHz, CDCl_3) δ 8.78 (dd, $J = 2.9, 1.0$ Hz, 1H), 8.60 (t, $J = 5.7$ Hz, 1H), 8.22 (dd,

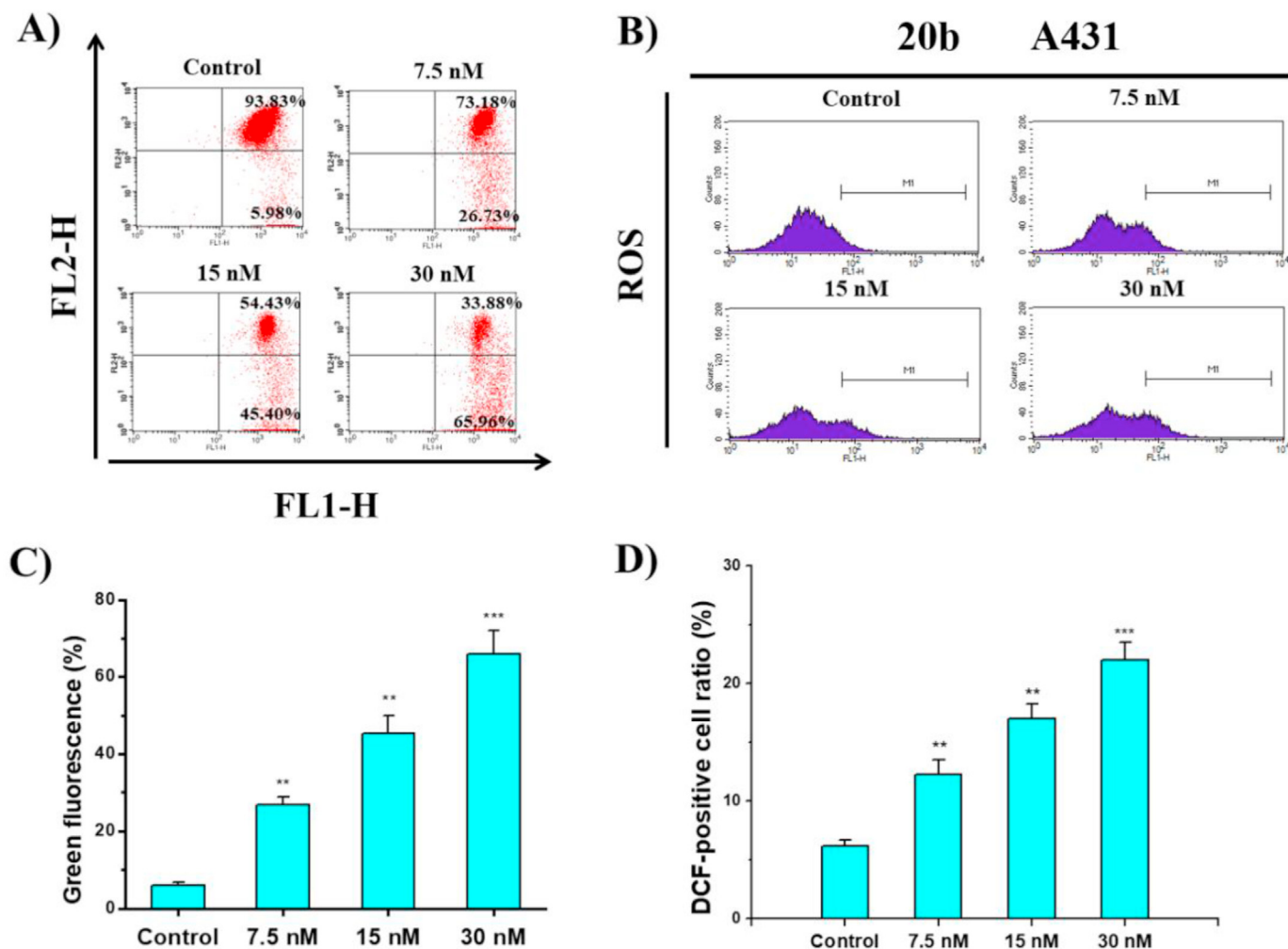


Fig. 10. A) Effects of **20b** on the MMP of A431 cells; (B) The generation of ROS was measured using DCF-DA in combination with FACScan flow cytometry; (C) Histograms display the FACScan flow cytometry; (D) Histograms display the intracellular ROS contents in the absence or presence of **20b**. ** $p < 0.01$, *** $p < 0.001$ vs. control group.

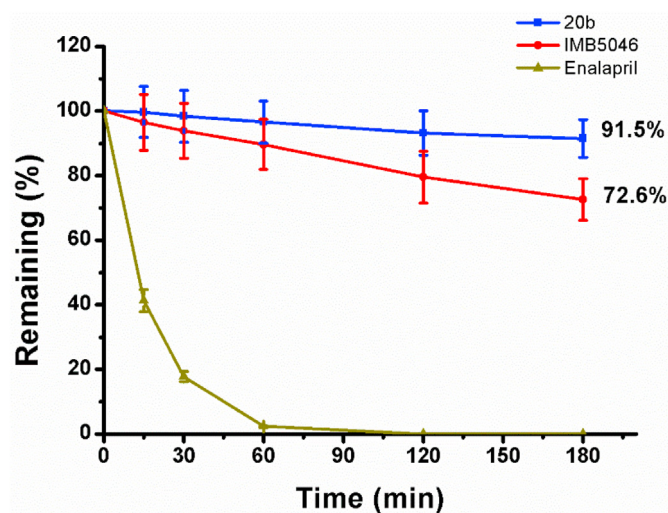


Fig. 11. Stability of **20b** and IMB5046 in rat plasma.

$J = 8.9, 2.0$ Hz, 1H), 7.31 (d, $J = 8.2$ Hz, 2H), 7.24 (d, $J = 8.1$ Hz, 2H), 7.15 (d, $J = 8.9$ Hz, 1H), 4.60 (d, $J = 5.8$ Hz, 2H), 3.58 (t, $J = 4.6$ Hz, 4H), 3.02 (t, $J = 4.6$ Hz, 4H), 2.48 (s, 3H); ^{13}C NMR (75 MHz, CDCl_3)

Table 10

Acute toxicity of **20b-P** in mice.

dose (mg/kg)	num. of mice	total mortality	survival (%)	LD ₅₀ (mg/kg) ^a
327.7	10	1	90	599.7
409.6	10	2	80	
512.0	10	3	70	
640.0	10	5	50	
800.0	10	8	20	

^a The 95% confidence limits: 530.8–677.5 mg/kg.

δ 165.01, 155.49, 143.31, 138.60, 134.53, 128.93, 128.18, 127.35, 127.02, 127.00, 119.43, 66.47, 52.80, 43.64, 15.91; HR-MS (ESI) m/z : calcd for $\text{C}_{19}\text{H}_{22}\text{N}_3\text{O}_4\text{S} [\text{M}+\text{H}]^+$ 388.1326, found 388.1320.

N-(4-methoxybenzyl)-2-morpholino-5-nitrobenzamide (13d). Yellow solid (103 mg, yield 88.0%). ^1H NMR (300 MHz, CDCl_3) δ 8.84 (d, $J = 2.7$ Hz, 1H), 8.50 (s, 1H), 8.24 (dd, $J = 9.0, 2.7$ Hz, 1H), 7.31 (d, $J = 8.3$ Hz, 2H), 7.16 (d, $J = 8.9$ Hz, 1H), 6.90 (d, $J = 8.2$ Hz, 2H), 4.58 (d, $J = 5.6$ Hz, 2H), 3.81 (s, 3H), 3.55 (t, $J = 4.5$ Hz, 4H), 3.01 (t, $J = 4.5$ Hz, 4H); ^{13}C NMR (75 MHz, CDCl_3) δ 164.82, 159.45, 155.50, 143.32, 129.84, 129.78, 128.28, 127.36, 126.93, 119.40, 114.40, 66.41, 55.43, 52.77, 43.57; HR-MS (ESI) m/z : calcd for $\text{C}_{19}\text{H}_{22}\text{N}_3\text{O}_5 [\text{M}+\text{H}]^+$ 372.1554, found 372.1548.

N-(4-ethoxybenzyl)-2-morpholino-5-nitrobenzamide (13e). Yellow solid (80 mg, yield 77.9%). ^1H NMR (300 MHz, CDCl_3) δ 8.85

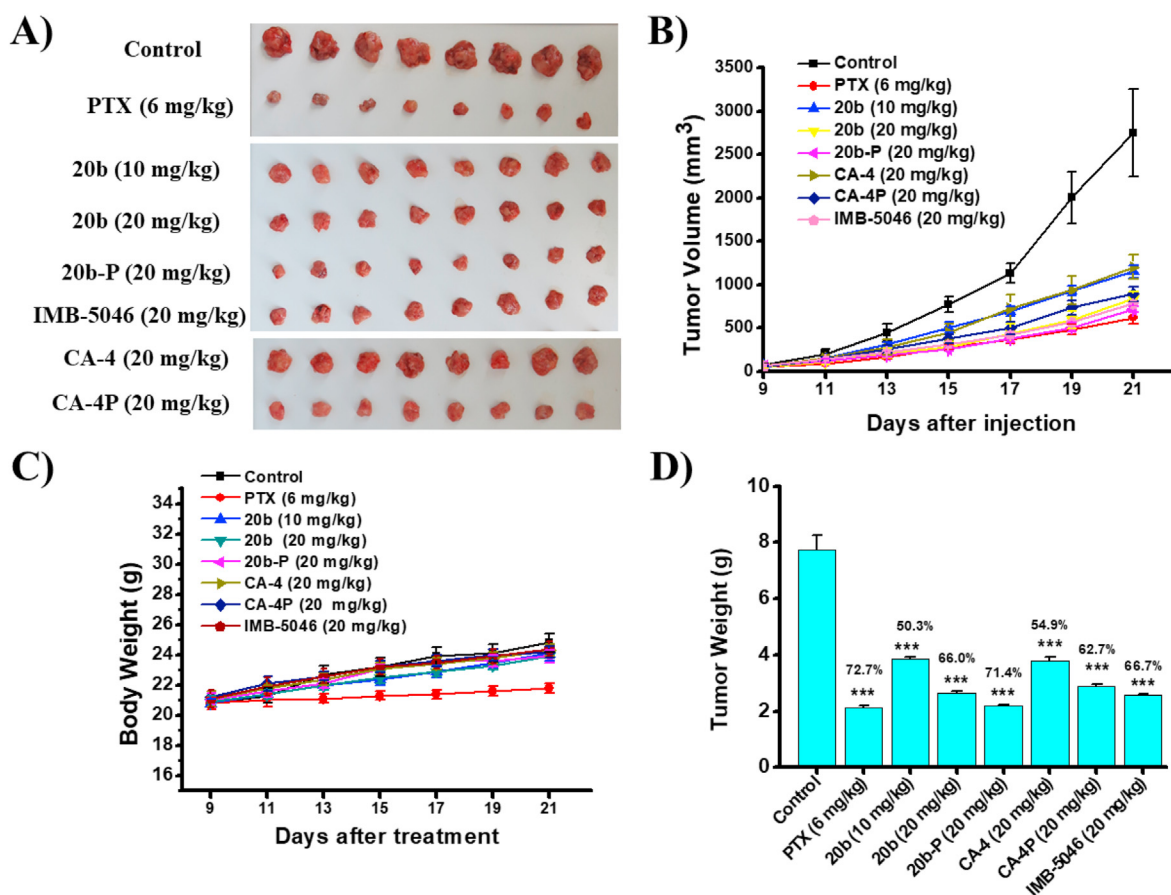


Fig. 12. **20b** and **20b-P** inhibited liver cancer xenograft growth *in vivo*. Mice were treated with vehicle, PTX (6 mg/kg every other day), **20b** (10 or 20 mg/kg per day), **20b-P** (20 mg/kg per day), IMB5046 (20 mg/kg per day), CA-4 (20 mg/kg per day), and CA-4P (20 mg/kg per day) for three weeks, and then sacrificed for analysis. All the groups were administered by intravenous injection. The treatments started the day after cell inoculum and the statistics started since the tumor grew out on the 9th day. (A) The images of tumors isolated from the mice at the end of the experiment; (B) Tumor volume changes of mice during treatment; (C) Body weight changes of mice during treatment; (D) The weight of the excised tumors of each group. ****P* < 0.001 vs. control group.

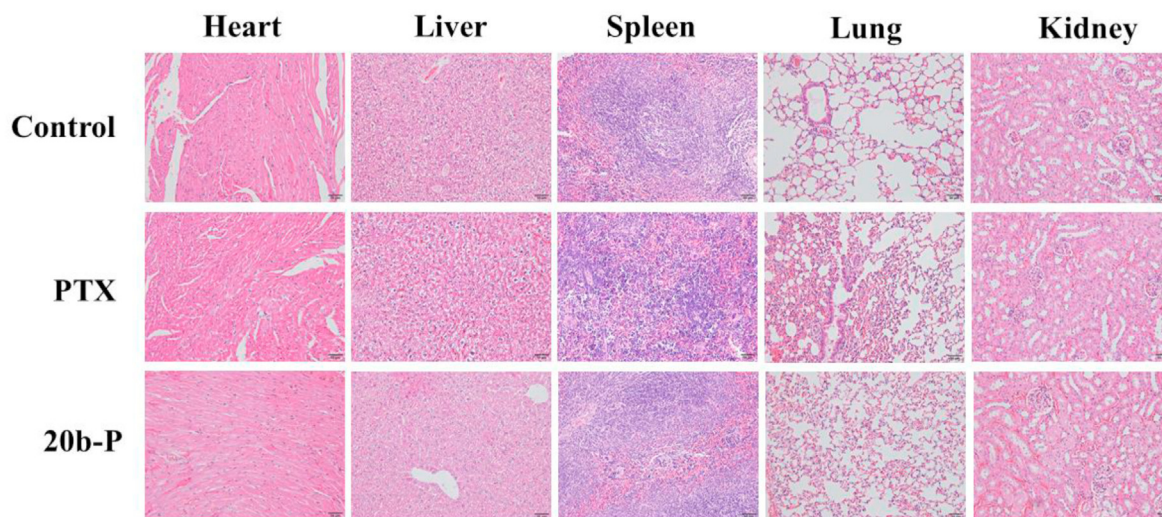


Fig. 13. HE staining of vital organs of mice including heart, liver, spleen, lung and kidney.

(d, *J* = 2.8 Hz, 1H), 8.51 (s, 1H), 8.25 (dd, *J* = 8.9, 2.8 Hz, 1H), 7.30 (d, *J* = 8.6 Hz, 2H), 7.16 (d, *J* = 8.9 Hz, 1H), 6.89 (d, *J* = 8.6 Hz, 2H), 4.58 (d, *J* = 5.6 Hz, 2H), 4.03 (q, *J* = 7.0 Hz, 2H), 3.58–3.48 (m, 4H), 3.06–2.97 (m, 4H), 1.42 (t, *J* = 7.0 Hz, 3H); ¹³C NMR (75 MHz, CDCl₃)

δ 164.69, 158.83, 155.51, 143.39, 129.77, 129.73, 128.41, 127.43, 126.90, 119.40, 114.96, 66.42, 63.61, 52.81, 43.59, 14.89; HR-MS (ESI) *m/z*: calcd for C₂₀H₂₄N₃O₅ [M+H]⁺ 386.1710, found 386.1712.

2-Morpholino-5-nitro-*N*-(4-(trifluoromethyl)benzyl)

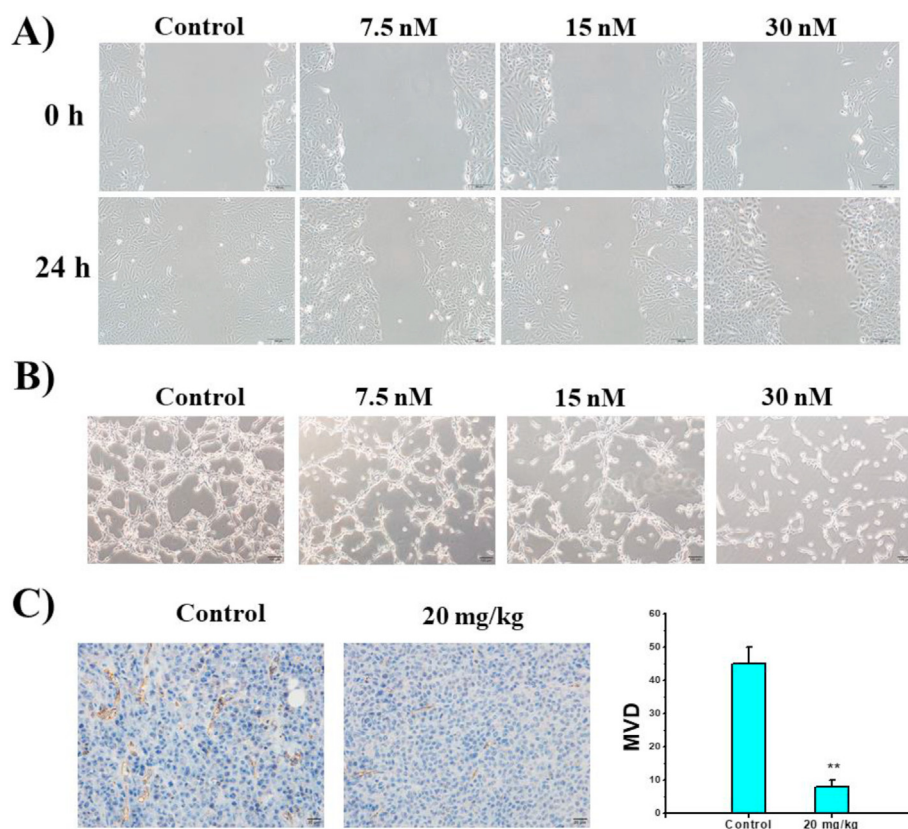


Fig. 14. *In vitro* and *in vivo* anti-vascular activity of **20b**. (A) Scratches were made with 200 μ L sterile pipette tips, and images were taken at 0 h and 24 h with a phase contrast microscopy after treatments with 0, 7.5, 15 and 30 nM of **20b**; (B) HUVEC capillary-like tubular network formation after treatments with 0, 7.5, 15 and 30 nM of **20b** for 6 h; (C) Immunohistochemical staining of CD31 in tumors treated with vehicle or **20b** (20 mg/kg). ** $P < 0.01$ vs. control group.

benzamide (13f). Yellow solid (99 mg, yield 81.1%). ^1H NMR (300 MHz, CDCl_3) δ 8.81 (d, $J = 2.8$ Hz, 1H), 8.77 (t, $J = 6.5$ Hz, 1H), 8.25 (dd, $J = 8.9$, 2.8 Hz, 1H), 7.63 (d, $J = 8.0$ Hz, 2H), 7.51 (d, $J = 8.0$ Hz, 2H), 7.20 (d, $J = 8.9$ Hz, 1H), 4.72 (d, $J = 6.0$ Hz, 2H), 3.70–3.55 (m, 4H), 3.14–2.99 (m, 4H); ^{13}C NMR (75 MHz, CDCl_3) δ 165.19, 155.56, 143.50, 142.09, 130.31 (q, $J = 32.6$ Hz), 128.54, 128.07, 127.48, 127.18, 125.99 (q, $J = 3.8$ Hz), 124.05 (q, $J = 270.5$ Hz), 119.66, 66.58, 52.92, 43.51; HR-MS (ESI) m/z : calcd for $\text{C}_{19}\text{H}_{19}\text{F}_3\text{N}_3\text{O}_4$ $[\text{M}+\text{H}]^+$ 410.1322 found 410.1319.

2-Morpholino-5-nitro-*N*-(4-(trifluoromethoxy)benzyl)benzamide (13g). Yellow solid (79 mg, yield 58.6%). ^1H NMR (300 MHz, CDCl_3) δ 8.86 (d, $J = 2.8$ Hz, 1H), 8.67 (s, 1H), 8.27 (dd, $J = 8.9$, 2.8 Hz, 1H), 7.43 (d, $J = 8.6$ Hz, 2H), 7.23 (d, $J = 8.6$ Hz, 2H), 7.20 (d, $J = 9.0$ Hz, 1H), 4.67 (d, $J = 5.9$ Hz, 2H), 3.62–3.54 (m, 4H), 3.06–2.98 (m, 4H); ^{13}C NMR (75 MHz, CDCl_3) δ 165.04, 155.54, 148.93, 143.46, 136.88, 129.84, 128.17, 127.44, 127.10, 121.60, 120.51 (q, $J = 255.8$ Hz), 119.59, 66.51, 52.89, 43.25; HR-MS (ESI) m/z : calcd for $\text{C}_{19}\text{H}_{19}\text{F}_3\text{N}_3\text{O}_5$ $[\text{M}+\text{H}]^+$ 426.1271, found 426.1267.

***N*-(4-(dimethylamino)benzyl)-2-morpholino-5-nitrobenzamide (13h).** Yellow solid (99 mg, yield 81.2%). ^1H NMR (300 MHz, CDCl_3) δ 8.86 (d, $J = 2.8$ Hz, 1H), 8.37 (s, 1H), 8.25 (dd, $J = 8.9$, 2.9 Hz, 1H), 7.24 (d, $J = 9.4$ Hz, 2H), 7.15 (d, $J = 8.9$ Hz, 1H), 6.71 (d, $J = 8.5$ Hz, 2H), 4.55 (d, $J = 5.5$ Hz, 2H), 3.56 (t, $J = 4.6$ Hz, 4H), 3.08–2.99 (m, 4H), 2.95 (s, 6H); ^{13}C NMR (75 MHz, CDCl_3) δ 164.66, 155.49, 150.49, 143.37, 129.53, 128.57, 127.42, 126.83, 125.20, 119.26, 112.85, 66.44, 52.80, 43.76, 40.69; HR-MS (ESI) m/z : calcd for $\text{C}_{20}\text{H}_{25}\text{N}_4\text{O}_4$ $[\text{M}+\text{H}]^+$ 385.1870, found 385.1873.

***N*-(4-chlorobenzyl)-2-morpholino-5-nitrobenzamide (13i).** Yellow solid (91 mg, yield 82.4%). ^1H NMR (300 MHz, CDCl_3) δ 8.85 (d, $J = 2.8$ Hz, 1H), 8.66 (s, 1H), 8.27 (dd, $J = 8.9$, 2.8 Hz, 1H), 7.34 (d,

$J = 1.8$ Hz, 4H), 7.19 (d, $J = 8.9$ Hz, 1H), 4.63 (d, $J = 5.8$ Hz, 2H), 3.65–3.53 (m, 4H), 3.09–2.98 (m, 4H); ^{13}C NMR (75 MHz, CDCl_3) δ 165.16, 155.51, 143.33, 136.41, 133.94, 129.74, 129.20, 128.01, 127.36, 127.10, 119.53, 66.52, 52.83, 43.38; HR-MS (ESI) m/z : calcd for $\text{C}_{18}\text{H}_{19}\text{ClN}_3\text{O}_4$ $[\text{M}+\text{H}]^+$ 376.1059 found 376.1058.

***N*-(4-hydroxybenzyl)-2-morpholino-5-nitrobenzamide (13j).** Yellow solid (65 mg, yield 81.1% over 2 steps). ^1H NMR (300 MHz, $\text{DMSO}-d_6$) δ 9.35 (s, 1H), 9.01 (t, $J = 6.0$ Hz, 1H), 8.17 (dd, $J = 9.0$, 2.9 Hz, 1H), 8.12 (d, $J = 2.8$ Hz, 1H), 7.15 (t, $J = 8.1$ Hz, 3H), 6.73 (d, $J = 8.4$ Hz, 2H), 4.32 (d, $J = 5.9$ Hz, 2H), 3.51 (t, $J = 4.5$ Hz, 4H), 3.09 (t, $J = 4.6$ Hz, 4H); ^{13}C NMR (75 MHz, $\text{DMSO}-d_6$) δ 166.37, 156.47, 154.38, 139.00, 129.33, 129.15, 126.89, 126.14, 125.50, 117.56, 115.09, 65.53, 50.48, 42.33; HR-MS (ESI) m/z : calcd for $\text{C}_{18}\text{H}_{20}\text{N}_3\text{O}_5$ $[\text{M}+\text{H}]^+$ 358.1397 found 358.1396.

***N*-(1-(4-methoxyphenyl)ethyl)-2-morpholino-5-nitrobenzamide (13k).** Yellow solid (99 mg, yield 81.1%). ^1H NMR (300 MHz, CDCl_3) δ 8.82 (d, $J = 2.8$ Hz, 1H), 8.43 (d, $J = 7.7$ Hz, 1H), 8.24 (dd, $J = 8.9$, 2.8 Hz, 1H), 7.34 (d, $J = 8.7$ Hz, 2H), 7.16 (d, $J = 8.9$ Hz, 1H), 6.92 (d, $J = 8.7$ Hz, 2H), 5.36–5.27 (m, 1H), 3.82 (s, 3H), 3.64–3.43 (m, 4H), 3.00 (dd, $J = 5.5$, 3.9 Hz, 4H), 1.61 (d, $J = 6.9$ Hz, 3H); ^{13}C NMR (75 MHz, CDCl_3) δ 164.15, 159.34, 155.47, 143.29, 134.58, 128.46, 127.84, 127.35, 126.85, 119.39, 114.36, 66.32, 55.46, 52.75, 49.02, 21.47; HR-MS (ESI) m/z : calcd for $\text{C}_{20}\text{H}_{24}\text{N}_3\text{O}_5$ $[\text{M}+\text{H}]^+$ 343.1401 found 343.1399.

***N*-(3-fluoro-4-methoxybenzyl)-2-morpholino-5-nitrobenzamide (13l).** Yellow solid (52 mg, yield 42.0%). ^1H NMR (300 MHz, CDCl_3) δ 8.82 (s, 1H), 8.62 (s, 1H), 8.25 (d, $J = 8.9$ Hz, 1H), 7.46–7.03 (m, 3H), 6.95 (t, $J = 8.4$ Hz, 1H), 4.57 (d, $J = 5.8$ Hz, 2H), 3.90 (s, 3H), 3.60 (s, 4H), 3.03 (s, 4H); ^{13}C NMR (75 MHz, CDCl_3) δ 165.01, 161.69, 160.45, 155.53, 154.18, 149.95 (d, $J = 20.1$ Hz), 143.57,

130.81 (d, $J = 7.1$ Hz), 128.25, 127.48, 127.10, 124.30 (d, $J = 3.4$ Hz), 119.58, 116.33, 116.08, 113.76, 66.56, 56.47, 52.93, 43.28; HR-MS (ESI) m/z : calcd for $C_{19}H_{21}FN_3O_5$ $[M+H]^+$ 390.1460, found 390.1467.

***N*-(3,4-dimethoxybenzyl)-2-morpholino-5-nitrobenzamide (13m)**. Yellow solid (85 mg, yield 66.9%). 1H NMR (300 MHz, $CDCl_3$) δ 8.85 (d, $J = 2.8$ Hz, 1H), 8.55 (s, 1H), 8.26 (dd, $J = 8.9, 2.8$ Hz, 1H), 7.17 (d, $J = 8.9$ Hz, 1H), 6.93 (dt, $J = 4.9, 2.0$ Hz, 2H), 6.86 (d, $J = 8.6$ Hz, 1H), 4.59 (d, $J = 5.7$ Hz, 2H), 3.89 (s, 3H), 3.88 (s, 3H), 3.61–3.51 (m, 4H), 3.07–2.97 (m, 4H); ^{13}C NMR (75 MHz, $CDCl_3$) δ 164.84, 155.49, 149.44, 148.94, 143.39, 130.35, 128.27, 127.40, 126.97, 120.78, 119.43, 111.68, 111.35, 66.44, 56.09, 56.07, 52.83, 43.98; HR-MS (ESI) m/z : calcd for $C_{20}H_{24}N_3O_6$ $[M+H]^+$ 402.1660, found 402.1658.

***N*-(3-hydroxy-4-methoxybenzyl)-2-morpholino-5-nitrobenzamide (13n)**. Yellow solid (75 mg, yield 61.5% over 2 steps). 1H NMR (300 MHz, $CDCl_3$) δ 8.85 (d, $J = 2.8$ Hz, 1H), 8.51 (s, 1H), 8.25 (dd, $J = 8.9, 2.9$ Hz, 1H), 7.17 (d, $J = 8.9$ Hz, 1H), 6.94 (d, $J = 1.9$ Hz, 1H), 6.89–6.81 (m, 2H), 4.55 (d, $J = 5.6$ Hz, 2H), 3.90 (s, 3H), 3.57 (t, $J = 4.7$ Hz, 4H), 3.07–3.00 (m, 4H); ^{13}C NMR (75 MHz, $DMSO-d_6$) δ 166.46, 154.37, 146.80, 146.44, 138.95, 131.56, 126.81, 126.17, 125.53, 118.70, 117.51, 115.40, 112.13, 65.57, 55.71, 50.50, 42.39; HR-MS (ESI) m/z : calcd for $C_{19}H_{22}N_3O_6$ $[M+H]^+$ 388.1503 found 388.1502.

***N*-(3,4,5-trimethoxybenzyl)-2-morpholino-5-nitrobenzamide (13o)**. Yellow solid (63 mg, yield 46.1%). 1H NMR (300 MHz, $CDCl_3$) δ 8.85 (d, $J = 2.8$ Hz, 1H), 8.55 (s, 1H), 8.27 (dd, $J = 8.9, 2.8$ Hz, 1H), 7.18 (d, $J = 8.9$ Hz, 1H), 6.61 (s, 2H), 4.58 (d, $J = 5.8$ Hz, 2H), 3.86 (s, 6H), 3.84 (s, 3H), 3.64–3.56 (m, 4H), 3.08–2.98 (m, 4H); ^{13}C NMR (75 MHz, $CDCl_3$) δ 164.94, 155.47, 153.74, 143.37, 137.94, 133.58, 128.26, 127.36, 126.99, 119.45, 105.58, 66.47, 61.03, 56.36, 52.85, 44.45; HR-MS (ESI) m/z : calcd for $C_{21}H_{26}N_3O_7$ $[M+H]^+$ 432.1765, found 432.1768.

2-Morpholino-5-nitro-*N*-(pyridin-4-ylmethyl)benzamide (13p). Yellow solid (89 mg, yield 82.4%). 1H NMR (300 MHz, $CDCl_3$) δ 8.97–8.76 (m, 2H), 8.60 (d, $J = 6.1$ Hz, 2H), 8.29 (dd, $J = 8.9, 2.8$ Hz, 1H), 7.29 (d, $J = 6.1$ Hz, 2H), 7.23 (d, $J = 8.9$ Hz, 1H), 4.68 (d, $J = 6.0$ Hz, 2H), 3.76–3.63 (m, 4H), 3.15–3.03 (m, 4H); ^{13}C NMR (75 MHz, $CDCl_3$) δ 165.45, 155.56, 150.36, 146.94, 143.43, 127.88, 127.45, 127.26, 122.79, 119.70, 66.67, 52.93, 42.85; HR-MS (ESI) m/z : calcd for $C_{17}H_{19}N_4O_4$ $[M+H]^+$ 343.1401 found 343.1399.

***N*-((6-methoxypyridin-3-yl)methyl)-2-morpholino-5-nitrobenzamide (13q)**. Yellow solid (79 mg, yield 58.6%). 1H NMR (300 MHz, $CDCl_3$) δ 8.85 (d, $J = 2.8$ Hz, 1H), 8.58 (s, 1H), 8.27 (dd, $J = 8.9, 2.8$ Hz, 1H), 8.17 (d, $J = 2.4$ Hz, 1H), 7.65 (dd, $J = 8.5, 2.5$ Hz, 1H), 7.19 (d, $J = 8.9$ Hz, 1H), 6.79–6.73 (m, 1H), 4.59 (d, $J = 5.8$ Hz, 2H), 3.94 (s, 3H), 3.65–3.59 (m, 4H), 3.07–3.01 (m, 4H); ^{13}C NMR (75 MHz, $CDCl_3$) δ 165.07, 164.04, 155.46, 146.55, 143.29, 139.12, 128.09, 127.35, 127.03, 126.35, 119.44, 111.35, 66.55, 53.65, 52.78, 40.89; HR-MS (ESI) m/z : calcd for $C_{18}H_{21}N_4O_5$ $[M+H]^+$ 373.1506, found 373.1509.

4.1.5. General procedures for the preparation of intermediates 14a-h and 22a-b

The synthesis methods of intermediates 14a-h and 22a-b were the same as that of 12.

5-Nitro-2-(piperidin-1-yl)benzoic acid (14a). Yellow solid, yield 80.5%. 1H NMR (300 MHz, $DMSO-d_6$) δ 13.62 (s, 1H), 8.36 (d, $J = 3.0$ Hz, 1H), 8.16 (dd, $J = 9.2, 3.0$ Hz, 1H), 7.19 (d, $J = 9.3$ Hz, 1H), 3.24 (t, $J = 5.2$ Hz, 4H), 1.71–1.51 (m, 6H); ^{13}C NMR (75 MHz, $DMSO-d_6$) δ 167.49, 155.35, 137.66, 127.33, 127.19, 120.78, 117.94, 51.86, 25.14, 23.18; ESI-MS m/z 250.1 $[M - H]^-$ 249.1.

5-Nitro-2-(pyrrolidin-1-yl)benzoic acid (14b). Yellow solid, yield 76.3%. 1H NMR (300 MHz, $DMSO-d_6$) δ 13.21 (s, 1H), 8.26 (d, $J = 2.8$ Hz, 1H), 8.05 (dd, $J = 9.4, 2.8$ Hz, 1H), 6.83 (d, $J = 9.5$ Hz, 1H), 3.29 (t, $J = 6.2$ Hz, 4H), 1.90 (t, $J = 6.1$ Hz, 4H); ^{13}C NMR (75 MHz,

$DMSO-d_6$) δ 168.51, 151.04, 135.17, 127.59, 126.96, 117.24, 114.34, 51.42, 25.70; ESI-MS m/z 236.1 $[M - H]^-$ 235.1.

2-(Diethylamino)-5-nitrobenzoic acid (14c). Yellow solid, yield 85.9%. 1H NMR (300 MHz, $DMSO-d_6$) δ 8.34 (d, $J = 2.9$ Hz, 1H), 8.17 (dd, $J = 9.4, 3.0$ Hz, 1H), 7.22 (d, $J = 9.4$ Hz, 1H), 3.40 (q, $J = 7.0$ Hz, 4H), 1.12 (t, $J = 7.0$ Hz, 6H); ^{13}C NMR (75 MHz, $DMSO-d_6$) δ 168.40, 153.06, 137.84, 127.31, 127.26, 121.67, 118.01, 46.90, 12.32; ESI-MS m/z 238.1 $[M - H]^-$ 237.1.

2-(Dimethylamino)-5-nitrobenzoic acid (14d). Yellow solid, yield 88.2%. 1H NMR (300 MHz, $DMSO-d_6$) δ 13.27 (s, 1H), 8.35 (d, $J = 2.9$ Hz, 1H), 8.11 (dd, $J = 9.5, 2.9$ Hz, 1H), 7.02 (d, $J = 9.4$ Hz, 1H), 3.03 (s, 6H); ^{13}C NMR (75 MHz, $DMSO-d_6$) δ 168.26, 154.89, 136.06, 128.05, 127.15, 117.94, 115.35, 42.99; ESI-MS m/z 210.1 $[M - H]^-$ 209.1.

2-(4-(Tert-butoxycarbonyl)piperazin-1-yl)-5-nitrobenzoic acid (14e). Yellow solid, yield 70.3%. 1H NMR (300 MHz, $DMSO-d_6$) δ 8.41 (d, $J = 2.9$ Hz, 1H), 8.19 (dd, $J = 9.2, 2.9$ Hz, 1H), 7.17 (d, $J = 9.3$ Hz, 1H), 3.48 (t, $J = 4.7$ Hz, 4H), 3.28 (dd, $J = 6.8, 3.6$ Hz, 4H), 1.42 (s, 9H); ^{13}C NMR (75 MHz, $DMSO-d_6$) δ 167.30, 155.06, 153.83, 138.06, 127.47, 127.22, 120.62, 117.84, 79.12, 50.22, 27.99; ESI-MS m/z 251.1 $[M - H]^-$ 250.1.

5-Nitro-2-thiomorpholinobenzoic acid (14f). Yellow solid, yield 76.5%. 1H NMR (300 MHz, $DMSO-d_6$) δ 8.38 (d, $J = 3.0$ Hz, 1H), 8.19 (dd, $J = 9.3, 3.0$ Hz, 1H), 7.21 (d, $J = 9.3$ Hz, 1H), 3.52 (t, $J = 2.5$ Hz, 4H), 2.75 (t, 4H); ^{13}C NMR (75 MHz, $DMSO-d_6$) δ 167.37, 155.78, 138.26, 127.28, 127.15, 121.60, 118.79, 53.35, 26.31; ESI-MS m/z 268.1 $[M - H]^-$ 267.1.

2-(1,1-Dioxidothiomorpholino)-5-nitrobenzoic acid (14g). Yellow solid, yield 78.3%. 1H NMR (300 MHz, $DMSO-d_6$) δ 13.55 (s, 1H), 8.47 (d, $J = 2.9$ Hz, 1H), 8.25 (dd, $J = 9.2, 2.9$ Hz, 1H), 7.35 (d, $J = 9.2$ Hz, 1H), 3.76–3.64 (m, 4H), 3.41–3.17 (m, 4H); ^{13}C NMR (101 MHz, $DMSO$) δ 167.45, 155.44, 139.80, 127.89, 127.74, 122.26, 120.64, 51.39, 50.35; ESI-MS m/z 300.0 $[M - H]^-$ 209.0.

2-((2-Methoxyethyl)amino)-5-nitrobenzoic acid (14h). Yellow solid, yield 83.2%. 1H NMR (300 MHz, $DMSO-d_6$) δ 8.87 (s, 1H), 8.63 (d, $J = 2.8$ Hz, 1H), 8.16 (dd, $J = 9.4, 2.9$ Hz, 1H), 6.92 (d, $J = 9.5$ Hz, 1H), 3.58 (t, $J = 5.0$ Hz, 2H), 3.51 (t, $J = 5.2$ Hz, 2H), 3.30 (s, 3H); ^{13}C NMR (75 MHz, $DMSO-d_6$) δ 168.51, 154.63, 134.64, 129.29, 128.51, 111.67, 109.14, 69.90, 58.08, 41.99; ESI-MS m/z 240.1 $[M - H]^-$ 239.1.

4-Morpholinonicotinic acid (22a). Yellow solid, yield 88.2%. 1H NMR (300 MHz, $DMSO-d_6$) δ 10.00 (s, 1H), 8.60 (s, 1H), 8.40 (d, $J = 7.2$ Hz, 1H), 7.48 (d, $J = 7.3$ Hz, 1H), 3.75 (t, $J = 4.5$ Hz, 4H), 3.59 (t, $J = 4.5$ Hz, 4H); ^{13}C NMR (75 MHz, $DMSO-d_6$) δ 165.90, 156.79, 143.29, 140.30, 115.45, 112.19, 63.49, 42.89; ESI-MS m/z 208.1 $[M - H]^-$ 207.1.

3-Morpholinoisonicotinic acid (22b). Yellow solid, yield 90.3%. 1H NMR (300 MHz, $DMSO-d_6$) δ 8.53 (d, $J = 3.1$ Hz, 1H), 8.32 (d, $J = 4.3$ Hz, 1H), 7.51 (d, $J = 4.4$ Hz, 1H), 3.72 (t, 4H), 3.11 (t, $J = 4.4$ Hz, 4H); ^{13}C NMR (75 MHz, $DMSO-d_6$) δ 168.12, 144.98, 144.13, 142.79, 132.75, 123.43, 66.62, 52.04; ESI-MS m/z 208.1 $[M - H]^-$ 207.1.

4.1.6. General procedures for the preparation of target compounds 16a-h

To the solutions of 14a-h (0.32 mmol) in 10 mL anhydrous DCM, 15 (93 mg, 0.64 mmol), EDCI (296 mg, 1.6 mmol), HOBT (52 mg, 0.38 mmol) and catalytic amount of DMAP were added. The mixtures were stirred for 2 h, and extracted with DCM (3 \times 25 mL). The combined organic layers were then washed with brine, dried over anhydrous Na_2SO_4 , and concentrated in vacuo to provide the crude products, which were purified by column chromatography with petroleum/ethyl acetate (4:1) to give products. Then, above obtained products were dissolved into 10 mL THF, and TBAF (1.2 e.q) was added. The mixtures were stirred for 15 min, and extracted with DCM (3 \times 25 mL). The combined organic layers were then washed with brine, dried over anhydrous Na_2SO_4 , and concentrated

in vacuo to provide the crude products, which were purified by column chromatography with petroleum/ethyl acetate (2:1) to give target compounds **16a-d** and **16f-h**. For piperazine compound **16e**, the product obtained in above procedure was dissolved into 10 mL anhydrous DCM, and 2 mL CF₃COOH was added. The mixture was stirred for 2 h, and neutralize with saturated NaHCO₃ aqueous. The mixture was then extracted with DCM (3 × 25 mL), and the combined organic layers were then washed with brine, dried over anhydrous Na₂SO₄, and concentrated in vacuo to provide the crude products, which were purified by column chromatography with DCM/MeOH (40:1) to give target compound **16e**.

N-(3-hydroxy-4-methoxybenzyl)-5-nitro-2-(piperidin-1-yl)benzamide (16a). Yellow solid, yield 44.4% over 2 steps. ¹H NMR (300 MHz, DMSO-*d*₆) δ 9.00 (t, *J* = 6.0 Hz, 1H), 8.95 (s, 1H), 8.13 (q, *J* = 3.3 Hz, 2H), 7.16–7.08 (m, 1H), 6.87 (d, *J* = 8.2 Hz, 1H), 6.80 (d, *J* = 2.1 Hz, 1H), 6.73 (dd, *J* = 8.2, 2.1 Hz, 1H), 4.31 (d, *J* = 5.9 Hz, 2H), 3.74 (s, 3H), 3.13 (s, 4H), 1.50 (s, 6H); ¹³C NMR (75 MHz, DMSO-*d*₆) δ 166.56, 155.06, 146.74, 146.45, 138.05, 131.68, 126.24, 126.17, 125.74, 118.48, 117.56, 115.26, 112.11, 55.71, 51.51, 42.34, 25.08, 23.38; HR-MS (ESI) *m/z*: calcd for C₂₀H₂₄N₃O₅ [M+H]⁺ 386.1710 found 386.1710.

N-(3-hydroxy-4-methoxybenzyl)-5-nitro-2-(pyrrolidin-1-yl)benzamide (16b). Yellow solid, yield 50.2% over 2 steps. ¹H NMR (300 MHz, DMSO-*d*₆) δ 8.98 (s, 2H), 8.27–7.77 (m, 2H), 7.17–6.56 (m, 4H), 4.46–4.19 (m, 2H), 3.74 (s, 3H), 3.30 (s, 4H), 1.85 (s, 4H); ¹³C NMR (75 MHz, DMSO-*d*₆) δ 167.85, 149.75, 146.75, 146.43, 138.62, 134.36, 131.62, 125.84, 121.48, 118.45, 115.25, 113.36, 112.10, 55.71, 49.85, 42.43, 25.15; HR-MS (ESI) *m/z*: calcd for C₁₉H₂₂N₃O₅ [M+H]⁺ 372.1554 found 372.1551.

2-(Diethylamino)-N-(3-hydroxy-4-methoxybenzyl)-5-nitrobenzamide (16c). Yellow solid, yield 55.3% over 2 steps. ¹H NMR (300 MHz, CDCl₃) δ 9.09 (t, *J* = 5.4 Hz, 1H), 8.85 (d, *J* = 2.9 Hz, 1H), 8.19 (dd, *J* = 8.9, 2.9 Hz, 1H), 7.16 (d, *J* = 9.0 Hz, 1H), 6.97–6.88 (m, 1H), 6.83 (d, *J* = 2.2 Hz, 2H), 5.86 (s, 1H), 4.53 (d, *J* = 5.4 Hz, 2H), 3.88 (s, 3H), 3.12 (q, *J* = 7.1 Hz, 4H), 0.98 (t, *J* = 7.1 Hz, 6H); ¹³C NMR (75 MHz, CDCl₃) δ 165.07, 154.85, 146.25, 145.99, 142.78, 131.10, 129.04, 127.26, 126.22, 121.87, 119.80, 114.36, 110.92, 56.12, 47.60, 43.77, 11.85; HR-MS (ESI) *m/z*: calcd for C₁₉H₂₄N₃O₅ [M+H]⁺ 374.1710 found 374.1714.

2-(Dimethylamino)-N-(3-hydroxy-4-methoxybenzyl)-5-nitrobenzamide (16d). Yellow solid, yield 62.9% over 2 steps. ¹H NMR (300 MHz, DMSO-*d*₆) δ 8.97 (d, *J* = 7.4 Hz, 2H), 8.31–7.68 (m, 2H), 6.89 (t, *J* = 11.3 Hz, 2H), 6.85–6.45 (m, 2H), 4.29 (d, *J* = 5.7 Hz, 2H), 3.74 (s, 3H), 2.95 (s, 6H); ¹³C NMR (75 MHz, DMSO-*d*₆) δ 167.61, 153.46, 146.70, 146.41, 135.46, 131.66, 126.02, 125.79, 122.66, 118.38, 115.18, 114.32, 112.11, 55.67, 42.35, 41.89; HR-MS (ESI) *m/z*: calcd for C₁₇H₂₀N₃O₅ [M+H]⁺ 346.1397 found 346.1393.

N-(3-hydroxy-4-methoxybenzyl)-5-nitro-2-(piperazin-1-yl)benzamide (16e). Yellow solid, yield 43.9% over 3 steps. ¹H NMR (300 MHz, DMSO-*d*₆) δ 9.04 (s, 2H), 8.15 (s, 2H), 7.15 (s, 1H), 6.82 (d, *J* = 25.3 Hz, 2H), 5.76 (s, 1H), 4.30 (s, 2H), 4.10–3.56 (m, 3H), 3.15 (s, 4H), 2.80 (s, 4H); ¹³C NMR (75 MHz, DMSO-*d*₆) δ 166.49, 154.41, 146.74, 146.43, 138.71, 131.61, 126.54, 126.18, 125.64, 118.48, 117.70, 115.21, 112.12, 55.69, 50.13, 44.20, 42.36; HR-MS (ESI) *m/z*: calcd for C₁₉H₂₃N₄O₅ [M+H]⁺ 387.1663 found 387.1664.

N-(3-hydroxy-4-methoxybenzyl)-5-nitro-2-thiomorpholinobenzamide (16f). Yellow solid, yield 56.0% over 2 steps. ¹H NMR (300 MHz, DMSO-*d*₆) δ 9.02 (t, *J* = 6.0 Hz, 1H), 8.97 (s, 1H), 8.15 (d, *J* = 9.3 Hz, 2H), 7.17 (d, *J* = 8.9 Hz, 1H), 6.88 (d, *J* = 8.1 Hz, 1H), 6.80 (s, 1H), 6.73 (d, *J* = 8.1 Hz, 1H), 4.31 (d, *J* = 6.0 Hz, 2H), 3.74 (s, 3H), 3.49–3.38 (m, 4H), 2.60 (d, *J* = 4.7 Hz, 4H); ¹³C NMR (75 MHz, DMSO-*d*₆) δ 166.42, 155.04, 146.76, 146.45, 138.94, 131.63, 127.23, 126.07, 125.54, 118.58, 118.50, 115.24, 112.21, 55.74, 52.96, 42.35, 26.22; HR-MS (ESI) *m/z*: calcd for C₁₉H₂₂N₃O₅S [M+H]⁺ 404.1275 found 404.1277.

2-(1,1-Dioxidothiomorpholino)-N-(3-hydroxy-4-methoxybenzyl)-5-nitrobenzamide (16g). Yellow solid, yield 53.4% over 2 steps. ¹H NMR (300 MHz, DMSO-*d*₆) δ 9.09–9.00 (m, 1H), 8.97 (s, 1H), 8.27–8.08 (m, 2H), 7.28 (d, *J* = 8.8 Hz, 1H), 6.88 (d, *J* = 8.2 Hz, 1H), 6.78 (d, *J* = 2.1 Hz, 1H), 6.73 (dd, *J* = 8.1, 2.1 Hz, 1H), 4.32 (d, *J* = 5.9 Hz, 2H), 3.74 (s, 3H), 3.65–3.48 (m, 4H), 3.11 (t, *J* = 5.1 Hz, 4H); ¹³C NMR (75 MHz, DMSO-*d*₆) δ 166.27, 153.54, 146.79, 146.48, 139.92, 131.58, 127.65, 126.01, 125.41, 119.67, 118.39, 115.10, 112.28, 55.70, 50.61, 49.39, 42.39; HR-MS (ESI) *m/z*: calcd for C₁₉H₂₂N₃O₇S [M+H]⁺ 436.1173 found 436.1166.

N-(3-hydroxy-4-methoxybenzyl)-2-((2-methoxyethyl)amino)-5-nitrobenzamide (16h). Yellow solid, yield 62.4% over 2 steps. ¹H NMR (300 MHz, DMSO-*d*₆) δ 9.31 (s, 1H), 9.16 (s, 1H), 8.95 (s, 1H), 8.62 (s, 1H), 8.14 (d, *J* = 9.3 Hz, 1H), 6.77 (dd, *J* = 32.8, 16.3 Hz, 4H), 4.32 (s, 2H), 3.75 (s, 3H), 3.56 (s, 2H), 3.45 (s, 2H), 3.30 (s, 3H); ¹³C NMR (75 MHz, DMSO-*d*₆) δ 167.30, 154.08, 146.68, 146.44, 134.63, 131.83, 128.12, 125.51, 118.11, 114.86, 113.11, 112.20, 111.07, 70.00, 58.13, 55.71, 54.93, 42.05; HR-MS (ESI) *m/z*: calcd for C₁₈H₂₂N₃O₆ [M+H]⁺ 376.1503 found 376.1496.

4.1.7. General procedures for the preparation of target compounds 20a-p

Target compounds **20a-p** were synthesized by two methods. Method A: the same as the synthesis of **16a-h**. Method B: To the solutions of various benzoic acids (0.32 mmol) in 10 mL anhydrous CH₃CN, **15** (93 mg, 0.64 mmol), HATU (145 mg, 0.38 mmol), and Et₃N (53 μL, 0.38 mmol) were added. The mixtures were stirred for 2 h, and extracted with DCM (3 × 25 mL). The combined organic layers were then washed with brine, dried over anhydrous Na₂SO₄, and concentrated in vacuo to provide the crude products, which were purified by column chromatography with petroleum/ethyl acetate (4:1) to give products. Then, above obtained products were dissolved into 10 mL THF, and TBAF was added. The mixtures were stirred for 15 min, and extracted with DCM (3 × 25 mL). The combined organic layers were then washed with brine, dried over anhydrous Na₂SO₄, and concentrated in vacuo to provide the crude products, which were purified by column chromatography with petroleum/ethyl acetate (2:1) to give target compounds. For compound **20o**, the obtained product (56 mg, 0.13 mmol) in above procedure was dissolved into 10 mL CH₃OH, Pd–C (5 mg) was added. The reaction was stirred for 2 h under hydrogen atmosphere, then the mixture was filtered and the filtrate was concentrated in vacuo to provide the crude product, which were purified by column chromatography with petroleum/ethyl acetate (1:1) to give target compound **20o**.

N-(3-hydroxy-4-methoxybenzyl)-2-morpholinobenzamide (20a). Method A, white solid, yield 54.9% over 2 steps. ¹H NMR (300 MHz, CDCl₃) δ 10.04 (s, 1H), 8.22 (dd, *J* = 7.8, 1.8 Hz, 1H), 7.44 (td, *J* = 7.7, 1.8 Hz, 1H), 7.26 (dd, *J* = 7.5, 1.4 Hz, 1H), 7.20 (td, *J* = 8.0, 1.2 Hz, 1H), 6.97 (d, *J* = 2.0 Hz, 1H), 6.87 (dd, *J* = 8.2, 2.0 Hz, 1H), 6.82 (d, *J* = 8.2 Hz, 1H), 6.02 (s, 1H), 4.55 (d, *J* = 5.3 Hz, 2H), 3.88 (s, 3H), 3.61–3.44 (m, 4H), 2.98–2.85 (m, 4H); ¹³C NMR (75 MHz, CDCl₃) δ 165.99, 150.82, 146.35, 146.13, 132.22, 131.87, 131.60, 127.77, 125.29, 120.50, 119.99, 114.70, 110.91, 66.88, 56.11, 53.47, 43.57; HR-MS (ESI) *m/z*: calcd for C₁₉H₂₃N₂O₄ [M+H]⁺ 343.1652 found 343.1645.

5-Fluoro-N-(3-hydroxy-4-methoxybenzyl)-2-morpholinobenzamide (20b). Method B, white solid, yield 46.5% over 2 steps. ¹H NMR (300 MHz, CDCl₃) δ 10.35 (t, *J* = 5.4 Hz, 1H), 7.96 (dd, *J* = 9.7, 3.0 Hz, 1H), 7.16 (m, 2H), 6.95 (s, 1H), 6.89–6.79 (m, 2H), 5.96 (s, 1H), 4.53 (d, *J* = 5.2 Hz, 2H), 3.89 (s, 3H), 3.50 (t, *J* = 4.4 Hz, 4H), 2.86 (t, *J* = 4.5 Hz, 4H); ¹³C NMR (75 MHz, CDCl₃) δ 164.47, 160.16 (d, *J* = 243.8 Hz), 146.85 (d, *J* = 3.0 Hz), 146.38, 146.13, 131.37, 130.09 (d, *J* = 6.9 Hz), 122.93 (d, *J* = 7.9 Hz), 120.06, 118.83 (d, *J* = 22.4 Hz), 118.37 (d, *J* = 24.0 Hz), 114.67, 110.91, 66.86,

56.13, 53.70, 43.72; HR-MS (ESI) m/z : calcd for $C_{19}H_{22}FN_2O_4$ $[M+H]^+$ 361.1558 found 361.1551.

N-(3-hydroxy-4-methoxybenzyl)-2-(piperidin-1-yl)benzamide (20c). Method A, white solid, yield 50.5% over 2 steps. 1H NMR (300 MHz, $CDCl_3$) δ 10.61 (s, 1H), 8.24 (dd, J = 8.1, 1.8 Hz, 1H), 7.40 (td, J = 7.6, 1.9 Hz, 1H), 7.20 (t, J = 7.7 Hz, 2H), 6.96 (d, J = 2.1 Hz, 1H), 6.86–6.78 (m, 2H), 5.99 (s, 1H), 4.55 (d, J = 5.4 Hz, 2H), 3.86 (s, 3H), 2.81 (d, J = 5.0 Hz, 4H), 1.44 (s, 6H); ^{13}C NMR (75 MHz, $CDCl_3$) δ 166.26, 152.69, 146.15, 146.00, 133.43, 131.98, 131.56, 127.66, 124.84, 120.98, 119.84, 114.68, 110.93, 56.16, 54.83, 43.49, 26.24, 23.72; HR-MS (ESI) m/z : calcd for $C_{20}H_{25}N_2O_3$ $[M+H]^+$ 341.1860 found 341.1862.

5-Fluoro-N-(3-hydroxy-4-methoxybenzyl)-2-(piperidin-1-yl)benzamide (20d). Method B, white solid, yield 55.7% over 2 steps. 1H NMR (300 MHz, $CDCl_3$) δ 10.79 (s, 1H), 7.97 (dd, J = 9.9, 3.2 Hz, 1H), 7.19 (dd, J = 8.8, 4.9 Hz, 1H), 7.08 (ddd, J = 8.8, 7.2, 3.2 Hz, 1H), 6.95 (d, J = 2.0 Hz, 1H), 6.87 (dd, J = 8.2, 2.0 Hz, 1H), 6.81 (d, J = 8.2 Hz, 1H), 5.62 (s, 1H), 4.54 (d, J = 5.3 Hz, 2H), 3.88 (s, 3H), 2.79 (d, J = 5.1 Hz, 4H), 1.51–1.42 (m, 6H); ^{13}C NMR (75 MHz, $CDCl_3$) δ 169.92, 159.94 (d, J = 243.4 Hz), 148.69 (d, J = 2.8 Hz), 146.15, 145.98, 139.31, 131.78, 123.20 (d, J = 7.9 Hz), 119.94, 118.57 (d, J = 22.1 Hz), 117.96 (d, J = 24.0 Hz), 118.12, 117.80, 114.63, 110.90, 56.19, 55.07, 43.61, 26.24, 23.62; HR-MS (ESI) m/z : calcd for $C_{20}H_{24}FN_2O_3$ $[M+H]^+$ 359.1765 found 359.1762.

N-(3-hydroxy-4-methoxybenzyl)-4-morpholinonicotinamide (20e). Method A, white solid, yield 40.7% over 2 steps. 1H NMR (300 MHz, $CDCl_3$) δ 8.96 (s, 1H), 8.52 (d, J = 5.6 Hz, 1H), 7.99 (s, 1H), 6.94 (d, J = 1.9 Hz, 1H), 6.88 (d, J = 5.6 Hz, 1H), 6.85 (d, J = 1.8 Hz, 1H), 6.82 (d, J = 8.1 Hz, 1H), 4.53 (d, J = 5.7 Hz, 2H), 3.90 (s, 3H), 3.59–3.47 (m, 4H), 3.04–2.93 (m, 4H); ^{13}C NMR (75 MHz, $CDCl_3$) δ 165.69, 156.51, 152.41, 151.94, 146.72, 146.38, 131.05, 122.44, 119.91, 114.78, 112.62, 111.04, 66.36, 56.11, 51.69, 43.52; HR-MS (ESI) m/z : calcd for $C_{18}H_{22}N_3O_4$ $[M+H]^+$ 344.1605 found 344.1599.

N-(3-hydroxy-4-methoxybenzyl)-3-morpholinoisonicotinamide (20f). Method A, white solid, yield 56.1% over 2 steps. 1H NMR (300 MHz, $CDCl_3$) δ 9.60 (t, J = 5.5 Hz, 1H), 8.53 (d, J = 4.3 Hz, 2H), 7.98 (d, J = 5.0 Hz, 1H), 6.97 (s, 1H), 6.85 (s, 2H), 4.54 (d, J = 5.5 Hz, 2H), 3.88 (s, 3H), 3.51 (t, J = 4.4 Hz, 4H), 2.99 (t, J = 4.6 Hz, 4H); ^{13}C NMR (75 MHz, $CDCl_3$) δ 164.00, 146.77, 146.68, 146.32, 145.05, 143.09, 134.62, 130.73, 124.40, 119.92, 114.83, 111.04, 66.62, 56.07, 53.12, 43.65; HR-MS (ESI) m/z : calcd for $C_{18}H_{22}N_3O_4$ $[M+H]^+$ 344.1605 found 344.1604.

5-Chloro-N-(3-hydroxy-4-methoxybenzyl)-2-morpholinobenzamide (20g). Method A, white solid, yield 53.2% over 2 steps. 1H NMR (300 MHz, $CDCl_3$) δ 9.93 (d, J = 6.6 Hz, 1H), 8.19 (d, J = 2.7 Hz, 1H), 7.39 (dd, J = 8.5, 2.8 Hz, 1H), 7.13 (d, J = 8.6 Hz, 1H), 6.95 (d, J = 2.0 Hz, 1H), 6.90–6.80 (m, 2H), 5.88 (s, 1H), 4.53 (d, J = 5.3 Hz, 2H), 3.89 (s, 3H), 3.50 (t, J = 4.5 Hz, 4H), 2.87 (t, J = 4.6 Hz, 4H); ^{13}C NMR (75 MHz, $CDCl_3$) δ 164.62, 149.28, 146.40, 146.15, 131.99, 131.78, 131.37, 131.15, 129.48, 122.17, 120.06, 114.66, 110.94, 66.79, 56.15, 53.51, 43.70; HR-MS (ESI) m/z : calcd for $C_{19}H_{22}ClN_2O_4$ $[M+H]^+$ 377.1263 found 377.1266.

5-Bromo-N-(3-hydroxy-4-methoxybenzyl)-2-morpholinobenzamide (20h). Method A, white solid, yield 59.0% over 2 steps. 1H NMR (300 MHz, $CDCl_3$) δ 9.86 (s, 1H), 8.33 (d, J = 2.5 Hz, 1H), 7.54 (dd, J = 8.5, 2.5 Hz, 1H), 7.06 (d, J = 8.6 Hz, 1H), 6.94 (s, 1H), 6.90–6.79 (m, 2H), 5.84 (s, 1H), 4.53 (d, J = 5.3 Hz, 2H), 3.89 (s, 3H), 3.50 (t, J = 4.5 Hz, 4H), 2.87 (t, J = 4.5 Hz, 4H); ^{13}C NMR (75 MHz, $CDCl_3$) δ 164.56, 149.78, 146.41, 146.15, 134.96, 134.70, 131.35, 129.68, 122.40, 120.04, 118.78, 114.66, 110.94, 66.75, 56.14, 53.42, 43.69; HR-MS (ESI) m/z : calcd for $C_{19}H_{22}BrN_2O_4$ $[M+H]^+$ 421.0757 found 421.0752.

N-(3-hydroxy-4-methoxybenzyl)-2-morpholino-5-(tri-fluoromethyl)benzamide (20i). Method A, white solid, yield 46.6%

over 2 steps. 1H NMR (300 MHz, $CDCl_3$) δ 9.39 (s, 1H), 8.43 (d, J = 2.3 Hz, 1H), 7.68 (dd, J = 8.4, 2.4 Hz, 1H), 7.24 (d, J = 8.4 Hz, 1H), 6.95 (d, J = 1.9 Hz, 1H), 6.93–6.85 (m, 1H), 6.83 (d, J = 8.2 Hz, 1H), 5.83 (s, 1H), 4.55 (d, J = 5.4 Hz, 2H), 3.89 (s, 3H), 3.68–3.36 (m, 4H), 2.95 (dd, J = 5.5, 3.6 Hz, 4H); ^{13}C NMR (75 MHz, $CDCl_3$) δ 164.92, 153.51, 146.40, 146.13, 131.25, 129.35 (q, J = 3.7 Hz), 128.90 (q, J = 3.6 Hz), 128.40, 126.99 (q, J = 33.2 Hz), 123.92 (q, J = 270.5 Hz), 120.31, 120.11, 114.61, 110.92, 66.69, 56.15, 53.29, 43.70; HR-MS (ESI) m/z : calcd for $C_{20}H_{22}F_3N_2O_4$ $[M+H]^+$ 411.1526 found 411.1519.

N-(3-hydroxy-4-methoxybenzyl)-2-morpholino-4-nitrobenzamide (20j). Method A, white solid, yield 56.5% over 2 steps. 1H NMR (300 MHz, $CDCl_3$) δ 9.34 (s, 1H), 8.31 (d, J = 8.6 Hz, 1H), 8.06 (dd, J = 8.6, 2.1 Hz, 1H), 8.00 (d, J = 2.2 Hz, 1H), 6.96 (d, J = 1.9 Hz, 1H), 6.91–6.80 (m, 2H), 5.73 (s, 1H), 4.56 (d, J = 5.5 Hz, 2H), 3.91 (s, 3H), 3.54 (t, J = 4.6 Hz, 4H), 3.02–2.91 (m, 4H); ^{13}C NMR (75 MHz, $CDCl_3$) δ 164.30, 151.56, 149.91, 146.49, 146.18, 133.50, 133.14, 130.92, 120.13, 119.43, 115.21, 114.62, 110.93, 66.55, 56.15, 53.33, 43.77; HR-MS (ESI) m/z : calcd for $C_{19}H_{22}N_3O_6$ $[M+H]^+$ 388.1503 found 388.1498.

5-Bromo-N-(3-hydroxy-4-methoxybenzyl)-2-(piperidin-1-yl)benzamide (20k). Method A, white solid, yield 46.3% over 2 steps. 1H NMR (300 MHz, $CDCl_3$) δ 10.34 (s, 1H), 8.36 (d, J = 2.6 Hz, 1H), 7.50 (dd, J = 8.5, 2.6 Hz, 1H), 7.06 (d, J = 8.5 Hz, 1H), 6.94 (d, J = 2.0 Hz, 1H), 6.86 (dd, J = 8.2, 2.0 Hz, 1H), 6.81 (d, J = 8.2 Hz, 1H), 5.62 (s, 1H), 4.54 (d, J = 5.4 Hz, 2H), 3.88 (s, 3H), 2.80 (d, J = 5.2 Hz, 4H), 1.50–1.44 (m, 6H); ^{13}C NMR (75 MHz, $CDCl_3$) δ 164.82, 151.61, 146.16, 145.97, 134.75, 134.40, 131.70, 129.58, 122.90, 119.91, 118.32, 114.59, 110.89, 56.19, 54.83, 43.59, 26.15, 23.61; HR-MS (ESI) m/z : calcd for $C_{20}H_{24}BrN_2O_3$ $[M+H]^+$ 419.0965 found 419.0961.

N-(3-hydroxy-4-methoxybenzyl)-2-(piperidin-1-yl)-5-(tri-fluoromethyl)benzamide (20l). Method A, white solid, yield 57.7% over 2 steps. 1H NMR (300 MHz, $CDCl_3$) δ 9.86 (d, J = 6.9 Hz, 1H), 8.47 (d, J = 2.4 Hz, 1H), 7.63 (dd, J = 8.5, 2.4 Hz, 1H), 7.23 (s, 1H), 6.94 (d, J = 2.0 Hz, 1H), 6.87 (dd, J = 8.2, 2.0 Hz, 1H), 6.81 (d, J = 8.2 Hz, 1H), 5.60 (s, 1H), 4.56 (d, J = 5.5 Hz, 2H), 3.88 (s, 3H), 2.88 (t, J = 4.7 Hz, 4H), 1.51 (d, J = 12.4 Hz, 6H); ^{13}C NMR (75 MHz, $CDCl_3$) δ 165.12, 155.37, 146.21, 146.00, 131.56, 129.07 (q, J = 3.9 Hz), 128.65 (q, J = 3.8 Hz), 128.25, 126.29, 120.87, 119.93, 114.57, 110.91, 56.17, 54.73, 43.61, 26.09, 23.60; HR-MS (ESI) m/z : calcd for $C_{21}H_{24}F_3N_2O_3$ $[M+H]^+$ 409.1734 found 409.1731.

5-(Dimethylamino)-N-(3-hydroxy-4-methoxybenzyl)-2-morpholinobenzamide (20m). Method B, white solid, yield 46.3% over 2 steps. 1H NMR (300 MHz, $CDCl_3$) δ 10.84 (s, 1H), 7.70 (d, J = 3.2 Hz, 1H), 7.13 (d, J = 8.8 Hz, 1H), 6.96 (d, J = 2.0 Hz, 1H), 6.89–6.76 (m, 3H), 5.91 (s, 1H), 4.54 (d, J = 5.2 Hz, 2H), 3.88 (s, 3H), 3.47 (d, J = 5.1 Hz, 4H), 2.97 (s, 6H), 2.82 (t, J = 4.6 Hz, 4H); ^{13}C NMR (75 MHz, $CDCl_3$) δ 166.21, 148.43, 146.23, 146.06, 140.19, 131.90, 128.07, 122.42, 119.99, 115.70, 115.08, 114.69, 110.86, 67.13, 56.14, 53.73, 43.65, 40.81; HR-MS (ESI) m/z : calcd for $C_{21}H_{28}N_3O_4$ $[M+H]^+$ 386.2074 found 386.2074.

N-(3-hydroxy-4-methoxybenzyl)-5-methoxy-2-morpholinobenzamide (20n). Method B, white solid, yield 54.9% over 2 steps. 1H NMR (300 MHz, $CDCl_3$) δ 10.67 (s, 1H), 7.84 (d, J = 3.2 Hz, 1H), 7.17 (d, J = 8.8 Hz, 1H), 7.03–6.94 (m, 2H), 6.87 (dd, J = 8.3, 2.0 Hz, 1H), 6.82 (d, J = 8.2 Hz, 1H), 5.87 (s, 1H), 4.54 (d, J = 5.2 Hz, 2H), 3.89 (s, 3H), 3.84 (s, 3H), 3.49 (t, J = 4.5 Hz, 4H), 2.85 (t, J = 4.6 Hz, 4H); ^{13}C NMR (75 MHz, $CDCl_3$) δ 165.47, 157.18, 146.29, 146.10, 143.97, 131.68, 128.93, 122.72, 120.02, 118.88, 115.11, 114.68, 110.88, 67.01, 56.14, 55.74, 53.72, 43.69; HR-MS (ESI) m/z : calcd for $C_{20}H_{25}N_2O_5$ $[M+H]^+$ 373.1758 found 373.1748.

5-Hydroxy-N-(3-hydroxy-4-methoxybenzyl)-2-morpholinobenzamide (20o). Method B, white solid, yield 16.8% over 3 steps. 1H NMR (300 MHz, $DMSO-d_6$) δ 10.32 (s, 1H), 9.50 (s, 1H), 8.96 (s, 1H), 7.37 (s, 1H), 7.20 (s, 1H), 6.88–6.74 (m, 4H), 4.35 (s, 2H), 3.74 (s, 3H), 3.43 (s, 4H), 2.75 (s, 4H); ^{13}C NMR (75 MHz,

DMSO- d_6) δ 164.98, 154.38, 146.86, 146.61, 142.56, 131.62, 129.42, 122.92, 118.65, 118.36, 116.46, 115.28, 112.25, 66.18, 55.73, 53.26, 42.38; HR-MS (ESI) m/z : calcd for $C_{19}H_{28}N_2O_5$ $[M+H]^+$ 359.1601 found 359.1597.

N-(3-hydroxy-4-methoxybenzyl)-5-methoxy-2-(piperidin-1-yl)benzamide (20p). Method B, white solid, yield 39.5% over 2 steps. 1H NMR (300 MHz, $CDCl_3$) δ 11.08 (s, 1H), 7.85 (d, J = 3.2 Hz, 1H), 7.16 (d, J = 8.8 Hz, 1H), 6.98–6.92 (m, 2H), 6.87 (dd, J = 8.2, 2.1 Hz, 1H), 6.81 (d, J = 8.2 Hz, 1H), 5.61 (s, 1H), 4.55 (d, J = 5.3 Hz, 2H), 3.88 (s, 3H), 3.83 (s, 3H), 2.78 (d, J = 5.2 Hz, 4H), 1.44 (s, 6H); ^{13}C NMR (75 MHz, $CDCl_3$) δ 165.82, 156.82, 146.08, 145.95, 145.86, 132.07, 128.72, 122.95, 119.88, 118.78, 116.32, 114.78, 114.64, 110.88, 56.19, 55.70, 55.02, 43.55, 26.35, 23.70; HR-MS (ESI) m/z : calcd for $C_{21}H_{27}N_2O_4$ $[M+H]^+$ 371.1965 found 371.1958.

4.1.8. The general procedures for the preparation of intermediates 19a-d

To the solutions of 2-fluorobenzoic acid (**10**) or 2,5-difluorobenzoic acid (**17**) (35.7 mmol) in 20 mL EtOH, a catalytic amount of concentrated H_2SO_4 was added, and the mixtures were refluxed overnight. The solvents were then removed and the residues were extracted with DCM (3×50 mL). The combined organic layers were then washed with brine, dried over anhydrous Na_2SO_4 , and concentrated in vacuo to provide **18a** or **18b**. To the solutions of intermediates **18a** or **18b** (29.1 mmol) in 20 mL DMSO, morpholine (14.3 mL, 145.7 mmol) or piperidine (13.3 mL, 145.7 mmol) were added. The mixtures were stirred at 120 °C for 6 h, and then diluted with 50 mL EtOAc, washed with water (20 mL \times 3), saturated brine, dried over anhydrous Na_2SO_4 , and concentrated in vacuo to afford crude products. To the solutions of the above crude products in 10 mL CH_3OH , 10 mL 10% NaOH aqueous was added and the mixtures were stirred at 80 °C for 30 min. CH_3OH was then removed in vacuo and acidized with 10% HCl aqueous to pH 3. The precipitates were collected by filtration, washed with water and dried to afford **19a-d**.

2-Morpholinobenzoic acid (19a). White solid, yield 55.4%. 1H NMR (300 MHz, DMSO- d_6) δ 8.02–7.93 (m, 1H), 7.64 (d, J = 2.9 Hz, 2H), 7.37 (td, J = 5.4, 2.5 Hz, 1H), 3.80 (t, J = 4.6 Hz, 4H), 3.06 (t, J = 4.6 Hz, 4H); ^{13}C NMR (75 MHz, DMSO- d_6) δ 167.29, 150.95, 134.12, 131.36, 126.58, 125.40, 123.04, 66.79, 53.06; ESI-MS m/z 207.1 $[M-H]^-$ 206.1.

5-Fluoro-2-morpholinobenzoic acid (19b). White solid, yield 44.9%. 1H NMR (300 MHz, DMSO- d_6) δ 7.75–7.68 (m, 1H), 7.68–7.59 (m, 1H), 7.52–7.39 (m, 1H), 3.76 (t, J = 4.4 Hz, 4H), 3.03 (t, J = 4.5 Hz, 4H); ^{13}C NMR (75 MHz, DMSO- d_6) δ 166.02, 160.09 (d, J = 243.0 Hz), 146.97 (d, J = 3.0 Hz), 127.82 (d, J = 7.5 Hz), 125.85 (d, J = 8.3 Hz), 120.95 (d, J = 21.8 Hz), 117.14 (d, J = 23.3 Hz), 66.74, 53.17; ESI-MS m/z 225.1 $[M-H]^-$ 224.1.

2-(Piperidin-1-yl)benzoic acid (19c). White solid, yield 49.3%. 1H NMR (300 MHz, DMSO- d_6) δ 8.01 (d, J = 7.8 Hz, 1H), 7.69 (d, J = 8.0 Hz, 1H), 7.66–7.59 (m, 1H), 7.45–7.36 (m, 1H), 3.01 (t, J = 5.2 Hz, 4H), 1.79–1.68 (m, 4H), 1.65–1.50 (m, 2H); ^{13}C NMR (75 MHz, DMSO- d_6) δ 167.14, 150.97, 134.08, 131.20, 127.76, 125.34, 123.47, 54.15, 26.07, 22.68; ESI-MS m/z 205.1 $[M-H]^-$ 204.1.

5-Fluoro-2-(piperidin-1-yl)benzoic acid (19d). White solid, yield 53.6%. 1H NMR (300 MHz, DMSO- d_6) δ 18.54 (s, 1H), 7.85 (dd, J = 8.9, 4.8 Hz, 1H), 7.73 (dd, J = 9.1, 3.2 Hz, 1H), 7.55 (td, J = 8.5, 3.2 Hz, 1H), 3.09 (t, J = 5.4 Hz, 4H), 1.76 (p, J = 5.5 Hz, 4H), 1.68–1.58 (m, 2H); ^{13}C NMR (75 MHz, DMSO- d_6) δ 166.01, 160.73 (d, J = 243.8 Hz), 146.59, 128.05 (d, J = 7.5 Hz), 126.05 (d, J = 8.3 Hz), 120.92 (d, J = 22.5 Hz), 116.92 (d, J = 23.3 Hz), 54.20, 25.95, 22.48; ESI-MS m/z 223.1 $[M-H]^-$ 222.1.

4.1.9. The general procedures for the preparation of intermediates 24a-f

To the solutions of various 2-fluorobenzoic acids **23a-d** (2.7 mmol) in 20 mL dioxane, morpholine (1.2 mL, 13.5 mmol) or piperidine (1.1 mL, 13.5 mmol) was added in one portion. The reactions were stirred at refluxing temperature, after the reactions completed, solvents and remaining morpholine or piperidine were removed in vacuo. Then, the residues were dissolved into water and neutralized by 10% HCl aqueous. The resulting precipitate were collected, washed by water, and dried to give intermediates **24a-f**.

5-Chloro-2-morpholinobenzoic acid (24a). White solid, yield 84.5%. 1H NMR (300 MHz, DMSO- d_6) δ 15.54 (s, 1H), 7.78 (d, J = 2.7 Hz, 1H), 7.62 (dd, J = 8.8, 2.6 Hz, 1H), 7.50 (d, J = 8.7 Hz, 1H), 3.73 (t, J = 4.5 Hz, 4H), 3.01 (t, J = 4.6 Hz, 4H); ^{13}C NMR (75 MHz, DMSO- d_6) δ 166.62, 149.77, 133.35, 130.48, 129.50, 127.30, 124.33, 66.65, 52.78; ESI-MS m/z 241.1 $[M-H]^-$ 240.1.

5-Bromo-2-morpholinobenzoic acid (24b). White solid, yield 73.8%. 1H NMR (300 MHz, DMSO- d_6) δ 15.47 (s, 1H), 7.96 (d, J = 2.6 Hz, 1H), 7.76 (dd, J = 8.6, 2.6 Hz, 1H), 7.46 (d, J = 8.7 Hz, 1H), 3.77 (t, J = 4.4 Hz, 4H), 3.05 (t, J = 4.5 Hz, 4H); ^{13}C NMR (75 MHz, DMSO- d_6) δ 166.54, 150.22, 136.23, 133.47, 127.43, 124.45, 117.34, 66.64, 52.73; ESI-MS m/z 285.0 $[M-H]^-$ 284.0.

2-Morpholino-5-(trifluoromethyl)benzoic acid (24c). White solid, yield 79.6%. 1H NMR (300 MHz, DMSO- d_6) δ 13.91 (s, 1H), 7.96 (d, J = 2.4 Hz, 1H), 7.80 (dd, J = 8.7, 2.4 Hz, 1H), 7.36 (d, J = 8.6 Hz, 1H), 3.76 (t, J = 4.5 Hz, 4H), 3.13 (t, J = 4.5 Hz, 4H); ^{13}C NMR (75 MHz, DMSO- d_6) δ 167.89, 154.15, 129.61 (d, J = 3.8 Hz), 128.34 (d, J = 3.8 Hz), 126.36, 124.33, 121.97 (q, J = 37.0 Hz), 120.26, 66.43, 52.00; ESI-MS m/z 275.0 $[M-H]^-$ 274.0.

2-Morpholino-4-nitrobenzoic acid (24d). Yellow solid, yield 93.4%. 1H NMR (300 MHz, DMSO- d_6) δ 7.81 (s, 1H), 7.79 (s, 2H), 3.69 (t, J = 4.6 Hz, 4H), 3.06 (t, J = 4.6 Hz, 4H); ^{13}C NMR (75 MHz, DMSO- d_6) δ 168.09, 151.66, 150.04, 132.17, 131.10, 116.60, 114.08, 66.44, 52.02; ESI-MS m/z 252.1 $[M-H]^-$ 251.1.

5-Bromo-2-(piperidin-1-yl)benzoic acid (24e). White solid, yield 86.8%. 1H NMR (300 MHz, DMSO- d_6) δ 17.90 (s, 1H), 8.08 (d, J = 2.6 Hz, 1H), 7.85 (dd, J = 8.6, 2.6 Hz, 1H), 7.69 (d, J = 8.6 Hz, 1H), 3.07 (t, J = 5.2 Hz, 4H), 1.73 (q, J = 5.5 Hz, 4H), 1.68–1.56 (m, 2H); ^{13}C NMR (75 MHz, DMSO- d_6) δ 166.00, 149.89, 136.54, 133.38, 127.62, 125.77, 119.95, 53.94, 25.93, 22.63; ESI-MS m/z 283.0 $[M-H]^-$ 282.0.

2-(Piperidin-1-yl)-5-(trifluoromethyl)benzoic acid (24f). White solid, yield 83.5%. 1H NMR (300 MHz, DMSO- d_6) δ 15.90 (s, 1H), 8.03 (d, J = 2.5 Hz, 1H), 7.84 (dd, J = 8.6, 2.5 Hz, 1H), 7.59 (d, J = 8.6 Hz, 1H), 3.06 (t, J = 5.1 Hz, 4H), 1.71–1.62 (m, 4H), 1.61–1.53 (m, 2H); ^{13}C NMR (75 MHz, DMSO- d_6) δ 167.09, 154.41, 129.99 (d, J = 3.0 Hz), 127.99 (d, J = 3.8 Hz), 126.15, 125.21, 124.32 (q, J = 32.5 Hz), 122.47, 53.37, 25.83, 23.16; ESI-MS m/z 273.0 $[M-H]^-$ 272.0.

4.1.10. Ethyl 5-amino-2-morpholinobenzoate (26)

To the solutions of **12** (39.7 mmol) in 20 mL EtOH, a catalytic amount of concentrated H_2SO_4 was added, and the mixtures were refluxed overnight. The solvents were then removed and the residues were extracted with DCM (3×50 mL). The combined organic layers were then washed with brine, dried over anhydrous Na_2SO_4 , and concentrated in vacuo to provide **25**. Ethyl 2-morpholino-5-nitrobenzoate (**25**) (5 g, 17.9 mmol) was dissolved into the mixture solvent of 20 mL EtOH and 20 mL AcOH, Fe powder (6 g, 107.2 mmol) was added, and the mixture was stirred at 65 °C for 30 min. Then, the solvent was removed in vacuo, and the residue was neutralized by saturated $NaHCO_3$ aqueous. The mixture was

filtrated, and the filtrates was extracted with EtOAc (3 × 50 mL), the combined organic layers were then washed with saturated brine, dried over anhydrous Na₂SO₄, and concentrated in vacuo to afford the crude product, which was purified by column chromatography with petroleum/ethyl acetate (2:1) to give 3.5 g **26** as yellow solid, yield 76.1%. ¹H NMR (300 MHz, DMSO-*d*₆) δ 6.90 (d, *J* = 8.7 Hz, 1H), 6.71 (s, 1H), 6.67–6.57 (m, 1H), 5.02 (s, 2H), 4.17 (q, *J* = 8.7 Hz, 2H), 3.59 (s, 4H), 2.73 (s, 4H), 1.34–1.14 (m, 3H); ¹³C NMR (75 MHz, DMSO-*d*₆) δ 168.39, 145.05, 141.21, 129.00, 121.79, 117.56, 114.83, 67.09, 60.71, 53.77, 14.66; ESI-MS *m/z* 250.1 [M+H]⁺ 251.1.

4.1.11. 5-(Dimethylamino)-2-morpholinobenzoic acid (**27**)

To a solution of **26** (200 mg, 0.8 mmol) in 5 mL AcOH, NaBH₃CN (200 mg, 3.2 mmol) was added. The mixture was stirred at room temperature for 30 min. Then, the solvent was removed in vacuo and the residue was neutralized by saturated NaHCO₃ aqueous. The mixture was filtrated, and the filtrates was extracted with EtOAc (3 × 25 mL), the combined organic layers were then washed with saturated brine, dried over anhydrous Na₂SO₄, and concentrated in vacuo to afford the crude product. To the solution of the above crude product in 10 mL CH₃OH, 10 mL 10% NaOH aqueous was added and the mixtures were stirred at 80 °C for 30 min CH₃OH was then removed in vacuo and acidized with 10% HCl aqueous to pH 3. The precipitates were collected by filtration, washed with water and dried to afford 154 mg **27** as grey solid, yield 65.4% over 2 steps. ¹H NMR (300 MHz, DMSO-*d*₆) δ 17.78 (s, 1H), 7.61 (dd, *J* = 8.9, 4.5 Hz, 1H), 7.34 (d, *J* = 1.8 Hz, 0H), 7.04 (d, 1H), 3.83 (t, *J* = 4.8 Hz, 4H), 3.05 (t, *J* = 4.8 Hz, 4H), 2.99 (s, 2H); ¹³C NMR (75 MHz, DMSO-*d*₆) δ 167.39, 149.47, 139.07, 125.52, 124.47, 117.61, 113.10, 66.88, 53.38, 40.50; ESI-MS *m/z* 250.1 [M – H][–] 249.1.

4.1.12. Ethyl 2-morpholino-5-(4,4,5,5-tetramethyl-1,3,2-dioxaborolan-2-yl)benzoate (**30a**)

To the solutions of **28a** (35.0 mmol) in 20 mL EtOH, a catalytic amount of concentrated H₂SO₄ was added, and the mixtures were refluxed overnight. The solvents were then removed and the residues were extracted with DCM (3 × 50 mL). The combined organic layers were then washed with brine, dried over anhydrous Na₂SO₄, and concentrated in vacuo to provide **29a**. To a solution of intermediate **29a** (500 mg, 1.59 mmol) in 20 mL dioxane, PdCl₂(CH₃CN)₂ (110 mg, 0.16 mmol), bis(pinacolato)diboron (613 mg, 2.39 mmol), and KOAc (470 mg, 4.77 mmol) were added. The mixture was stirred at 80 °C for 3 h. Then, the mixture was filtrated and the filtrate was concentrated in vacuo to afford the crude product, which was purified by column chromatography with petroleum/ethyl acetate (20:1) to give 495 mg **30a** as colorless oil, yield 86.1%. ¹H NMR (300 MHz, CDCl₃) δ 8.14 (d, *J* = 1.9 Hz, 1H), 7.89–7.81 (m, 1H), 6.98 (dd, *J* = 8.3, 1.6 Hz, 1H), 4.35 (q, *J* = 6.6, 6.0 Hz, 2H), 3.86 (t, *J* = 3.9 Hz, 4H), 3.10 (t, *J* = 3.4 Hz, 4H), 1.40 (t, *J* = 7.1 Hz, 3H), 1.33 (s, 12H); ¹³C NMR (75 MHz, CDCl₃) δ 168.19, 154.03, 139.08, 138.18, 123.21, 117.36, 83.80, 66.91, 60.94, 52.25, 25.01, 24.83, 24.54, 14.37; ESI-MS *m/z* 261.2 [M+H]⁺ 262.2.

The synthetic methods of intermediates **29b** and **30b** were the same as methods for the preparation of **29a** and **30a**.

Ethyl 5-bromo-2-(piperidin-1-yl)benzoate (29b). colorless oil, yield 89.5%. ¹H NMR (300 MHz, CDCl₃) δ 7.81 (d, *J* = 2.5 Hz, 1H), 7.48 (dd, *J* = 8.8, 2.5 Hz, 1H), 6.92 (d, *J* = 8.8 Hz, 1H), 4.40 (q, *J* = 7.1 Hz, 2H), 3.09–2.88 (m, 4H), 1.85–1.67 (m, 4H), 1.65–1.55 (m, 2H), 1.43 (t, *J* = 7.1 Hz, 3H); ¹³C NMR (75 MHz, CDCl₃) δ 167.02, 152.15, 134.92, 133.75, 125.89, 120.57, 112.75, 61.21, 53.72, 26.04, 24.10, 14.32; ESI-MS *m/z* 311.1 [M+H]⁺ 312.1.

Ethyl 2-(piperidin-1-yl)-5-(4,4,5,5-tetramethyl-1,3,2-dioxaborolan-2-yl)benzoate (30b). colorless oil, yield 85.4%. ¹H NMR (300 MHz, CDCl₃) δ 8.10 (d, *J* = 1.6 Hz, 1H), 7.81 (dd, *J* = 8.2, 1.7 Hz, 1H), 6.99 (d, *J* = 8.3 Hz, 1H), 4.39 (q, *J* = 7.1 Hz, 2H), 3.15–3.04

(m, 4H), 1.74 (p, *J* = 5.6 Hz, 4H), 1.67–1.56 (m, 2H), 1.43 (t, *J* = 7.1 Hz, 3H), 1.37 (s, 12H); ¹³C NMR (100 MHz, CDCl₃) δ 168.77, 154.82, 138.69, 137.96, 122.95, 117.36, 83.62, 60.80, 53.16, 25.97, 24.85, 24.25, 14.38; ESI-MS *m/z* 359.2 [M+H]⁺ 360.2.

4.1.13. Ethyl 5-hydroxy-2-morpholinobenzoate (**31a**)

To a solution of **30a** (320 mg, 0.89 mmol) in 20 mL CH₃OH, 2 mL 30% H₂O₂ aqueous was added dropwise. The mixture was stirred at room temperature for 30 min. Then, the CH₃OH was removed in vacuo. The residue was extracted with EtOAc (3 × 25 mL), and the combined organic layers were then washed with saturated brine, dried over anhydrous Na₂SO₄, and concentrated in vacuo to afford the crude product, which was purified by column chromatography with petroleum/ethyl acetate (5:1) to give 208 mg **31a** as white solid, yield 93.4%. ¹H NMR (300 MHz, CDCl₃) δ 7.19 (d, *J* = 2.9 Hz, 1H), 7.00 (d, *J* = 8.7 Hz, 1H), 6.95–6.90 (m, 1H), 4.35 (q, *J* = 7.1 Hz, 2H), 3.85 (t, 4H), 2.96 (t, 4H), 1.38 (t, *J* = 7.1 Hz, 3H); ¹³C NMR (75 MHz, CDCl₃) δ 167.93, 151.77, 145.21, 127.55, 121.30, 119.44, 117.41, 67.31, 61.23, 53.49, 24.79; ESI-MS *m/z* 251.1 [M+H]⁺ 252.1.

The synthesis method of intermediate **31b** was the same as that of **31a**.

Ethyl 5-hydroxy-2-(piperidin-1-yl)benzoate (31b). white solid, yield 89.7%. ¹H NMR (300 MHz, CDCl₃) δ 7.21 (dd, *J* = 9.1, 2.9 Hz, 1H), 7.04–6.97 (m, 1H), 6.97–6.90 (m, 1H), 4.38 (p, *J* = 7.0 Hz, 2H), 3.92 (s, 1H), 3.01–2.71 (m, 4H), 1.73 (p, *J* = 5.6 Hz, 4H), 1.57 (q, *J* = 5.6, 5.1 Hz, 2H), 1.42 (t, *J* = 7.1 Hz, 3H); ¹³C NMR (75 MHz, CDCl₃) δ 168.66, 150.72, 146.81, 126.95, 121.05, 119.32, 117.28, 61.28, 54.70, 26.35, 24.16, 14.28; ESI-MS *m/z* 249.1 [M+H]⁺ 250.1.

4.1.14. The general procedures for the preparation of intermediates **32a-c**

To the solutions of **31a-b** (0.48 mmol) in anhydrous THF, NaH (29 mg, 0.72 mmol, 60%) was added and stirred at 0 °C under nitrogen atmosphere for 15 min. Then, (CH₃)₂SO₄ (0.45 mL, 0.53 mmol) or benzyl bromide (63 μL, 0.53 mmol) were added, and the mixtures were stirred at 0 °C for another 30 min. The mixtures were extracted with EtOAc (3 × 25 mL), and the combined organic layers were washed with saturated brine, dried over anhydrous Na₂SO₄, and concentrated in vacuo to afford the crude products. To the solutions of the above crude products in 10 mL CH₃OH, 10 mL 10% NaOH aqueous was added and the mixtures were stirred at 80 °C for 30 min CH₃OH was then removed in vacuo and acidized with 10% HCl aqueous to pH 3. The precipitates were collected by filtration, washed with water and dried to afford **32a-c**.

Ethyl 5-methoxy-2-morpholinobenzoate (32a). White solid, yield 57.5% over 2 steps. ¹H NMR (300 MHz, DMSO-*d*₆) δ 7.68 (d, *J* = 8.8 Hz, 1H), 7.47 (d, *J* = 3.1 Hz, 1H), 7.20 (dd, *J* = 8.9, 3.1 Hz, 1H), 3.78 (s, 3H), 3.75 (s, 4H), 3.02 (t, *J* = 4.6 Hz, 4H); ¹³C NMR (75 MHz, DMSO-*d*₆) δ 166.65, 158.13, 143.39, 126.61, 125.32, 120.39, 114.79, 66.83, 56.03, 53.29; ESI-MS *m/z* 237.1 [M – H][–] 236.1.

Ethyl 5-(benzyloxy)-2-morpholinobenzoate (32b). White solid, yield 63.3% over 2 steps. ¹H NMR (300 MHz, DMSO-*d*₆) δ 17.42 (s, 1H), 7.69 (d, *J* = 8.9 Hz, 1H), 7.58 (d, *J* = 3.1 Hz, 1H), 7.54–7.42 (m, 2H), 7.40 (s, 1H), 7.37 (d, *J* = 6.0 Hz, 1H), 7.31 (dd, *J* = 8.2, 5.0 Hz, 2H), 5.17 (s, 2H), 3.78 (t, *J* = 4.8 Hz, 4H), 3.04 (t, *J* = 5.0 Hz, 4H); ¹³C NMR (75 MHz, DMSO-*d*₆) δ 166.71, 157.12, 143.58, 137.14, 128.93, 128.38, 128.08, 125.22, 120.98, 115.87, 70.06, 66.83, 53.28; ESI-MS *m/z* 313.1 [M – H][–] 312.1.

Ethyl 5-methoxy-2-(piperidin-1-yl)benzoate (32c). White solid, yield 54.6% over 2 steps. ¹H NMR (300 MHz, DMSO-*d*₆) δ 18.73 (s, 1H), 7.69 (dd, *J* = 8.9, 3.6 Hz, 1H), 7.58–7.47 (m, 1H), 7.22 (d, *J* = 8.9 Hz, 1H), 3.80 (s, 3H), 3.04 (t, *J* = 5.2 Hz, 4H), 1.87–1.69 (m, 4H), 1.62 (s, 2H); ¹³C NMR (75 MHz, DMSO-*d*₆) δ 166.99, 158.36, 143.12, 126.76, 124.75, 120.01, 114.52, 55.99, 54.24, 26.02, 22.47; ESI-MS *m/z* 235.1 [M – H][–] 234.1.

4.1.15. The general procedures for the preparation of intermediates **33a-c**

To the solutions of intermediate **26** (200 mg, 0.8 mmol) in 10 mL CH₃OH, various aldehydes (0.96 mmol) were added and stirred for 30 min, then NaBH₄ (46 mg, 1.2 mmol) was added and stirred for another 15 min. The reactions were quenched with saturated NH₄Cl aqueous and extracted with EtOAc (3 × 25 mL), and the combined organic layers were washed with saturated brine, dried over anhydrous Na₂SO₄, and concentrated in vacuo to afford the crude products. To the solutions of the above crude products in 10 mL CH₃OH, 10 mL 10% NaOH aqueous was added and the mixtures were stirred at 80 °C for 30 min CH₃OH was then removed in vacuo and acidized with 10% HCl aqueous to pH 3. The precipitates were collected by filtration, washed with water and dried to afford **33a-c**.

5-((4-Methoxybenzyl)amino)-2-morpholinobenzoic acid (33a) Grey solid, yield 66.9% over 2 steps. ¹H NMR (300 MHz, DMSO-*d*₆) δ 7.39 (d, *J* = 8.5 Hz, 1H), 7.23 (d, *J* = 8.7 Hz, 2H), 6.85 (d, *J* = 8.2 Hz, 2H), 6.81–6.75 (m, 1H), 6.61 (d, *J* = 5.9 Hz, 1H), 4.19 (s, 2H), 3.75–3.70 (m, 4H), 3.68 (s, 3H), 2.93 (t, *J* = 4.6 Hz, 4H); ¹³C NMR (75 MHz, DMSO-*d*₆) δ 167.34, 158.63, 148.08, 138.74, 131.82, 128.75, 125.64, 124.38, 117.31, 114.25, 113.47, 66.87, 55.46, 53.38, 46.19; ESI-MS *m/z* 342.2 [M – H][–] 341.2.

2-Morpholino-5-((pyridin-4-ylmethyl)amino)benzoic acid (33b) Grey solid, yield 54.4% over 2 steps. ¹H NMR (300 MHz, DMSO-*d*₆) δ 17.73 (s, 1H), 8.48 (d, *J* = 5.1 Hz, 2H), 7.44 (d, *J* = 8.7 Hz, 1H), 7.33 (d, *J* = 5.2 Hz, 2H), 7.21 (d, *J* = 2.9 Hz, 1H), 6.82 (s, 1H), 6.78 (dd, *J* = 8.7, 3.0 Hz, 1H), 4.35 (d, *J* = 4.1 Hz, 2H), 3.75 (t, 4H), 2.95 (t, *J* = 4.4 Hz, 4H); ¹³C NMR (75 MHz, DMSO-*d*₆) δ 167.25, 149.99, 149.63, 147.69, 139.16, 125.78, 124.57, 122.61, 117.31, 113.53, 66.85, 53.35, 45.69; ESI-MS *m/z* 313.1 [M – H][–] 312.1.

5-((Furan-2-ylmethyl)amino)-2-morpholinobenzoic acid (33c) Grey solid, yield 49.8% over 2 steps. ¹H NMR (300 MHz, DMSO-*d*₆) δ 7.54 (s, 1H), 7.44 (d, *J* = 8.7 Hz, 1H), 7.27 (d, *J* = 2.7 Hz, 1H), 6.96–6.82 (m, 1H), 6.53 (t, *J* = 6.1 Hz, 1H), 6.35 (s, 1H), 6.25 (d, *J* = 3.1 Hz, 1H), 4.24 (d, *J* = 5.9 Hz, 2H), 3.74 (t, *J* = 4.5 Hz, 4H), 2.95 (t, *J* = 4.5 Hz, 4H); ¹³C NMR (75 MHz, DMSO-*d*₆) δ 167.30, 153.25, 147.74, 142.54, 139.09, 125.67, 124.43, 117.34, 113.55, 110.84, 107.45, 66.88, 53.38; ESI-MS *m/z* 302.1 [M – H][–] 301.1.

4.1.16. The general procedures for the preparation of intermediates **33d-g**

To the solutions of intermediate **26** (200 mg, 0.8 mmol) in 10 mL CH₃CN, various benzoic acids (0.96 mmol), HATU (366 mg, 0.96 mmol), and Et₃N (134 μL, 0.96 mmol) were added. The mixtures were stirred for 2 h, and extracted with DCM (3 × 25 mL). The combined organic layers were then washed with brine, dried over anhydrous Na₂SO₄, and concentrated in vacuo to provide the crude products. To the solutions of the above products in 10 mL CH₃OH, 10 mL 10% NaOH aqueous was added and the mixtures were stirred at 80 °C for 30 min CH₃OH was then removed in vacuo and acidized with 10% HCl aqueous to pH 3. The precipitates were collected by filtration, washed with water and dried to afford **33d-f**. For intermediate **33g**, intermediate **26** (200 mg, 0.8 mmol) in 10 mL CH₃CN, acetic anhydride (91 μL, 0.96 mmol), and Et₃N (134 μL, 0.96 mmol) were added. The mixtures were stirred for 2 h, and extracted with EtOAc (3 × 25 mL). The combined organic layers were then washed with brine, dried over anhydrous Na₂SO₄, and concentrated in vacuo to provide the crude product, which was further hydrolyzed in above procedure to afford **33g**.

5-(4-Methoxybenzamido)-2-morpholinobenzoic acid (33d) White solid, yield 42.5% over 2 steps. ¹H NMR (300 MHz, DMSO-*d*₆) δ 10.30 (s, 1H), 8.39 (s, 1H), 8.09 (d, *J* = 8.7 Hz, 1H), 7.96 (d, *J* = 8.4 Hz, 1H), 7.86 (d, *J* = 8.3 Hz, 2H), 7.04 (d, *J* = 8.3 Hz, 1H), 6.98 (d, *J* = 8.4 Hz, 2H), 3.81 (s, 3H), 3.79 (s, 4H), 3.03 (s, 4H); ¹³C NMR (75 MHz, DMSO-*d*₆) δ 167.44, 163.27, 138.41, 138.41, 131.78, 130.17,

125.61, 123.89, 123.44, 122.60, 114.24, 114.10, 66.82, 55.87, 53.24; ESI-MS *m/z* 356.1 [M – H][–] 355.1.

5-(Isonicotinamido)-2-morpholinobenzoic acid (33e) Grey solid, yield 46.8% over 2 steps. ¹H NMR (300 MHz, DMSO-*d*₆) δ 16.83 (s, 1H), 10.69 (s, 1H), 8.77 (s, 2H), 8.38 (s, 1H), 8.07 (d, *J* = 8.7 Hz, 1H), 7.85 (s, 2H), 7.69 (d, *J* = 8.7 Hz, 1H), 3.77 (s, 4H), 3.04 (s, 4H); ¹³C NMR (75 MHz, DMSO-*d*₆) δ 172.36, 166.90, 164.54, 150.80, 146.49, 141.84, 137.37, 125.72, 123.93, 122.88, 122.01, 66.83, 53.24; ESI-MS *m/z* 327.1 [M – H][–] 326.1.

5-(Furan-2-carboxamido)-2-morpholinobenzoic acid (33f) Grey solid, yield 50.9% over 2 steps. ¹H NMR (300 MHz, DMSO-*d*₆) δ 16.84 (s, 1H), 10.34 (s, 1H), 8.31 (d, *J* = 2.6 Hz, 1H), 7.98 (dd, *J* = 8.8, 2.7 Hz, 1H), 7.86 (d, *J* = 1.6 Hz, 1H), 7.59 (d, *J* = 8.8 Hz, 1H), 7.30 (d, *J* = 3.5 Hz, 1H), 6.62 (dd, *J* = 3.5, 1.7 Hz, 1H), 3.71 (t, 4H), 2.96 (t, *J* = 4.6 Hz, 4H); ¹³C NMR (75 MHz, DMSO-*d*₆) δ 166.87, 161.45, 156.75, 147.59, 146.45, 146.05, 137.51, 125.70, 123.98, 122.60, 115.57, 112.67, 66.81, 53.19; ESI-MS *m/z* 316.1 [M – H][–] 315.1.

5-Acetamido-2-morpholinobenzoic acid (33g) White solid, yield 64.5% over 2 steps. ¹H NMR (300 MHz, DMSO-*d*₆) δ 10.14 (s, 1H), 8.17 (d, *J* = 2.6 Hz, 1H), 7.86 (dd, *J* = 8.8, 2.6 Hz, 1H), 7.61 (d, *J* = 8.7 Hz, 1H), 3.76 (t, *J* = 4.5 Hz, 4H), 3.00 (t, *J* = 4.5 Hz, 4H), 2.02 (s, 3H); ¹³C NMR (75 MHz, DMSO-*d*₆) δ 168.99, 166.82, 145.37, 138.34, 125.70, 124.32, 124.12, 121.16, 66.80, 53.21, 24.40; ESI-MS *m/z* 264.1 [M – H][–] 263.1.

4.1.17. The general procedures for the preparation of intermediates **33h-j**

To a solution of **30a** (200 mg, 0.55 mmol) in 20 mL DMF, various bromobenzenes (0.66 mmol), Pd(PPh₃)₄ (60 mg, 0.06 mmol), and K₂CO₃ (152 mg, 1.1 mmol) were added. The mixture was stirred at 90 °C for 2 h. Then, the mixtures were filtered and the filtrates were concentrated in vacuo to afford the crude products, which were dissolved into 10 mL CH₃OH, 10 mL 10% NaOH aqueous was added and the mixtures were stirred at 80 °C for 30 min CH₃OH was then removed in vacuo and acidized with 10% HCl aqueous to pH 3. The precipitates were collected by filtration, washed with water and dried to afford **33h-j**.

4'-Methoxy-4-morpholino-[1,1'-biphenyl]-3-carboxylic acid (33h) White solid, yield 57.9% over 2 steps. ¹H NMR (300 MHz, DMSO-*d*₆) δ 8.11 (s, 1H), 7.82 (s, 1H), 7.59 (s, 2H), 7.00 (s, 2H), 3.77 (s, 7H), 3.05 (s, 4H); ¹³C NMR (75 MHz, DMSO-*d*₆) δ 167.40, 166.41, 159.64, 149.46, 137.85, 131.46, 128.56, 128.21, 125.88, 123.46, 114.97, 66.80, 55.64, 53.03; ESI-MS *m/z* 313.1 [M – H][–] 312.1.

2-Morpholino-5-(pyridin-4-yl)benzoic acid (33i) Grey solid, yield 44.3% over 2 steps. ¹H NMR (300 MHz, DMSO-*d*₆) δ 15.71 (s, 1H), 8.10 (s, 2H), 7.89 (d, *J* = 8.4 Hz, 2H), 7.79–7.38 (m, 3H), 3.77 (s, 4H), 3.07 (s, 6H); ¹³C NMR (75 MHz, DMSO-*d*₆) δ 167.54, 156.64, 150.41, 146.73, 135.80, 131.70, 128.98, 125.89, 123.16, 116.74, 66.75, 53.35, 52.88; ESI-MS *m/z* 282.1 [M – H][–] 281.1.

5-(Furan-2-yl)-2-morpholinobenzoic acid (33j) White solid, yield 55.4% over 2 steps. ¹H NMR (300 MHz, DMSO-*d*₆) δ 15.93 (s, 1H), 8.23 (d, *J* = 2.2 Hz, 1H), 7.91 (dd, *J* = 8.5, 2.3 Hz, 1H), 7.78 (d, *J* = 1.7 Hz, 1H), 7.59 (d, *J* = 8.5 Hz, 1H), 7.03 (d, *J* = 3.4 Hz, 1H), 6.62 (dd, *J* = 3.4, 1.8 Hz, 1H), 3.88–3.69 (m, 4H), 3.16–2.98 (m, 4H); ¹³C NMR (75 MHz, DMSO-*d*₆) δ 167.36, 152.19, 149.77, 143.76, 128.56, 127.92, 125.90, 125.78, 123.13, 112.70, 106.94, 66.71, 52.85; ESI-MS *m/z* 273.1 [M – H][–] 272.1.

4.1.18. The general procedures for the preparation of target compounds **34a-j**

The synthetic methods of **34a-j** were the same as method B for the preparation of **20a-p**.

N-(3-hydroxy-4-methoxybenzyl)-5-((4-methoxybenzyl)amino)-2-morpholinobenzoamide (34a) White solid, yield 66.9% over 2 steps. ¹H NMR (300 MHz, CDCl₃) δ 10.84 (d, *J* = 5.4 Hz, 1H),

7.62 (d, $J = 3.0$ Hz, 1H), 7.32–7.25 (m, 2H), 7.05 (d, $J = 8.6$ Hz, 1H), 6.96 (d, $J = 1.9$ Hz, 1H), 6.92–6.74 (m, 4H), 6.65 (dd, $J = 8.5, 3.0$ Hz, 1H), 5.95 (s, 1H), 4.52 (d, $J = 5.1$ Hz, 2H), 4.27 (s, 2H), 3.87 (s, 3H), 3.79 (s, 3H), 3.46 (s, 4H), 2.79 (d, $J = 4.7$ Hz, 4H); ^{13}C NMR (75 MHz, CDCl_3) δ 165.92, 158.94, 146.27, 146.08, 146.00, 140.98, 131.80, 131.19, 128.88, 128.44, 122.73, 119.99, 115.62, 115.55, 114.72, 114.13, 110.86, 67.08, 56.12, 55.39, 53.75, 47.87, 43.64; HR-MS (ESI) m/z : calcd for $\text{C}_{27}\text{H}_{32}\text{N}_3\text{O}_5$ $[\text{M}+\text{H}]^+$ 478.2336 found 478.2333.

N-(3-hydroxy-4-methoxybenzyl)-2-morpholino-5-(pyridin-4-ylmethyl)amino benzamide (34b). White solid, yield 50.2% over 2 steps. ^1H NMR (300 MHz, $\text{DMSO}-d_6$) δ 10.45 (d, $J = 6.3$ Hz, 1H), 8.95 (d, $J = 3.0$ Hz, 1H), 8.56–8.42 (m, 2H), 7.38–7.29 (m, 2H), 7.24 (d, $J = 2.9$ Hz, 1H), 7.10 (d, $J = 8.6$ Hz, 1H), 6.86 (d, $J = 8.2$ Hz, 1H), 6.79 (s, 1H), 6.74 (dd, $J = 8.1, 2.1$ Hz, 1H), 6.62 (dd, $J = 8.7, 3.0$ Hz, 1H), 6.53 (d, $J = 6.9$ Hz, 1H), 4.39–4.26 (m, 4H), 3.73 (s, 3H), 3.40 (dd, $J = 5.9, 3.2$ Hz, 4H), 2.70 (t, $J = 4.6$ Hz, 4H); ^{13}C NMR (75 MHz, $\text{DMSO}-d_6$) δ 165.23, 149.56, 146.83, 146.59, 146.45, 140.22, 131.66, 128.78, 122.71, 122.18, 118.62, 115.27, 115.17, 114.83, 113.92, 112.23, 66.22, 55.71, 53.28, 45.47, 42.37; HR-MS (ESI) m/z : calcd for $\text{C}_{25}\text{H}_{29}\text{N}_4\text{O}_4$ $[\text{M}+\text{H}]^+$ 449.2183 found 449.2184.

5-((Furan-2-ylmethyl)amino)-N-(3-hydroxy-4-methoxybenzyl)-2-morpholinobenzamide (34c). White solid, yield 54.2% over 2 steps. ^1H NMR (300 MHz, CDCl_3) δ 10.84 (t, $J = 5.3$ Hz, 1H), 7.63 (d, $J = 3.0$ Hz, 1H), 7.35 (d, $J = 1.8$ Hz, 1H), 7.08 (d, $J = 8.6$ Hz, 1H), 6.95 (d, $J = 1.9$ Hz, 1H), 6.88–6.80 (m, 2H), 6.73 (dd, $J = 8.6, 3.0$ Hz, 1H), 6.31 (dd, $J = 3.2, 1.8$ Hz, 1H), 6.25 (d, $J = 3.2$ Hz, 1H), 6.01 (s, 1H), 4.52 (d, $J = 5.2$ Hz, 2H), 4.33 (s, 2H), 4.23 (s, 1H), 3.88 (s, 3H), 3.45 (d, $J = 4.8$ Hz, 4H), 2.80 (t, $J = 4.6$ Hz, 4H); ^{13}C NMR (75 MHz, CDCl_3) δ 165.84, 152.46, 146.28, 146.07, 145.41, 142.04, 141.45, 131.70, 128.38, 122.70, 119.94, 116.10, 115.65, 114.66, 110.88, 110.43, 107.26, 67.02, 56.11, 53.70, 43.59, 41.45; HR-MS (ESI) m/z : calcd for $\text{C}_{24}\text{H}_{28}\text{N}_3\text{O}_5$ $[\text{M}+\text{H}]^+$ 438.2023 found 438.2022.

N-(3-hydroxy-4-methoxybenzyl)-5-(4-methoxybenzamido)-2-morpholinobenzamide (34d). White solid, yield 46.8% over 2 steps. ^1H NMR (300 MHz, CDCl_3) δ 10.49 (s, 1H), 8.48 (s, 1H), 8.41–8.34 (m, 1H), 8.09 (s, 1H), 7.89 (d, $J = 8.5$ Hz, 2H), 7.23 (s, 1H), 6.96 (s, 1H), 6.93 (s, 2H), 6.81 (d, $J = 1.2$ Hz, 2H), 5.94 (s, 1H), 4.46 (d, $J = 5.2$ Hz, 2H), 3.89 (s, 3H), 3.85 (s, 3H), 3.49 (s, 4H), 2.88 (s, 4H); ^{13}C NMR (75 MHz, $\text{DMSO}-d_6$) δ 165.48, 164.71, 161.93, 146.84, 146.58, 146.08, 135.66, 131.70, 129.61, 128.76, 126.70, 123.24, 122.24, 120.86, 118.65, 115.35, 113.60, 112.22, 66.04, 55.72, 55.44, 52.91, 42.38; HR-MS (ESI) m/z : calcd for $\text{C}_{27}\text{H}_{30}\text{N}_3\text{O}_6$ $[\text{M}+\text{H}]^+$ 492.2129 found 492.2126.

N-(3-((3-hydroxy-4-methoxybenzyl)carbamoyl)-4-morpholinophenyl)isonicotinamide (34e). White solid, yield 44.4% over 2 steps. ^1H NMR (300 MHz, $\text{DMSO}-d_6$) δ 10.57 (s, 1H), 9.77 (t, $J = 5.8$ Hz, 1H), 8.94 (s, 1H), 8.83–8.70 (m, 2H), 8.19 (d, $J = 2.6$ Hz, 1H), 7.95 (dd, $J = 8.7, 2.7$ Hz, 1H), 7.92–7.79 (m, 2H), 7.29 (d, $J = 8.8$ Hz, 1H), 6.88 (d, $J = 8.2$ Hz, 1H), 6.83 (d, $J = 2.0$ Hz, 1H), 6.77 (dd, $J = 8.2, 2.0$ Hz, 1H), 4.38 (d, $J = 5.7$ Hz, 2H), 3.74 (s, 3H), 3.48 (t, $J = 4.2$ Hz, 4H), 2.83 (t, $J = 4.5$ Hz, 4H); ^{13}C NMR (75 MHz, $\text{DMSO}-d_6$) δ 165.42, 163.74, 150.30, 146.84, 146.72, 146.56, 141.65, 134.74, 131.67, 128.91, 123.34, 122.41, 121.57, 120.88, 118.67, 115.35, 112.20, 66.00, 55.72, 52.82, 42.38; HR-MS (ESI) m/z : calcd for $\text{C}_{25}\text{H}_{27}\text{N}_4\text{O}_5$ $[\text{M}+\text{H}]^+$ 463.1976 found 463.1970.

N-(3-((3-hydroxy-4-methoxybenzyl)carbamoyl)-4-morpholinophenyl)furan-2-carboxamide (34f). White solid, yield 42.9% over 2 steps. ^1H NMR (300 MHz, CDCl_3) δ 10.35 (t, $J = 5.4$ Hz, 1H), 8.32 (m, 2H), 8.02 (d, $J = 2.8$ Hz, 1H), 7.53 (s, 1H), 7.24 (d, $J = 4.4$ Hz, 1H), 6.97 (s, 1H), 6.83 (t, $J = 6.1$ Hz, 2H), 6.56 (s, 1H), 5.89 (s, 1H), 4.55 (d, $J = 5.2$ Hz, 2H), 3.89 (s, 3H), 3.55–3.44 (m, 4H), 2.89 (t, $J = 4.5$ Hz, 4H); ^{13}C NMR (75 MHz, CDCl_3) δ 165.20, 156.35, 147.70, 147.04, 146.43, 146.19, 144.60, 135.07, 131.47, 128.33, 123.87, 122.73, 122.19, 120.02, 115.56, 114.75, 112.71, 110.96, 66.91, 56.16, 53.62, 43.72; HR-MS (ESI) m/z : calcd for $\text{C}_{24}\text{H}_{25}\text{N}_2\text{O}_6$ $[\text{M}+\text{H}]^+$

452.1816 found 452.1817.

5-Acetamido-N-(3-hydroxy-4-methoxybenzyl)-2-morpholinobenzamide (34g). White solid, yield 43.3% over 2 steps. ^1H NMR (300 MHz, $\text{DMSO}-d_6$) δ 10.02 (s, 1H), 9.89 (d, $J = 5.9$ Hz, 1H), 8.96 (s, 1H), 7.98 (s, 1H), 7.77 (d, $J = 8.6$ Hz, 1H), 7.22 (d, $J = 8.7$ Hz, 1H), 6.87 (d, $J = 8.2$ Hz, 1H), 6.82 (s, 1H), 6.76 (d, $J = 8.1$ Hz, 1H), 4.36 (s, 2H), 3.74 (s, 3H), 3.45 (t, $J = 4.2$ Hz, 4H), 2.96–2.67 (m, 4H), 2.03 (s, 3H); ^{13}C NMR (75 MHz, $\text{DMSO}-d_6$) δ 168.22, 165.34, 146.79, 146.57, 145.74, 135.73, 131.66, 128.82, 121.99, 121.18, 120.76, 118.68, 115.33, 112.22, 66.04, 55.73, 52.92, 42.38, 23.91; HR-MS (ESI) m/z : calcd for $\text{C}_{21}\text{H}_{26}\text{N}_3\text{O}_5$ $[\text{M}+\text{H}]^+$ 400.1867 found 400.1868.

N-(3-hydroxy-4-methoxybenzyl)-4'-methoxy-4-morpholino-[1,1'-biphenyl]-3-carboxamide (34h). White solid, yield 57.9% over 2 steps. ^1H NMR (300 MHz, CDCl_3) δ 10.06 (d, $J = 4.8$ Hz, 1H), 8.44 (d, $J = 2.4$ Hz, 1H), 7.62 (d, $J = 8.3, 2.5$ Hz, 1H), 7.60–7.51 (m, 2H), 7.22 (d, $J = 8.3$ Hz, 1H), 7.05–6.90 (m, 3H), 6.88 (dd, $J = 8.2, 2.0$ Hz, 1H), 6.83 (d, $J = 8.2$ Hz, 1H), 5.88 (s, 1H), 4.57 (d, $J = 5.3$ Hz, 2H), 3.88 (s, 3H), 3.85 (s, 3H), 3.52 (t, $J = 4.4$ Hz, 4H), 2.92 (t, $J = 4.6$ Hz, 4H); ^{13}C NMR (75 MHz, CDCl_3) δ 166.00, 159.37, 149.36, 146.31, 146.10, 137.67, 132.33, 131.68, 129.95, 129.89, 128.09, 127.98, 121.00, 120.04, 114.68, 114.35, 110.90, 66.94, 56.14, 55.46, 53.54, 43.64; HR-MS (ESI) m/z : calcd for $\text{C}_{26}\text{H}_{29}\text{N}_2\text{O}_5$ $[\text{M}+\text{H}]^+$ 449.2071 found 449.2069.

N-(3-hydroxy-4-methoxybenzyl)-2-morpholino-5-(pyridin-4-yl)benzamide (34i). White solid, yield 53.4% over 2 steps. ^1H NMR (300 MHz, CDCl_3) δ 9.74 (t, $J = 5.4$ Hz, 1H), 8.66 (d, $J = 5.1$ Hz, 2H), 8.51 (d, $J = 2.3$ Hz, 1H), 7.73 (dd, $J = 8.4, 2.3$ Hz, 1H), 7.55 (d, $J = 5.1$ Hz, 2H), 7.30 (s, 1H), 6.98 (s, 1H), 6.86 (q, $J = 8.3$ Hz, 2H), 6.15 (s, 1H), 4.58 (d, $J = 5.3$ Hz, 2H), 3.90 (s, 3H), 3.55 (t, $J = 4.4$ Hz, 4H), 2.96 (t, $J = 4.5$ Hz, 4H); ^{13}C NMR (75 MHz, CDCl_3) δ 165.61, 151.52, 150.24, 147.11, 146.52, 146.28, 134.44, 131.44, 130.54, 130.32, 128.47, 121.46, 121.01, 119.98, 114.75, 110.99, 66.81, 56.14, 53.44, 43.68; HR-MS (ESI) m/z : calcd for $\text{C}_{23}\text{H}_{26}\text{N}_3\text{O}_4$ $[\text{M}+\text{H}]^+$ 420.1918 found 420.1910.

5-(Furan-2-yl)-N-(3-hydroxy-4-methoxybenzyl)-2-morpholinobenzamide (34j). White solid, yield 56.9% over 2 steps. ^1H NMR (300 MHz, CDCl_3) δ 9.94 (s, 1H), 8.49 (d, $J = 2.3$ Hz, 1H), 7.75 (dd, $J = 8.4, 2.4$ Hz, 1H), 7.47 (d, $J = 1.8$ Hz, 1H), 7.20 (d, $J = 8.4$ Hz, 1H), 6.97 (d, $J = 2.1$ Hz, 1H), 6.94–6.78 (m, 2H), 6.71 (d, $J = 3.4$ Hz, 1H), 6.48 (dd, $J = 3.5, 1.8$ Hz, 1H), 5.74 (s, 1H), 4.57 (d, $J = 5.4$ Hz, 2H), 3.90 (s, 3H), 3.66–3.39 (m, 4H), 2.92 (t, $J = 4.6$ Hz, 4H); ^{13}C NMR (75 MHz, CDCl_3) δ 165.75, 153.01, 149.58, 146.33, 146.12, 142.31, 131.56, 128.03, 128.01, 127.34, 127.03, 120.84, 120.02, 114.69, 111.89, 110.92, 105.59, 66.86, 56.12, 53.44, 43.64; HR-MS (ESI) m/z : calcd for $\text{C}_{23}\text{H}_{25}\text{N}_2\text{O}_5$ $[\text{M}+\text{H}]^+$ 409.1758 found 409.1752.

4.1.19. 5-((5-fluoro-2-morpholinobenzamido)methyl)-2-methoxyphenyl phosphate disodium (20b-P)

To a solution of **20b** (1.0 g, 2.77 mmol) in anhydrous THF, NaH (133 mg, 3.33 mmol, 60%) was added and stirred at 0 °C under nitrogen atmosphere for 15 min. Then, newly prepared dibenzylphosphoryl chloride (988 mg, 3.33 mmol) was added, and the mixture was stirred at room temperature for 2 h. The mixture was extracted with EtOAc (3 × 25 mL), and the combined organic layers were washed with saturated brine, dried over anhydrous Na_2SO_4 , and concentrated in vacuo to afford the crude product, which was purified by column chromatography with petroleum/ethyl acetate (5:1) to give 1.1 g **20b-Bn** as white solid, yield 63.8%. **20b-Bn** (1.1 g, 2.77 mmol) was dissolved into 20 mL CH_3OH , Pd–C (100 mg) was added. The reaction was stirred for 2 h under hydrogen atmosphere, then the mixture was filtered and the filtrate was concentrated in vacuo to provide 750 mg crude product as white solid, which was dissolved into 20 mL CH_3OH , and NaOH (129 mg, 3.24 mmol) was added. After stirring for 30 min, the mixture was

concentrated in vacuo. The residue was solidified and washed with EtOAc to afford 769 mg **20b-P** as white solid, yield 89.6% over 2 steps. ^1H NMR (300 MHz, MeOD) δ 7.71 (d, J = 1.7 Hz, 1H), 7.62 (dd, J = 9.5, 3.1 Hz, 1H), 7.32 (dd, J = 8.9, 4.9 Hz, 1H), 7.20 (ddd, J = 8.9, 7.7, 3.2 Hz, 1H), 6.97–6.91 (m, 2H), 4.51 (s, 2H), 3.85 (s, 3H), 3.53–3.46 (m, 4H), 2.89–2.84 (m, 4H); ^{13}C NMR (75 MHz, MeOD) δ 165.83, 161.09, 157.87, 149.52 (d, J = 3.0 Hz), 147.29, 144.43, 130.37 (d, J = 17.3 Hz), 122.77 (d, J = 7.5 Hz), 120.71, 119.97, 118.07 (d, J = 21.8 Hz), 116.45 (d, J = 24.0 Hz), 111.51, 66.49, 55.23, 53.09, 43.24. HR-MS (ESI) m/z : calcd for $\text{C}_{19}\text{H}_{21}\text{FN}_2\text{Na}_2\text{O}_7\text{P}$ [$\text{M} - \text{Na}$] $^-$ 461.0895 found 461.0861.

4.2. Biology

4.2.1. Materials

3-(4,5-Dimethylthiazol-2-yl)-2,5-diphenyl-2-H-tetrazolium bromide (MTT), propidium iodide (PI), Hoechst 33342, the Annexin V-FITC apoptosis detection kit, 5,5',6,6'-tetrachloro-1,1',3,3'-tetraethyl-imidacarbocyanine iodide (JC-1) were purchased from Nanjing KeyGen Biotech Co. Ltd. (Nanjing, China). Goat antimouse IgG/Alexa-Fluor 488 antibody was purchased from Jackson ImmunoResearch in USA. Primary antibodies against cdc2, cyclin B1, p-histone-H3, Bax, Bcl-2, caspase 3, caspase 9, p53, and PARP were purchased from Beyotime (Jiangsu, China). The purified tubulin polymerization kit was purchased from Cytoskeleton Inc. (Denver, USA). Rat plasma and Enalapril were purchased from Tripod (Jiangsu, China). Other reagents were purchased from Sigma-Aldrich (St. Louis, MO, USA) unless otherwise specified.

4.2.2. Cell lines and cell culture

Human chronic myelogenous leukemia cells (K562), hepatocellular carcinoma cells (HepG2), human colon cancer cells (HCT-8), and human breast cancer cells (MDA-MB-231), mouse liver cancer cells (H22) were grown in RPMI 1640 medium (KeyGen Biotech Co. Ltd., Nanjing, China). Human umbilical vein endothelial cells (HUVECs) and human normal hepatocytes LO2 cells were grown in F12K medium (KeyGen Biotech Co. Ltd., Nanjing, China). The medium for all cell lines were supplemented with 10% fetal bovine serum (Life Technologies, USA), 100 $\mu\text{g}/\text{mL}$ streptomycin (Life Technologies, USA), and 100 U/mL penicillin (Life Technologies, USA) and maintained at 37 °C in a humidified atmosphere with 5% CO_2 .

4.2.3. MTT assay

The overall growth of human cancer cell lines was determined using the colorimetric MTT assay. Briefly, the cell lines were incubated at 37 °C in a humidified 5% CO_2 incubator for 24 h in 96-well plates prior to the experiments. K562, HepG2, H22, HCT-8, MDA-MB-231 and L-O2 cells were seeded at a density of 5×10^3 cells/well. After removal of medium, 100 μL of fresh medium containing the test compounds at different concentrations was added to each well and incubated at 37 °C for 72 h (or 6 h). The percentage of DMSO in the medium did not exceeded 0.25%. The number of living cells after 72 h (or 6 h) of culture in the presence (or absence, as in the case of the control) of the various compounds was directly proportional to the intensity of the blue color of media, which is quantitatively measured by spectrophotometry (Biorad, Nazareth, Belgium) at a 570 nm wavelength. The experiment was performed in quadruplicate and repeated three times.

4.2.4. In vitro tubulin polymerization inhibitory assay

The tubulin reaction mix in 100 μL PEM buffer contained 2 mg/mL tubulin (Cytoskeleton), 80 mM piperazine- $\text{N,N}'$ -bis(2-ethanesulfonic acid) sequisodium salt PIPES (pH 6.9), 0.5 mM EGTA, 2 mM MgCl_2 , and 15% glycerol. Then, the mixture was

preincubated with compounds or vehicle DMSO on ice. PEG containing GTP was added to the final concentration of 3 mg/mL before detecting the tubulin polymerization reaction. After 30 min, the absorbance was detected by a spectrophotometer at 340 nm at 37 °C every 2 min for 60 min. The area under the curve was used to determine the concentration that inhibited tubulin polymerization by 50% (IC50), which was calculated with GraphPad Prism Software version 5.02.

4.2.5. Competitive inhibition assays

The competitive binding activity of inhibitors was evaluated using a radiolabeled [3H]-colchicine competition scintillation proximity (SPA) assay. In brief, 0.08 μM [3H]-colchicine was mixed with **20b** (1 μM , 5 μM) or CA-4 (1 μM , 5 μM) and biotinylated porcine tubulin (0.5 μg) in a buffer of 100 μL containing 80 mM PIPES (pH 6.8), 1 mM EGTA, 10% glycerol, 1 mM MgCl_2 , and 1 mM GTP for 2 h at 37 °C. Then streptavidin-labeled SPA beads (80 μg) were added to each mixture. The radioactive counts were measured directly with a scintillation counter.

4.2.6. Immunofluorescent staining

A431 cells were seeded into 6-well plates and then treated with vehicle control 0.1% DMSO, and **20b** (7.5 nM, 15 nM, 30 nM). The cells were fixed with 4% paraformaldehyde and then washed three times with PBS. After blocking for 20 min by adding 50–100 μL goat serum albumin at room temperature, cells were incubated with a monoclonal antibody (anti- α -tubulin) at 37 °C for 2 h. Then the cells were washed three times by PBS following staining by fluorescence secondary antibody and labeling of nuclei by 4,6-diamidino-2-phenylindole (DAPI). Cells were visualized on a Zeiss LSM 570 laser scanning confocal microscope (Carl Zeiss, Germany).

4.2.7. Molecular modeling

The 2D structures of **20b**, IMB5046, and CA-4 were generated on ChemBioDraw Ultra 12.0. Ligprep module implemented in Schrödinger was used to generate energy minimized 3D structures. The X-ray structure of CA-4- α , β -tubulin complex was downloaded from the Protein Data Bank (PDB code 5lyj) and prepared for docking using Protein Preparation Wizard. Default settings were used for all the remaining parameters and no constraints were specified separately. All ligand conformers were docked to each of the receptor grid structures using Glide extra precision (XP) mode. The 2D interactions between ligands and tubulin were generated by Ligand Interaction Diagram module, and the structural image was obtained using PyMOL software.

4.2.8. Cell cycle analysis

A431 cells were seeded into 6-well plates and incubated at 37 °C in a humidified 5% CO_2 incubator for 24 h, and then treated with or without **20b** at indicated concentrations (7.5 nM, 15 nM, 30 nM) for another 48 h. The collected cells were fixed by adding 70% ethanol at 4 °C for 12 h. Subsequently, the cells were resuspended in PBS containing 100 mL RNase A and 400 mL of propidium iodide for 30 min. The DNA content of the cells was measured using a FACS Calibur flow cytometer (Bectone Dickinson, San Jose, CA, USA).

4.2.9. Hoechst 33342 staining

Approximately 5×10^4 cells per well were plated in six-well plates, and the cells were then incubated with **20b** (7.5 nM, 15 nM, 30 nM) for 48 h. After incubation, cells were washed with PBS, fixed in 4% paraformaldehyde for 30 min, and then stained with 20 $\mu\text{g}/\text{mL}$ Hoechst 33342 for 15 min at room temperature in the dark. Cells were then assessed by fluorescence microscopy for morphological changes after **20b** treatment.

4.2.10. Cell apoptosis analysis

After treatment with or without **20b** at indicated concentrations (7.5 nM, 15 nM, 30 nM) for 48 h, A431 cells were washed twice in PBS, centrifuged and resuspended in 500 μ L AnnexinV binding buffer. The cells were then harvested, washed and stained with 5 mL Annexin V-APC and 5 mL 7-AAD in the dark for 15 min. Apoptosis was analyzed using a FACS Calibur flow cytometer (Bectone Dickinson, San Jose, CA, USA).

4.2.11. Mitochondrial membrane potential analysis

After treatment with vehicle control 0.1% DMSO, and **20b** (7.5 nM, 15 nM, 30 nM) for 48 h, the cells were washed in PBS and resuspended in 500 μ L JC-1 incubation buffer at 37 °C for 15 min. The percentage of cells with healthy or collapsed mitochondrial membrane potentials was monitored by flow cytometry analysis (Bectone-Dickinson, San Jose, CA, USA).

4.2.12. Measurement of intracellular ROS generation

Intracellular ROS production was detected by using the peroxide-sensitive fluorescent probe DCF-DA. In brief, after treatment with **20b** (7.5 nM, 15 nM, 30 nM) for 48 h, A431 cells were incubated with 10 mM DCF-DA at 37 °C for 15 min. The intracellular ROS mediated oxidation of DCF-DA to the fluorescent compound 2',7'-dichlorofluorescein (DCF). Then cells were harvested, and the pellets were suspended in 1 mL PBS. Samples were analyzed at an excitation wavelength of 480 nm and an emission wavelength of 525 nm by flow cytometry on a FC500 cytometer (Beckman Coulter).

4.2.13. Solubility evaluation

Solubility was measured separately at pH 7.4 and pH 2.0 by using an HPLC–UV method. Compounds **20b** and **20d** were added to phosphate buffer (pH 7.4) or HCl aqueous (pH 2.0) at 20 °C. After shaking and centrifuging, the supernatant was taken to determine the concentration of compounds **20b** and **20d** in each solvent for calculation of the corresponding solubility. The mobile phase was menthol-water (80/20, v/v) at a flow rate of 1.0 mL/min with the detection wavelength at 254 nm. This experiment was repeated in triplicates.

4.2.14. log P measurement

The DMSO stock solution (10 mg/mL, 20 μ L) of **20b**, **20d** and CA-4 were added into the mixture solvents of *n*-octane (1 mL) and water (1 mL). The mixtures were stirred at room temperature for 24 h and then stood overnight. Each solution (0.5 mL) was transferred from two phases respectively into other vials for HPLC analysis. The instrument and conditions were the same as those for solubility determination. The log *P* was calculated by the peak area ratios in *n*-octane and in water.

4.2.15. Plasma stability measurement

The stability of compounds **20b** and **20d** in rat plasma was determined using HPLC method. Rat blood plasma was diluted with distilled water until the indicated volume, and then the solution was pre-incubated for 5 min at 37 °C. The stock solutions of the test compounds **20b**, **20d** and positive control (100 nM, 20 μ L) were added to the rat plasma (480 μ L), and the mixtures were incubated at 37 °C. The incubations were terminated at 0, 15, 30, 60, 120, and 180 min, by removing aliquots (80 μ L) of the plasma samples and mixing them with an equal volume of acetonitrile. The mixture was stirred vigorously and centrifuged (5500 rpm, 5 min). The supernatant was filtered, and the filtrate was analyzed by HPLC. These tests were conducted three times for each compound. Remaining (%) was calculate by the ratio of peak area at each time point and peak area at 0 min.

4.2.16. Determination of acute toxicity

Five-week-old male Institute of Cancer Research (ICR) mice were purchased from Shanghai SLAC Laboratory Animals Co. Ltd. An acute toxicity study by intravenous injection was conducted according to the guidelines of the Organization for Economic Co-operation and Development. The animals were weighed and divided at random into five groups of ten animals. Then, the mice were intravenously injected with **20b-P** (327.7, 409.6, 512.0, 640, and 800 mg/kg) in saline solutions. The animals were observed continuously for 14 days.

4.2.17. Evaluation of in vivo anti-tumor effect

A total of 1×10^6 H22 cells were subcutaneously inoculated into the right flank of ICR mice according to protocols of tumor transplant research. After incubation for one day, mice were weighted and divided at random into eight groups with eight animals per groups. The groups treated with **20b**, IMB5046, and CA-4 were administered in a vehicle of 10% DMF/2% Tween 80/88% saline, respectively. The groups treated with **20b-P** and CA-4P were administered 20 mg/kg in a vehicle of saline. The positive control group was treated with PTX (6 mg/kg) by intravenous injection. The negative control group received a vehicle of 10% DMF/2% Tween 80/88% saline through intravenous injection. Treatments of **20b**, **20b-P**, IMB5046, and CA-4 were conducted at a frequency of intravenous injection one dose per day for a total 21 consecutive days while the positive group was treated with PTX at a dose of 6 mg/kg every other day. Body weights and tumor volumes were measured every 2 days. After the treatments, all the mice were sacrificed and weighed. The following formula was used to determine tumor volumes: tumor volume = $L \times W^2/2$, where *L* is the length and *W* is the width. Ratio of inhibition of tumor (%) = $(1 - \text{average tumor weight of treated group/average tumor weight of control group}) \times 100\%$. All procedures were performed following institutional approval in accordance with the NIH Guide for the Care and Use of Laboratory Animals.

4.2.18. Wound healing assays

HUVEC cells were grown in 6-well plates for 24 h. Scratches were made in confluent monolayers using 200 μ L pipette tips. Then, wounds were washed twice with PBS to remove non-adherent cell debris. Media containing different concentrations of **20b** (7.5 nM, 15 nM, 30 nM) were added to the petri dishes. Cells which migrated across the wound area were photographed using phase contrast microscopy at 0 h and 24 h.

4.2.19. Tube formation assay

EC Matrigel matrix was thawed at 4 °C overnight, and HUVECs suspended in F12K were seeded in 96-well culture plates at a cell density of 50,000 cells/well after polymerization of the Matrigel at 37 °C for 30 min. They were then treated with 20 μ L different concentrations of **20b** or vehicle for 6 h at 37 °C. Then, the morphological changes of the cells and tubes formed were observed and photographed under inverted microscope (OLYMPUS, Japan).

4.2.20. Immunohistochemistry assay

Slides from mice tissues (control group and **20b**-treated group at 20 mg/kg in *in vivo* antitumor experiments) were embedded in paraffin and cut to sections of 4 μ m, deparaffinized, and treated with citrate buffer. Then, they were blocked with avidin/biotin for 20 min. The slides were incubated with CD31 overnight at 4 °C. Next, the slides were treated with secondary antibody with horseradish peroxidase goat anti-rabbit for 1–3 h and developed with 3, 3'-diaminobenzidine. Finally, the slides were counterstained with hematoxylin. The mean microvessel density (MVD) was

measured by calculating the CD31-positive cells in randomly selected areas in each section using image analysis software and then analyzed with OriginPro 8.0 software.

Declaration of competing interest

The authors declare that they have no known competing financial interests or personal relationships that could have appeared to influence the work reported in this paper.

Acknowledgments

This study was supported from the National Natural Science Foundation of China (No. 81673306, 81703348, 81874289 and 81973167) for financial support, and “Double First-Class” University project CPU2018GY04, CPU2018GY35, China Pharmaceutical University.

Appendix A. Supplementary data

Supplementary data to this article can be found online at <https://doi.org/10.1016/j.ejmech.2021.113316>.

References

- [1] J. Howard, A.A. Hyman, Dynamics and mechanics of the microtubule plus end, *Nature* 422 (2003) 753–758.
- [2] S. Etienne-Manneville, From signaling pathways to microtubule dynamics: the key players, *Curr. Opin. Cell Biol.* 22 (2010) 104–111.
- [3] M.A. Jordan, L. Wilson, Microtubules as a target for anticancer drugs, *Nat. Rev. Cancer* 4 (2004) 253–265.
- [4] R.A. Stanton, K.M. Gernert, J.H. Nettles, R. Aneja, Drugs that target dynamic microtubules: a new molecular perspective, *Med. Res. Rev.* 31 (2011) 443–481.
- [5] T. Hohmann, F. Dehghani, The cytoskeleton-A complex interacting meshwork, *Cells* 8 (2019).
- [6] C. Dumontet, M.A. Jordan, Microtubule-binding agents: a dynamic field of cancer therapeutics, *Nat. Rev. Drug Discov.* 9 (2010) 790–803.
- [7] K. Haider, S. Rahaman, M.S. Yar, A. Kamal, Tubulin inhibitors as novel anticancer agents: an overview on patents (2013–2018), *Expert Opin. Ther. Pat.* 29 (2019) 623–641.
- [8] M.O. Steinmetz, A.E. Protá, Microtubule-targeting agents: strategies to hijack the cytoskeleton, *Trends Cell Biol.* 28 (2018) 776–792.
- [9] G.R. Pettit, S.B. Singh, E. Hamel, C.M. Lin, D.S. Alberts, D. Garcia-Kendall, Isolation and structure of the strong cell growth and tubulin inhibitor combretastatin A-4, *Experientia* 45 (1989) 209–211.
- [10] F. Yakushiji, H. Tanaka, K. Murguruma, T. Iwahashi, Y. Yamazaki, Y. Hayashi, Prodrug study of plinabulin using a click strategy focused on the effects of a replaceable water-solubilizing moiety, *Chem. Pharm. Bull.* 60 (2012) 877–881.
- [11] C. Stengel, S.P. Newman, M.P. Leese, B.V. Potter, M.J. Reed, A. Purohit, Class III beta-tubulin expression and in vitro resistance to microtubule targeting agents, *Br. J. Cancer* 102 (2010) 316–324.
- [12] E.C. McLoughlin, N.M. O’Boyle, Colchicine-binding site inhibitors from chemistry to clinic: a review, *Pharmaceuticals* 13 (2020).
- [13] K.E. Arnst, Y. Wang, Z.N. Lei, D.J. Hwang, G. Kumar, D. Ma, D.N. Parke, Q. Chen, J. Yang, S.W. White, T.N. Seagroves, Z.S. Chen, D.D. Miller, W. Li, Colchicine binding site agent DJ95 overcomes drug resistance and exhibits antitumor efficacy, *Mol. Pharmacol.* 96 (2019) 73–89.
- [14] W. Li, H. Sun, S. Xu, Z. Zhu, J. Xu, Tubulin inhibitors targeting the colchicine binding site: a perspective of privileged structures, *Future Med. Chem.* 9 (2017) 1765–1794.
- [15] V. Spanò, M. Pennati, B. Parrino, A. Carbone, A. Montalbano, V. Cilibrasi, V. Zuco, A. Loperigolo, D. Cominetti, P. Diana, G. Cirrincione, P. Barraja, N. Zaffaroni, Preclinical activity of new [1,2]oxazolo[5,4-*e*]isindole derivatives in diffuse malignant peritoneal mesothelioma, *J. Med. Chem.* 59 (2016) 7223–7238.
- [16] V. Spanò, M. Pennati, B. Parrino, A. Carbone, A. Montalbano, A. Loperigolo, V. Zuco, D. Cominetti, P. Diana, G. Cirrincione, N. Zaffaroni, P. Barraja, [1,2] Oxazolo[5,4-*e*]isindoles as promising tubulin polymerization inhibitors, *Eur. J. Med. Chem.* 124 (2016) 840–851.
- [17] V. Spanò, R. Rocca, M. Barreca, D. Giallombardo, A. Montalbano, A. Carbone, M.V. Raimondi, E. Gaudio, R. Bortolozzi, R. Bai, P. Tassone, S. Alcaro, E. Hamel, G. Viola, F. Bertoni, P. Barraja, Pyrrolo[2,3-*c*]cyclohepta[1,2-*d*][1,2]oxazoles, a new class of antimitotic agents active against multiple malignant cell types, *J. Med. Chem.* 63 (2020) 12023–12042.
- [18] V. Spanò, M. Barreca, R. Rocca, R. Bortolozzi, R. Bai, A. Carbone, M.V. Raimondi, A.P. Piccionello, A. Montalbano, S. Alcaro, E. Hamel, G. Viola, P. Barraja, Insight on [1,3]thiazolo[4,5-*e*]isindoles as tubulin polymerization inhibitors, *Eur. J. Med. Chem.* 212 (2021) 113122.
- [19] M.J. Pérez-Pérez, E.M. Priego, O. Bueno, M.S. Martins, M.D. Canela, S. Liekens, Blocking blood flow to solid tumors by destabilizing tubulin: an approach to targeting tumor growth, *J. Med. Chem.* 59 (2016) 8685–8711.
- [20] D.W. Siemann, The unique characteristics of tumor vasculature and preclinical evidence for its selective disruption by tumor-vascular disrupting agents, *Cancer Treat. Rev.* 37 (2011) 63–74.
- [21] C.M. Lin, S.B. Singh, P.S. Chu, R.O. Dempcy, J.M. Schmidt, G.R. Pettit, E. Hamel, Interactions of tubulin with potent natural and synthetic analogs of the antimitotic agent combretastatin: a structure-activity study, *Mol. Pharmacol.* 34 (1988) 200–208.
- [22] K. Grosios, S.E. Holwell, A.T. McGown, G.R. Pettit, M.C. Bibby, In vivo and in vitro evaluation of combretastatin A-4 and its sodium phosphate prodrug, *Br. J. Cancer* 81 (1999) 1318–1327.
- [23] G.M. Tozer, V.E. Prise, J. Wilson, R.J. Locke, B. Vojnovic, M.R. Stratford, M.F. Dennis, D.J. Chaplin, Combretastatin A-4 phosphate as a tumor vascular-targeting agent: early effects in tumors and normal tissues, *Cancer Res* 59 (1999) 1626–1634.
- [24] <http://investor.mateon.com/releasedetail.cfm?ReleaseID=1041745>.
- [25] N. Sirisoma, A. Pervin, H. Zhang, S. Jiang, J.A. Willardson, M.B. Anderson, G. Mather, C.M. Pleiman, S. Kasibhatla, B. Tseng, J. Drewe, S.X. Cai, Discovery of *N*-(4-methoxyphenyl)-*N*,2-dimethylquinazolin-4-amine, a potent apoptosis inducer and efficacious anticancer agent with high blood brain barrier penetration, *J. Med. Chem.* 52 (2009) 2341–2351.
- [26] K. Mahal, M. Resch, R. Ficner, R. Schobert, B. Biersack, T. Mueller, Effects of the tumor-vasculature-disrupting agent verubulin and two heteroaryl analogues on cancer cells, endothelial cells, and blood vessels, *ChemMedChem* 9 (2014) 847–854.
- [27] X.F. Wang, F. Guan, E. Ohkoshi, W. Guo, L. Wang, D.Q. Zhu, S.B. Wang, L.T. Wang, E. Hamel, D. Yang, L. Li, K. Qian, S.L. Morris-Natschke, S. Yuan, K.H. Lee, L. Xie, Optimization of 4-(*N*-cycloamino)phenylquinazolines as a novel class of tubulin-polymerization inhibitors targeting the colchicine site, *J. Med. Chem.* 57 (2014) 1390–1402.
- [28] M.T. Cui, L. Jiang, M. Goto, P.L. Hsu, L. Li, Q. Zhang, L. Wei, S.J. Yuan, E. Hamel, S.L. Morris-Natschke, K.H. Lee, L. Xie, In vivo and mechanistic studies on antitumor lead 7-methoxy-4-(2-methylquinazolin-4-yl)-3,4-dihydroquinazolin-2(1*H*)-one and its modification as a novel class of tubulin-binding tumor-vascular disrupting agents, *J. Med. Chem.* 60 (2017) 5586–5598.
- [29] S. Banerjee, K.E. Arnst, Y. Wang, G. Kumar, S. Deng, L. Yang, G.B. Li, J. Yang, S.W. White, W. Li, D.D. Miller, Heterocyclic-fused pyrimidines as novel tubulin polymerization inhibitors targeting the colchicine binding site: structural basis and antitumor efficacy, *J. Med. Chem.* 61 (2018) 1704–1718.
- [30] I.M. Subbiah, D.J. Lenihan, A.M. Tsimberidou, Cardiovascular toxicity profiles of vascular-disrupting agents, *Oncologist* 16 (2011) 1120–1130.
- [31] K. Kanoh, S. Kohno, T. Asari, T. Harada, J. Katada, M. Muramatsu, H. Kawashima, H. Sekiya, I. Uno, (–)-Phenylalhistin: a new mammalian cell cycle inhibitor produced by *Aspergillus ustus*, *Bioorg. Med. Chem. Lett* 7 (1997) 2847–2852.
- [32] Y. Yamazaki, K. Tanaka, B. Nicholson, G. Deyanat-Yazdi, B. Potts, T. Yoshida, A. Oda, T. Kitagawa, S. Orikasa, Y. Kiso, H. Yasui, M. Akamatsu, T. Chinen, T. Usui, Y. Shinozaki, F. Yakushiji, B.R. Miller, S. Neuteboom, M. Palladino, K. Kanoh, G.K. Lloyd, Y. Hayashi, Synthesis and structure-activity relationship study of antimicrotubule agents phenylalhistin derivatives with a dihydrodiperazine-2,5-dione structure, *J. Med. Chem.* 55 (2012) 1056–1071.
- [33] <https://clinicaltrials.gov/show/NCT02504489>.
- [34] L. Li, S. Jiang, X. Li, Y. Liu, J. Su, J. Chen, Recent advances in trimethoxyphenyl (TMP) based tubulin inhibitors targeting the colchicine binding site, *Eur. J. Med. Chem.* 151 (2018) 482–494.
- [35] Q.-X. Yue, X. Liu, D.-A. Guo, Microtubule-binding natural products for cancer therapy, *Planta Med.* 76 (2010) 1037–1043.
- [36] X. Wu, Q. Wang, W. Li, Recent advances in heterocyclic tubulin inhibitors targeting the colchicine binding site, *Anti-Cancer Agents Med. Chem.* 16 (2016) 1325–1338.
- [37] Y. Pang, B. An, L. Lou, J. Zhang, J. Yan, L. Huang, X. Li, S. Yin, Design, synthesis, and biological evaluation of novel selenium-containing iso combretastatins and phenstatins as antitumor agents, *J. Med. Chem.* 60 (2017) 7300–7314.
- [38] Q. Wang, K.E. Arnst, Y. Wang, G. Kumar, D. Ma, H. Chen, Z. Wu, J. Yang, S.W. White, D.D. Miller, W. Li, Structural modification of the 3,4,5-trimethoxyphenyl moiety in the tubulin inhibitor VERU-111 leads to improved antiproliferative activities, *J. Med. Chem.* 61 (2018) 7877–7891.
- [39] W. Li, F. Xu, W. Shuai, H. Sun, H. Yao, C. Ma, S. Xu, H. Yao, Z. Zhu, D.H. Yang, Z.S. Chen, J. Xu, Discovery of novel quinoline-chalcone derivatives as potent antitumor agents with microtubule polymerization inhibitory activity, *J. Med. Chem.* 62 (2019) 993–1013.
- [40] Y.B. Zheng, J.H. Gong, X.J. Liu, S.Y. Wu, Y. Li, X.D. Xu, B.Y. Shang, J.M. Zhou, Z.L. Zhu, S.Y. Si, Y.S. Zhen, A novel nitrobenzoate microtubule inhibitor that overcomes multidrug resistance exhibits antitumor activity, *Sci. Rep.* 6 (2016) 31472.
- [41] K. Nepali, H.-Y. Lee, J.-P. Liou, Nitro-group-containing drugs, *J. Med. Chem.* 62 (2018) 2851–2893.
- [42] W. Li, Y. Yin, H. Yao, W. Shuai, H. Sun, S. Xu, J. Liu, H. Yao, Z. Zhu, J. Xu, Discovery of novel vinyl sulfone derivatives as anti-tumor agents with

- microtubule polymerization inhibitory and vascular disrupting activities, *Eur. J. Med. Chem.* 157 (2018) 1068–1080.
- [43] W. Li, W. Shuai, F. Xu, H. Sun, S. Xu, H. Yao, J. Liu, H. Yao, Z. Zhu, J. Xu, Discovery of novel 4-arylisochromenes as anticancer agents inhibiting tubulin polymerization, *ACS Med. Chem. Lett.* 9 (2018) 974–979.
- [44] W. Li, Y. Yin, W. Shuai, F. Xu, H. Yao, J. Liu, K. Cheng, J. Xu, Z. Zhu, S. Xu, Discovery of novel quinazolines as potential anti-tubulin agents occupying three zones of colchicine domain, *Bioorg. Chem.* 83 (2019) 380–390.
- [45] W. Li, W. Shuai, H. Sun, F. Xu, Y. Bi, J. Xu, C. Ma, H. Yao, Z. Zhu, S. Xu, Design, synthesis and biological evaluation of quinoline-indole derivatives as anti-tubulin agents targeting the colchicine binding site, *Eur. J. Med. Chem.* 163 (2019) 428–442.
- [46] W. Li, H. Sun, F. Xu, W. Shuai, J. Liu, S. Xu, H. Yao, C. Ma, Z. Zhu, J. Xu, Synthesis, molecular properties prediction and biological evaluation of indole-vinyl sulfone derivatives as novel tubulin polymerization inhibitors targeting the colchicine binding site, *Bioorg. Chem.* 85 (2019) 49–59.
- [47] H. Zhu, H. Sun, Y. Liu, Y. Duan, J. Liu, X. Yang, W. Li, S. Qin, S. Xu, Z. Zhu, J. Xu, Design, synthesis and biological evaluation of vinyl selenone derivatives as novel microtubule polymerization inhibitors, *Eur. J. Med. Chem.* 207 (2020) 112716.
- [48] W. Shuai, X. Li, W. Li, F. Xu, L. Lu, H. Yao, L. Yang, H. Zhu, S. Xu, Z. Zhu, J. Xu, Design, synthesis and anticancer properties of isocombretapyridines as potent colchicine binding site inhibitors, *Eur. J. Med. Chem.* 197 (2020) 112308.
- [49] S.-O. Li, R.E. Eakin, Synthesis of *N*-phosphorylated derivatives of amino acids, *J. Am. Chem. Soc.* 77 (1955) 1866–1870.
- [50] S.A. Patil, R. Patil, D.D. Miller, Indole molecules as inhibitors of tubulin polymerization: potential new anticancer agents, *Future Med. Chem.* 4 (2012) 2085–2115.
- [51] R. Patil, S.A. Patil, K.D. Beaman, S.A. Patil, Indole molecules as inhibitors of tubulin polymerization: potential new anticancer agents, an update (2013–2015), *Future Med. Chem.* 8 (2016) 1291–1316.
- [52] Z. Binkhathlan, A. Lavasanifar, P-glycoprotein inhibition as a therapeutic approach for overcoming multidrug resistance in cancer: current status and future perspectives, *Curr. Cancer Drug Targets* 13 (2013) 326–346.
- [53] G. Wuitschik, E.M. Carreira, B. Wagner, H. Fischer, I. Parrilla, F. Schuler, M. Rogers-Evans, K. Müller, Oxetanes in drug discovery: structural and synthetic insights, *J. Med. Chem.* 53 (2010) 3227–3246.
- [54] L.Q. Sun, L. Zhu, K. Qian, B. Qin, L. Huang, C.H. Chen, K.H. Lee, L. Xie, Design, synthesis, and preclinical evaluations of novel 4-substituted 1,5-diarylanilines as potent HIV-1 non-nucleoside reverse transcriptase inhibitor (NNRTI) drug candidates, *J. Med. Chem.* 55 (2012) 7219–7229.
- [55] J. Chen, Z. Wang, C.M. Li, Y. Lu, P.K. Vaddady, B. Meibohm, J.T. Dalton, D.D. Miller, W. Li, Discovery of novel 2-aryl-4-benzoyl-imidazoles targeting the colchicines binding site in tubulin as potential anticancer agents, *J. Med. Chem.* 53 (2010) 7414–7427.
- [56] A. Massarotti, A. Coluccia, R. Silvestri, G. Sorba, A. Brancale, The tubulin colchicine domain: a molecular modeling perspective, *ChemMedChem* 7 (2012) 33–42.
- [57] A. Dorléans, B. Gigant, R.B. Ravelli, P. Mailliet, V. Mikol, M. Knossow, Variations in the colchicine-binding domain provide insight into the structural switch of tubulin, *Proc. Natl. Acad. Sci. U.S.A.* 106 (2009) 13775–13779.
- [58] Y.N. Liu, J.J. Wang, Y.T. Ji, G.D. Zhao, L.Q. Tang, C.M. Zhang, X.L. Guo, Z.P. Liu, Design, synthesis, and biological evaluation of 1-methyl-1,4-dihydroindeno [1,2-*c*]pyrazole analogues as potential anticancer agents targeting tubulin colchicine binding site, *J. Med. Chem.* 59 (2016) 5341–5355.
- [59] R. Gaspari, A.E. Prota, K. Bargsten, A. Cavalli, M.O. Steinmetz, Structural basis of *cis*- and *trans*-combretastatin binding to tubulin, *Inside Chem.* 2 (2017) 102–113.
- [60] J.R. Jackson, D.R. Patrick, M.M. Dar, P.S. Huang, Targeted anti-mitotic therapies: can we improve on tubulin agents? *Nat. Rev. Cancer* 7 (2007) 107–117.
- [61] T. Moldoveanu, A.V. Follis, R.W. Kriwacki, D.R. Green, Many players in BCL-2 family affairs, *Trends Biochem. Sci.* 39 (2014) 101–111.
- [62] P. Hensley, M. Mishra, N. Kyprianou, Targeting caspases in cancer therapeutics, *Biol. Chem.* 394 (2013) 831–843.
- [63] D. Speidel, Transcription-independent p53 apoptosis: an alternative route to death, *Trends Cell Biol.* 20 (2010) 14–24.
- [64] G. Waris, H. Ahsan, Reactive oxygen species: role in the development of cancer and various chronic conditions, *J. Carcinog.* 5 (2006) 14.
- [65] E.L. Schwartz, Antivascular actions of microtubule-binding drugs, *Clin. Cancer Res.* 15 (2009) 2594–2601.
- [66] B.H. Hussein, H.A. Azab, M.F. el-Azab, A.I. el-Falouji, A novel anti-tumor agent, Ln(III) 2-thioacetate benzothiazole induces anti-angiogenic effect and cell death in cancer cell lines, *Eur. J. Med. Chem.* 51 (2012) 99–109.